Selected Methods of Precision Distance Determinations to Nearby Galaxies

by **Bartłomiej Otton Zgirski**

A PhD thesis written under the supervision of
prof. dr hab. Grzegorz Pietrzyński
and auxiliary supervision of
Dr. Marek Górski

Nicolaus Copernicus Astronomical Center
of the Polish Academy of Sciences
Warszawa, Poland
February 2022

Dedykuję M. oraz moim rodzicom

”The fault, dear Brutus, is not in our stars,
But in ourselves, that we are underlings.”
- Cassius in William Shakespeare’s ”Julius Caesar”

Abstract

Distance determinations are among the essential tasks of observational astronomy. Different methods that are subject to different systematic errors allow checking consistency and accuracy of distance determinations. Techniques of partially overlapping and increasing ranges constitute the *cosmic distance ladder*, whose calibration is pivotal in determining the *Hubble constant.* These are especially the nearby galaxies that provide excellent opportunities for testing different distance determination methods.

In my dissertation, I present three different distance determination methods based on two types of stellar distance indicators.

The first part of my thesis presents a new calibration of a distance determination method based on mean values of luminosity functions of carbon stars in the near-infrared (NIR) $J-$band. The calibrated mean absolute magnitude of carbon stars is $-6.212 \pm 0.010(\text{stat.}) \pm 0.030(\text{syst.})$ mag. I further use the new calibration to determine distances to nine nearby galaxies and compare my results with the corresponding results from classical Cepheids. I obtain a very good agreement between the two methods, with the mean distance difference of 0.01 mag and the corresponding standard deviation of 0.06 mag.

In the second part of the thesis, I describe two distance determination methods based on RR Lyrae stars. I provide a new calibration of the period-luminosity (PL) and period-luminosity-metallicity (PLZ) relations in NIR bands for RR Lyrae stars from the Milky Way. I compare my calibrations with the recent findings available in the literature, and I determine distances to four nearby galaxies. The zero point of my calibrations of period-luminosity-metallicity relations for RR Lyrae stars is in agreement with the very accurate distance to the Large Magellanic Cloud obtained using eclipsing binaries (Pietrzyński et al., 2019). However, my new calibrations yield distances to four nearby galaxies that are smaller by $0.013 - 0.020$ mag compared to distances based on previous calibrations available in the literature. Subsequently, I present my calibration of projection factors and determination of the mean radii for two Galactic RR Lyrae stars. My calibrations for RR Lyrae stars are based on data gathered at the Cerro Armazones Observatory and parallaxes from the Early Data Release 3 of the GAIA space mission.

My research on carbon stars provides a method allowing to determine the Hubble constant, independent of classical Cepheids and the Tip of the Red Giant Branch. The new calibration of P-L-Z relations for RR Lyrae stars allows testing of distance determination methods in the neighborhood of our Galaxy. Relations allow tracing the old stellar Population II. The precision calibration of projection factors for two RR Lyrae stars provides auspicious results and when applied to a larger sample of these stars, may provide a genuine breakthrough in distance determination using this technique.

Streszczenie

Wyznaczenia odległości są jednym z najważniejszych zadań w astronomii obserwacyjnej. Użycie różnych metod pomiaru podlegających różnym błędom systematycznym pozwala na sprawdzanie zgodności i dokładności wyznaczeń odległości. Metody o częściowo nakładających się na siebie, coraz większych zasięgach pozwalają na skonstruowanie kosmicznej drabiny odległości, kluczowej w wyznaczeniu *stałej Hubble'a.* W szczególności pobliskie galaktyki dostarczają doskonałych możliwości testowania róznych metod pomiarów odległości.

W mojej rozprawie przedstawiam trzy różne metody pomiarów odległości oparte na dwóch typach gwiazd - wskaźnikach odległości.

Pierwsza część mojej pracy przedstawia nową kalibrację metody pomiarów odległości na podstawie średnich wartości funkcji jasności gwiazd węglowych w podczerwonym paśmie J. Skalibrowana przeze mnie średnia jasność absolutna gwiazd węglowych wynosi $-6.212\pm 0.010(\text{stat.})\pm 0.030(\text{syst.})$ mag. Na podstawie tej kalibracji dokonuję następnie wyznaczeń odległości do dziewięciu pobliskich galaktych oraz porównuję moje wyniki z odległościami otrzymanymi przy użyciu Cefeid klasycznych. Otrzymuję bardzo dobrą zgodność pomiędzy dwoma metodami, ze średnią różnicą odległości 0.01 mag i opowiadającym jej odchyleniem standardowym 0.06 mag.

W drugiej części pracy opisuję dwie metody pomiarów odległości przy użyciu gwiazd typu RR Lutni. Przedstawiam nowe kalibracje zależności okres-jasność oraz okres-jasność-metaliczność w pasmach podczerwonych dla gwiazd typu RR Lutni z Drogi Mlecznej. Dokonuję porównania moich kalibracji z ostatnimi wynikami dostępnymi w literaturze oraz wyznaczam odległości do czterech pobliskich galaktyk. Punkt zerowy moich kalibracji zależności okres-jasność-metaliczność dla gwiazd RR Lutni jest zgodny z bardzo dokładną odległością do Wielkiego Obłoku Magellana wyznaczoną przy użyciu układów zaćmieniowych (Pietrzyński et al., 2019). Jednakże, odległości do czterech pobliskich galaktyk uzyskane na podstawie moich nowych kalibracji są mniejsze o $0.13-0.20$ mag w porównaniu do odległości otrzymanych na podstawie poprzednich kalibracji dostępnych w literaturze. Następnie przedstawiam kalibracje współczynników projekcji oraz wyznaczenia średnich promieni dla dwóch gwiazd typu RR Lutni z naszej Galaktyki. Moje kalibracje dotyczące gwiazd RR Lutni zostały dokonane na podstawie danych zebranych w Obserwatorium Cerro Armazones oraz precyzyjnych paralaks z trzeciego (wczesnego) udostępnienia danych z misji kosmicznej GAIA.

Moje badania dotyczące gwiazd węglowych dostarczają metody pozwalającej na wyznaczanie stałej Hubble'a, niezależnie od wyznaczeń dokonanych przy użyciu cefeid klasycznych i wierzchołka gałęzi czerwonych olbrzymów. Nowa kalibracja zależności okres-jasność-metaliczność dla gwiazd RR Lutni pozwala na sprawdzanie metod wyznaczania odległości w sąsiedztwie Drogi Mlecznej. Zależności pozwalają na badanie struktur związanych ze starą Populacją II. Precyzyjna kalibracja współczynników projekcji dla dwóch gwiazd RR Lutni dostarcza bardzo obiecujących wyników. Przy zastosowaniu jej do większej próbki tych gwiazd może umożliwić dokonanie prawdziwego przełomu w pomiarach odległości przy użyciu tej geometrycznej techniki.

Contents

1 Introduction

Distance determinations are among the most fundamental tasks in astronomy. They allow for proper calibration of the energetics of various astrophysical phenomena and are also essential for the establishment of important cosmological parameters, including the *Hubble parameter* - the rate of expansion of the Universe.

The use of various independent methods allows checking for possible systematic errors in our reasoning. Different techniques are sensitive to systematic errors of different sources. That is why determinations using various techniques are important. Nearby galaxies, where distance indicators are available to be observed from ground-based observatories, serve as laboratories where astronomers may test different methods. The proximity of nearby galaxies allows distances to be determined with greater precision and accuracy than for systems at the limit of our methods.

It is not possible to determine distances of different orders of magnitude using only one method. That is why astronomers rely on the concept of the *cosmic distance ladder* (Figure 1). Short-range geometrical measurements, based on, e.g., parallax or eclipsing binaries, calibrate absolute magnitudes of *standard candles* that provide secondary techniques. They allow determining distances to Supernova host galaxies in the *Hubble flow* (i.e., at distances where peculiar motions of galaxies are significantly smaller than those resulting from the expansion of the Universe). This allows us to determine the current value of the Hubble parameter – the *Hubble constant* H_0 in three steps.

At the beginning of the 21$^{\mathrm{st}}$ century, the *Hubble Space Telescope (HST) Key Project* (Freedman et al., 2001), devoted to determine the Hubble constant based on calibrations of four different long-range distance indicators[1] using the Leavitt law[2] for classical Cepheids, yielded the value of $H_0 = 72 \pm 8$ km s^{-1} Mpc^{-1}. The re-calibration (Freedman et al., 2012) of the zero point of period-luminosity relations for Cepheids using Spitzer Space Telescope's parallaxes of 10 Galactic Cepheids allowed determining the constant with significantly better accuracy: $H_0 = 74.3 \pm 1.5$(stat.)$\pm$2.1(syst.) km s^{-1} Mpc^{-1}.

Independent research performed as a part of the *SHOES Project* has relied on the calibration of type Ia Supernovae (SNIa) based on Cepheids. The possible influence of systematic errors was mitigated by relying on NIR observations, the larger sample of Cepheids used for the calibration, the use of a new anchor - NGC 4258 megamaser galaxy (Miyoshi et al. 1995, Herrstein et al. 2005), and the utilization of a single photometric system (Riess et al., 2011). The authors combined three calibrations: i) based on the geometric distance to the megamaser, ii) the Large Magellanic Cloud (LMC), and iii) HST together with Hipparcos parallaxes of Galactic Cepheids. They obtained $H_0 = 73.8 \pm 2.4$ km s^{-1} Mpc^{-1}.

At the same time, the cosmic microwave background (CMB) space observatory *WMAP* provided data that allowed determining H_0 independent of the calibration of the cosmic distance scale through analysis of the CMB anisotropy. Based on the nine-year data, the final estimation of the Hubble constant yielded 70.0 ± 2.2 km s^{-1} Mpc^{-1} (Hinshaw et al., 2013), which agreed with values based on the calibration of the cosmic distance scale using Cepheids. Different determinations yielded values of the Hubble constant that were in agreement, with increasingly better precision. The new space observatory *Planck*, launched in 2009, provides even better precision of determinations of H_0 resulting from the analysis of CMB anisotropy.

However, together with the expected increased precision, analyses based on Planck data yielded systematically smaller values for H_0 compared to results based on WMAP data. The most recent result from Planck is $H_0 = 67.4 \pm 0.5$ km s^{-1} Mpc^{-1} (Planck Collaboration, 2020) – a value that is based on the ΛCDM cosmological model. The uncertainty of H_0 resulting from the distance ladder calibrations decreased, too. Riess et al. (2016) improved the accuracy by

[1] HST Key Project relied on type Ia Supernovae, Tully-Fischer relation, surface-brightness fluctuations, type II Supernovae, and the fundamental plane in the final determination of the Hubble constant. The determination was anchored to the Large Magellanic Cloud distance of $\mu_{\mathrm{LMC}} = 18.5 \pm 0.1$ mag.

[2] The Leavitt law, i.e., the period-luminosity relations for classical Cepheids that were discovered by Henrietta Swan Leavitt at the beginning of the 20th century.

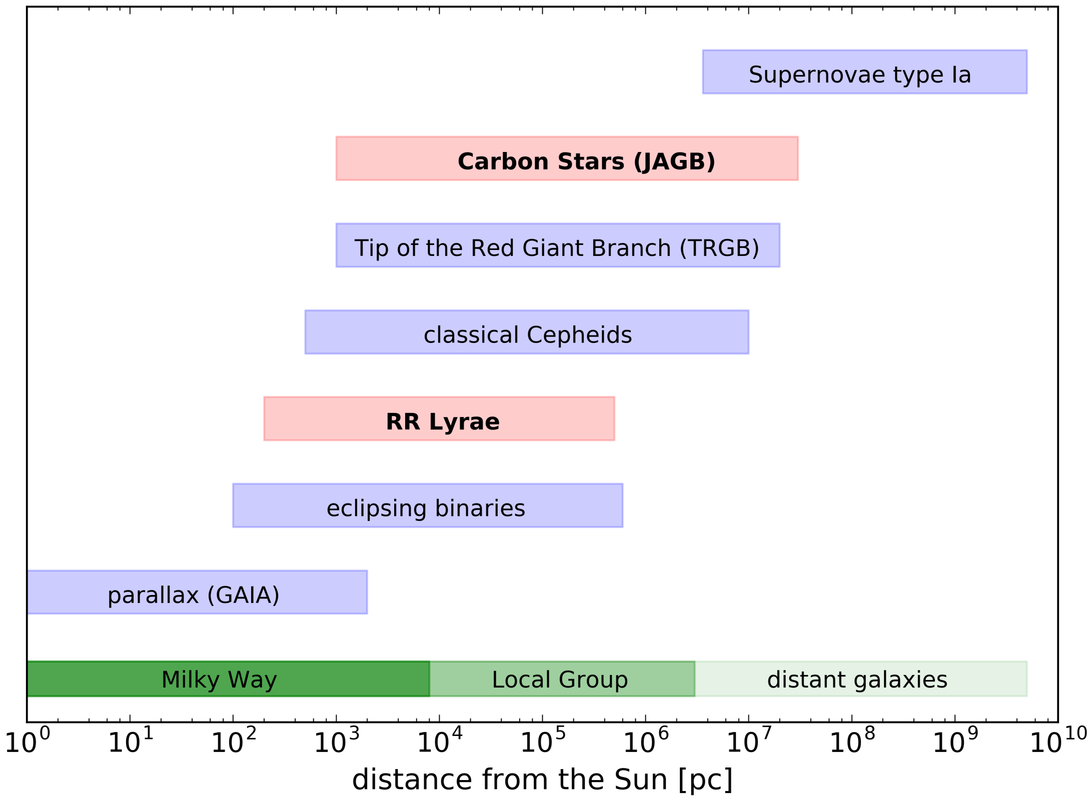

Figure 1: Ranges of the most important techniques used to calibrate the cosmic distance scale and determine the value of H_0. Geometric methods provide direct and the most accurate determinations of distances, but their range is limited. Standard candles such as classical Cepheids, TRGB, or carbon stars allow calibrating Supernovae in galaxies in the *Hubble flow*. Thus, we may determine the Hubble constant in three steps on the cosmic distance ladder. Distance indicators calibrated in this work are highlighted.

anchoring the zero point of the Leavitt law in the LMC to the accurate distance of Pietrzyński et al. (2013); the authors added a new anchor – the distance to M 31 as determined from two eclipsing binaries. In this way, Riess et al. (2016) obtained $H_0 = 73.24 \pm 1.74$ km s^{-1} Mpc^{-1} as their best value. The discrepancy between the two independent methods that is now estimated to be around 5σ (Riess et al. 2021 – calibration of the distance ladder based on GAIA Early Data Release 3 -EDR3- parallaxes, the LMC distance from eclipsing binaries, and masers in NGC 4258; consistent with the previous calibrations) caused a problem known as the *Hubble tension*. It may be related to the need to verify cosmological models, as results indicate that the Universe might have been expanding slower than expected (based on the late-universe determinations) at its early stage probed by the CMB.

The very existence of the Hubble tension results from the estimation of accuracy and precision of the calibration of the cosmic distance scale. Therefore, the calibration is fundamental and should be checked using various methods. The findings of the *Carnegie-Chicago Hubble Program* (Freedman et al. 2019, Freedman 2021) indicate that the Tip of the Red Giant Branch (TRGB) method provides the intermediate value of $H_0 = 69.8 \pm 0.6 \pm 1.6$ km s^{-1} Mpc^{-1} based on both the anchoring distance to the LMC (Pietrzyński et al., 2019) and GAIA EDR3 parallaxes (Gaia Collaboration et al., 2021). This would implicate that either TRGB or classical Cepheids are subject to yet unknown systematic errors. Proper calibration of distance determinations and evaluation of their uncertainties has been and will continue to be crucial in solving

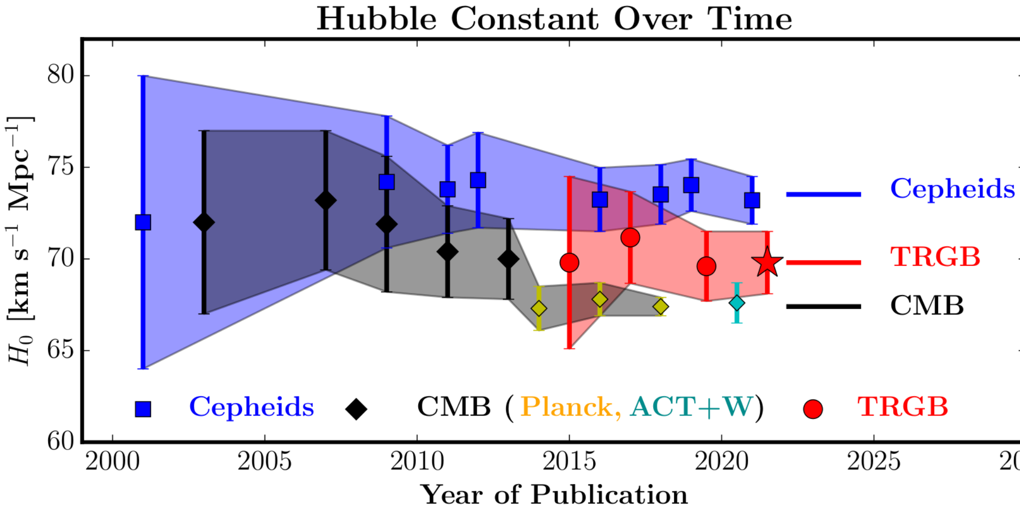

Figure 2: Values of H_0 determined using different methods – calibrations of the distance scale using Cepheids, TRGB, and based on measurements of the cosmic microwave background radiation assuming the ΛCDM cosmological model of a flat Universe. The figure is taken from `https://arxiv.org/abs/2106.15656` (Freedman, 2021).

this puzzle, strictly connected to the fundamental understanding of the Universe.

Alternative methods to determine the Hubble constant are also available. A novel method relies on the notion of *standard sirens* associated with the determination of distances to sources of gravitational waves (Abbott et al. 2017, Hotokezaka et al. 2019: $H_0 = 70.3^{+5.3}_{-5.0}$ km s^{-1} Mpc^{-1} based on the GW170817 event in NGC 4993). Although the accuracy of such determinations will enhance with future detections of more events, it is not yet comparable with the accuracy of the methods described above. Other determinations of H_0 are based on the baryon acoustic oscillations (BAO, e.g., Macaulay et al. 2019, $H_0 = 67.8 \pm 1.3$ km s^{-1} Mpc^{-1} – consistent with CMB measurements assuming the ΛCDM model), the strong gravitational lensing (e.g., Yang et al. 2020, $H_0 = 73.65^{+1.95}_{-2.26}$ km s^{-1} Mpc^{-1}), dust reverberation of active galactic nuclei (AGN, Yoshii et al. 2014, $H_0 = 73 \pm 3$ km s^{-1} Mpc^{-1} – only statistical error), or megamasers (Pesce et al. 2020, $H_0 = 73.9 \pm 3$ km s^{-1} Mpc^{-1}). In my work, I focus on classical methods, related to the cosmic distance ladder.

The aim of my thesis is not the determination of the Hubble constant but rather the introduction of tools that allow cross-checking of methods calibrating H_0 through the cosmic distance ladder. My work results in the calibration of methods that may be used in distance determinations to Supernova host galaxies and the inspection of systematic errors associated with distance determinations in the neighborhood of our Galaxy. The calibrations I present are founded on two independent zero points based on accurate geometric determinations of distances. The first one is associated with the LMC distance obtained with an accuracy of 1% using eclipsing binaries (Pietrzyński et al., 2019). The second one is based on GAIA EDR3 parallaxes of RR Lyrae stars from the Solar neighborhood (Gaia Collaboration et al., 2021). My calibrations prepare the ground for determinations of the Hubble constant in the era of the new generation of telescopes, such as the recently launched *James Webb Space Telescope* or the *Extremely Large Telescope* that is currently under construction.

In my thesis, I present three distance determination methods based on two types of distance indicators – carbon stars and RR Lyrae stars. Carbon stars allow us to determine distances at ranges similar to those probed by classical Cepheids and TRGB. It means that they may serve as independent calibrators of Supernovae. On the other hand, the RR Lyrae stars are fainter and allow to establish distances associated with the old stellar Population II. They may also be used in testing other methods, such as TRGB or the Leavitt law for classical Cepheids in the immediate neighborhood of the Milky Way.

In the third chapter, I propose an improved method for distance determinations using mean magnitudes of carbon stars. I provide calibration of this method and determine distances to nine galaxies using it. My calibration is based on carbon stars from the LMC. I will provide a calibration of this method and determine distances to nine galaxies.

The fourth chapter is devoted to RR Lyrae stars. In its first part, I present the new calibration of the NIR PL and PLZ relations for Galactic RR Lyrae stars based on the GAIA EDR3 parallaxes and photometry taken at the Cerro Armazones Observatory, especially for this project. The second part of the chapter covers a variation of the Baade-Wesselink technique of distance determinations to single pulsating objects applied to two RR Lyrae stars. The method requires both optical and NIR photometry, and well-covered radial velocity curves. It is a study focused on determinations of the crucial parameter of the method – the $p-$factor – that also takes advantage of the GAIA EDR3 parallaxes.

2 Observational data

The calibration of carbon stars as a distance indicator and the distance determinations to nearby galaxies are based on archival data, used before in another project devoted to classical Cepheids or published as separate photometric maps. Therefore, no calibration or data reduction was necessary. More details regarding this data set are given in the chapter about carbon stars.

As a part of my work associated with RR Lyrae stars, NIR photometry and radial velocities were required in an independent and coherent way. I personally took part in the observations using telescopes at the *Cerro Armazones Observatory* (OCA) and the *European Southern Observatory* (ESO).

OCA is located in the Chilean Atacama desert and is one of the best sites for observational astronomy in the world; especially its low water vapor content is ideal for NIR photometry. During the course of my PhD studies, I spent around 180 nights at this mountain.

Since 2010, the observatory has hosted four telescopes: the 0.8 m *Infra-Red Imaging Survey (IRIS)*, the 0.4,m *Bochum Monitoring Telescope (BMT)*, also known as *VYSOS 16*, the 0.25 m *Berlin Exoplanet Search Telescope II (BEST II)*, and the binocular 2×0.15 m *Robotic Bochum Twin Telescope (RoBoTT)*. I have used IRIS and VYSOS 16 (Figure 4) for the purpose of my research devoted to RR Lyrae stars.

The 0.8 m IRIS telescope is based on an alt-azimuth mount and equipped with a HAWAII-1 infrared camera (Hodapp et al. 2010, Watermann 2012) installed in a Nasmyth focus. Its field of view is 12.5×12.5 arcmin with a 0.73 arcsec/pix pixel scale. The focal length of the IRIS optical system is 5227 mm. The camera is cooled with 3.5 liters of liquid nitrogen to a temperature of about 77 K to minimize the instrumental thermal noise. The filter wheel includes $JHKs$[3] filters similar to those of 2MASS (Skrutskie et al., 2006). Figure 5 depicts transmission curves of the IRIS filters in comparison with those of the 2MASS system.

VYSOS 16 is installed on an equatorial fork mount. It is equipped with an SBIG STL-6303 camera installed in a Coudé focus. The field of view is 41.2×27.5 arcmin with a 0.79 arcsec/pix pixel scale. The focal length of the system is 2337 mm. The camera is cooled down to $-10°$C using a fan. Among others, Johnson BV filters made by Astrodon are installed in the filter wheel.

I have used IRIS photometry for the determination of PLZ relations for RR Lyrae stars. Moreover, the Baade-Wesselink determination required optical $V-$band photometry from VYSOS 16 and time-series of radial velocities based on stellar spectra. In this work, I am using radial velocities based on high-resolution ($R > 40000$) spectra obtained from three ESO spectrographs: HARPS (Mayor et al., 2003) at the 3.6 m telescope and FEROS (Kaufer et al., 1999) at the MPG/ESO 2.2 m telescope (both at the La Silla Observatory), and UVES (Dekker et al., 2000) at the Very Large Telescope (VLT - UT2) at the Paranal Observatory in Chile.

[3]For simplicity I use K instead of Ks (the abbreviation for $K-short$) throughout this dissertation.

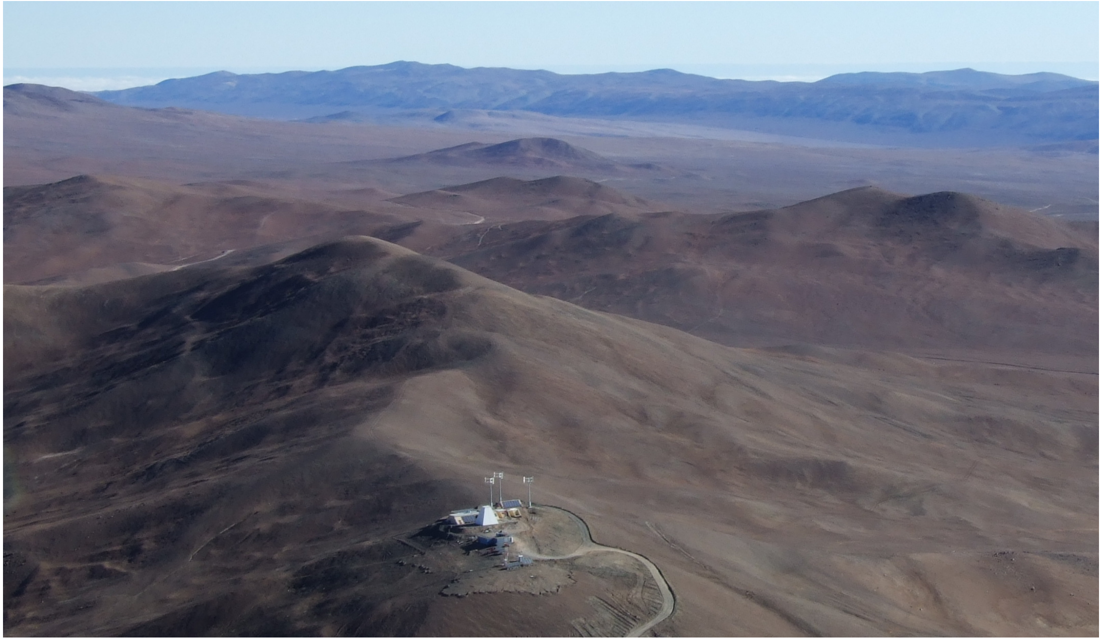

Figure 3: Cerro Armazones Observatory (OCA), located in the Chilean Atacama desert, provides excellent conditions for high-precision photometry – especially in the NIR domain (from the author's archive).

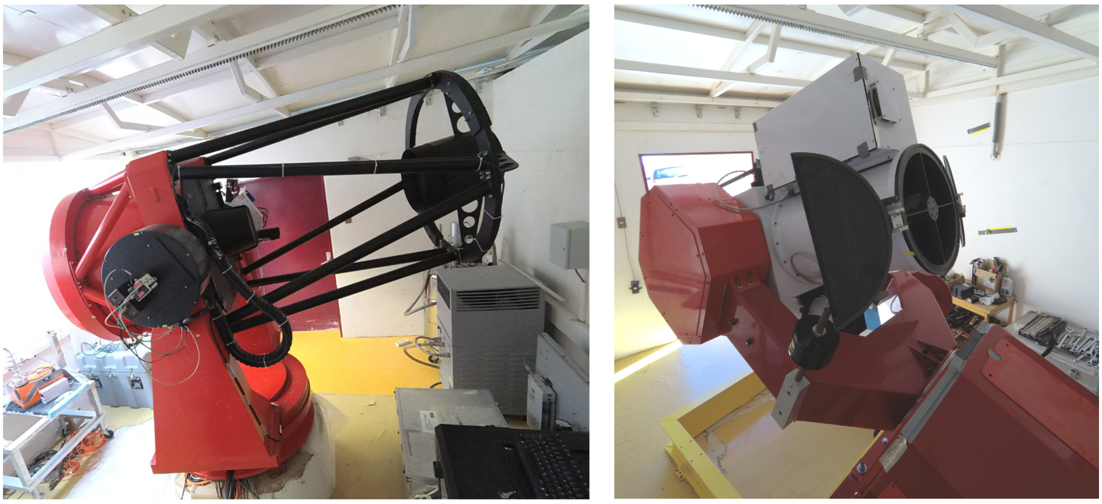

Figure 4: Two telescopes of OCA used in my project devoted to RR Lyrae stars. The 0.8 m IRIS providing JHK photometry and the 0.4,m VYSOS 16 for the Johnson BV photometry of stars in the Solar neighborhood (from the author's archive).

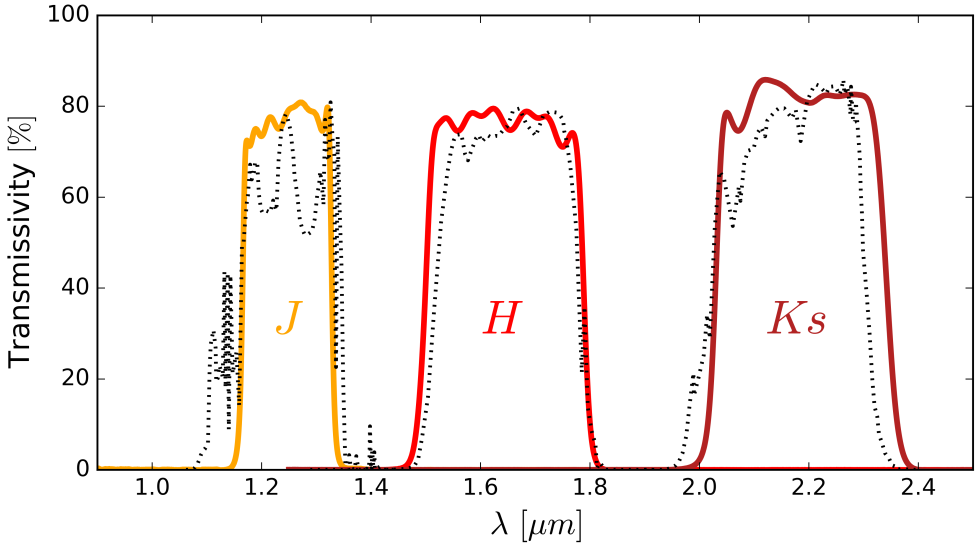

Figure 5: Transmission curves of IRIS filters (colored) compared with transmissivity of original 2MASS filters (dotted black curves). Transmission curves of 2MASS filters were normalized to correspond to IRIS filters.

Scientific frames obtained with IRIS and VYSOS 16 were calibrated using an automatic pipeline (Watermann, 2012) based on IRAF (Tody, 1986), SExtractor (Bertin & Arnouts, 1996), and SCAMP (Bertin, 2006) software with the courtesy of Dr. Martin Haas from the Astronomical Institute of the Ruhr University Bochum. The calibration pipeline includes:

- Flat-field correction - normalization of different sensitivities of camera pixels.
- Determination and subtraction of the sky thermal background based on the *dithering*[4] technique – i.e. the frequent change of the telescope pointing between the scientific target and some varying offset position. This differential method allows for an effective cancelling of the sky background.
- Stacking of individual frames into the final image. It requires precise values of dithering shifts determined using astrometric solutions derived by the SCAMP software.

I have performed photometric measurements using a custom photometric pipeline written together with my colleague Piotr Wielgórski. The photometric pipeline is based on the Python Astropy library (Astropy Collaboration, 2013) that allows data extraction from headers of .fits files and operations (such as arithmetic operations, cutting etc.) on data matrices. In the case of IRIS data, the photometry is standardized using photometry from the 2MASS catalog (Cutri et al., 2003). The VYSOS 16 data are tied up to the TYCHO-2 catalog (Høg et al., 2000). Photometric scripts are based on the DAOPHOT photometric package (Stetson, 1987). The photometric reduction pipeline includes:

- Manual designation of a scientific target and comparison stars in a reference frame.
- Aperture photometry of all frames corresponding to a given scientific object. Detection of sources using *find* and aperture photometry performed using *photometry* routines of DAOPHOT.
- Extraction of instrumental magnitudes $m_{\rm inst}$ of the scientific object for all frames based on positions of objects in the reference frame. Source-matching script based on APMATCH program authored by Dr. Wojciech Pych.

[4] Also known as *jittering*.

- Standardization of instrumental magnitudes to the 2MASS and Johnson photometric systems based on magnitudes of comparison stars from 2MASS and TYCHO-2 catalogs.

Both for IRIS and VYSOS 16 the usual precision of the instrumental photometry m_{inst} of $0.01 - 0.02$ mag was obtained.

The transformation equation that converts instrumental magnitudes of scientific sources into the standard magnitudes in a given system is given by:

$$m_{\text{stand}} = m_{\text{inst}} + \alpha X + \beta C + \gamma \tag{1}$$

where m_{stand} is the desired standard magnitude, m_{inst} is the measured instrumental magnitude, α is the atmospheric extinction term, X is the air mass (the integral of air density along a given line of sight, relative to zenith where $X_Z = 1$), β is the color term of the optical system, C is the apparent instrumental color of the object, and γ is the zero point of standardization.

Given the relatively small sizes of the field of view, comparison stars in a given field are located at the same air masses as the corresponding scientific sources. Thus, their instrumental magnitudes are equally affected by the atmospheric extinction ($\alpha X = const$).

Color coefficients $\beta = -0.070 \pm 0.027$, 0.015 ± 0.030, and 0.020 ± 0.036 for the $J-$, $H-$, and $K-$bands, respectively. Colors C corresponding to these coefficients are $(J - K)$ in the case of $J-$ and $K-$bands, and $(J - H)$ in the case of the $H-$band. Since for $H-$ and $K-$band magnitudes the corresponding β are consistent with 0, no color correction was applied in their standardization. In the case of the $J-$band $\beta = -0.07$ was applied.

In the case of VYSOS 16, where only $V-$band was used, $\beta = 0.006 \pm 0.01$ corresponds to the instrumental color $(B - V)$. Thus, the color correction has also been neglected here.

The accuracy of the overall photometric zero point calculated as an error on the mean of differences between the catalog and independently derived magnitudes of constant control stars is estimated at 0.002 mag (Wielgórski et al., 2021) with the mean shift between the standardization's and 2MASS catalog's zero points equal to zero.

In the case of VYSOS 16 data were tied up to the TYCHO-2 catalog - they were used only for the purpose of the Baade-Wesselink analysis. Johnson magnitudes of stars from the catalog are given with lower accuracy. Thus the estimated systematic uncertainty that affects the whole $V-$band light curves associated with the uncertainty of magnitudes of comparison stars is 0.05 mag.

High-resolution spectroscopic data from HARPS and UVES were calibrated using dedicated pipelines from ESO. Data from FEROS were calibrated by Piotr Wielgórski using the CERES pipeline (Brahm et al., 2017).

I have measured radial velocities using one-dimensional spectra using RaveSpan[5] (Pilecki et al. 2012, Pilecki et al. 2017). I have calculated radial velocities using two techniques implemented in the program. One of them is the *cross-correlation function* (CCF) of the template and the stellar spectra. The second approach is based on the *broadening function* (BF, Rucinski 2002). Both methods give virtually the same results. The most probable radial velocity is estimated based on a fit of a Gaussian to CCF/BF. The mean of estimated uncertainties of the measured radial velocities is about 200 m/s.

[5] RaveSpan is available for download at `https://users.camk.edu.pl/pilecki/ravespan/`.

3 Distances to nine nearby galaxies using carbon stars

3.1 Carbon stars as a distance indicator

Originally discovered using spectroscopy by Angelo Secchi in 1868 (Secchi 1868, McCarthy 1994), carbon stars are characterized by the presence of radical C_2 absorption bands in their spectra (Swan, 1857) that resemble those of cometary tails or products of combustion of hydrocarbon fuels.

Atmospheres of these thermally-pulsating[6] asymptotic giant branch (AGB) stars, with ages in the range (100 M − 3 G)yr, have a surplus of carbon relative to oxygen abundance. It makes them significantly redder (with temperatures between 2500 K and 3900 K) than their oxygen-rich evolutionary progenitors. The convective envelope of a carbon star transports carbon to the surface from its helium-burning shell during the third dredge-up[7]. It alters the molecular opacity of the stellar photosphere, which decreases its effective temperature (Marigo et al., 2008).

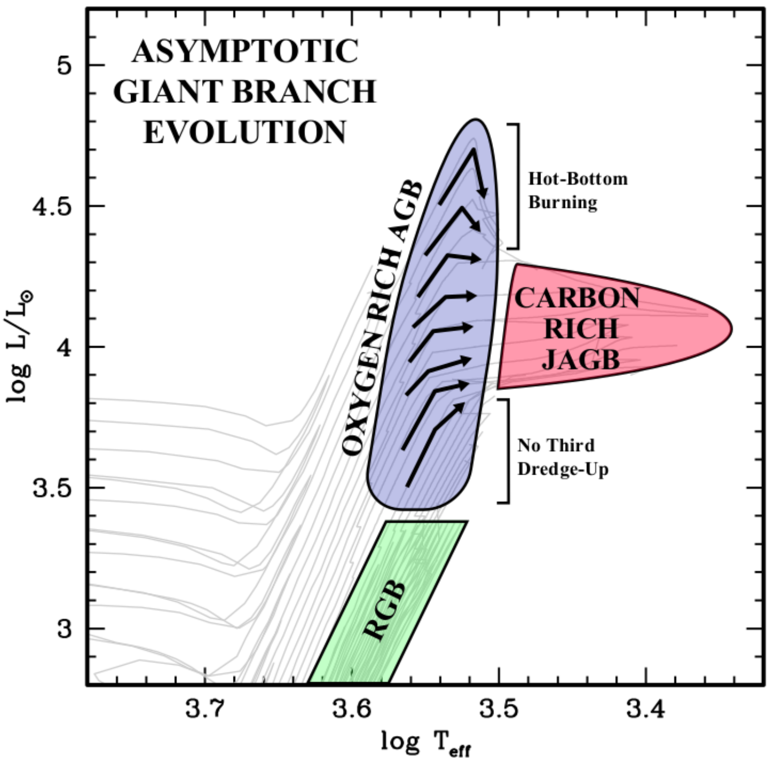

Figure 6: The *funneling effect* as depicted in the work of Madore & Freedman (2020) based on theoretical models of Marigo et al. (2008). Carbon stars exist as late evolutionary stages of the AGB for the tightly concentrated range of stellar masses only. The sketch of the HR diagram taken from `https://arxiv.org/abs/2005.10792`.

The effect of concentration of luminosities of carbon stars, which makes them interesting candidates for standard candles, has been explained in numerous theoretical works (e.g., Iben

[6]Thermal pulses, also known as He-shell flashes, occur during the late stages of the evolution of AGB stars that burned out helium above their carbon-nitrogen cores. Hydrogen above the thin layer of helium starts to burn, and, as a result, the helium shell is being rebuilt. After sufficient helium has accumulated, the fusion of this element reignites rapidly, and the stellar luminosity rises, which is the reason for periodic thermal pulses.

[7]Dredge-ups are periods in stellar evolution when a convective envelope penetrates stellar interior deep enough to reach nuclear fusion products. The third dredge-ups correspond precisely to the evolutionary phases of the late AGB stars. They accompany thermal pulse cycles and cause transport of, e.g., carbon to the stellar surface.

1973, Sackmann et al. 1974, Groenewegen & Marigo 2004, Karakas et al. 2018, Ventura et al. 2020). Carbon-rich photospheres are obtainable only for stars having masses from a relatively compact interval, which makes their magnitudes directly restricted. *Hot-bottom burning* that occurs in too massive AGB stars results in the conversion of carbon into nitrogen at the base of their convective envelopes. Even though the exact mass value needed for ignition of such a process depends on the metallicity of a star, it typically occurs for $M > 3.5\,M_{\odot}$ but may appear even for $M > 2M_{\odot}$ for stars of low metallicity. On the other hand, the convective envelopes of low-mass ($M < 1.3\,M_{\odot}$) AGB stars are not extensive enough to bring carbon to their surface.

Carbon stars were utilized for distance determinations for the first time by Richer et al. (1984), Richer et al. (1985), and Pritchet et al. (1987), who used optical photometry to determine distances to NGC 205, NGC 300, and NGC 55. These determinations were based on statistical studies on a sample of 70 carbon stars in the LMC in VRI (Richer, 1981), which proved that their bolometric and $I-$band magnitudes are relatively well concentrated with a spread of $\sigma_I = 0.47$ mag and the reported uncertainty of the mean $I-$band magnitude of ± 0.06 mag. However, in order to distinguish carbon stars from M-type stars having the same $(V-I)$ colors, authors used the $(8100-7800)$ Å color. These two narrow-band filters allow to easily separate stars having strong TiO absorption lines (M-type stars) from those having CN lines (carbon stars).

Important observational results were described in the work of Nikolaev & Weinberg (2000) who distinguished different stellar populations in the Large Magellanic Cloud (LMC) appearing in the color-magnitude diagram (CMD) based on the NIR 2MASS photometry. Among the described CMD zones, *Region J* corresponds to the population of carbon stars. The authors used this CMD feature to analyze the spatial structure of the LMC (Weinberg & Nikolaev, 2001), showing that the carbon-abundant long-period variables are standard candles for a given narrow interval of their colors with a well-defined color-luminosity relation[8]. They also estimated precision of a single carbon star as a standard candle in JHK of about 0.2 mag. The authors also outlined the advantages of using stars from the mentioned region as distance indicators, stressing their very high luminosities that potentially make it possible to reach farther than the Tip of the Red Giant Branch (TRGB) method.

The works of Nikolaev & Weinberg showed the advantages of statistical analysis of carbon stars using NIR rather than optical photometry. Indeed, NIR observations are less affected by extinction (which influences the significant differences between the spread of luminosities of carbon stars in optical and NIR bands). An important advantage is also that photometry in just two bands is needed to form a J vs. $(J-K)$ CMD where carbon stars are well separated from other populations through simple color cuts (see Figure 7).

A kind of hybrid solution was proposed by Battinelli & Demers (2005). The authors praised the selection of samples using $(J-K)$ colors, following the works of Nikolaev & Weinberg. They showed that samples with more than around 100 carbon stars have their mean absolute $I-$band magnitude constant. They also derived a metallicity-absolute magnitude dependence, obtaining $\langle M_I \rangle = -4.33 + 0.28\,[Fe/H]$, and laid prospects on developing the NIR version of the method in the era of the future *James Webb Space Telescope* already.

The revival of the topic of carbon stars as a distance indicator came along lately with the almost simultaneous publications of Ripoche et al. (2020) and Madore & Freedman (2020), who explicitly articulated for the first time the constant $J-$band magnitude of carbon stars occupying *Region J* in the whole of its $(J-K)$ color interval, i.e., $(J-K) \in (1.3, 2.0)$ mag. This trait allowed to utilize the mean $J-$band[9] magnitude of a population of carbon stars as

[8] Weinberg & Nikolaev (2001) established the relation of $< K >= -(0.99 \pm 0.80) < (J-K) > +K_0$ based on 14 carbon Miras from the LMC Region J and deduced that luminosity does not change a lot for carbon stars having $1.6 < (J-K) < 1.7$. They further used the mean NIR magnitudes of carbon stars having colors from this interval as standard candles.

[9] It is worth mentioning here that the NIR band J is not the reason for the naming of *Region J* described by Nikolaev & Weinberg (2000) - they just used subsequent letters of the alphabet to name different zones in the CMD of the LMC. It is a coincidence that carbon stars which have constant $J-$band magnitudes along the population's color interval appear in *Region J*; in addition, in their work, Weinberg & Nikolaev used carbon star luminosity functions in JHK. However, in the peer-reviewed version of their paper, Madore & Freedman

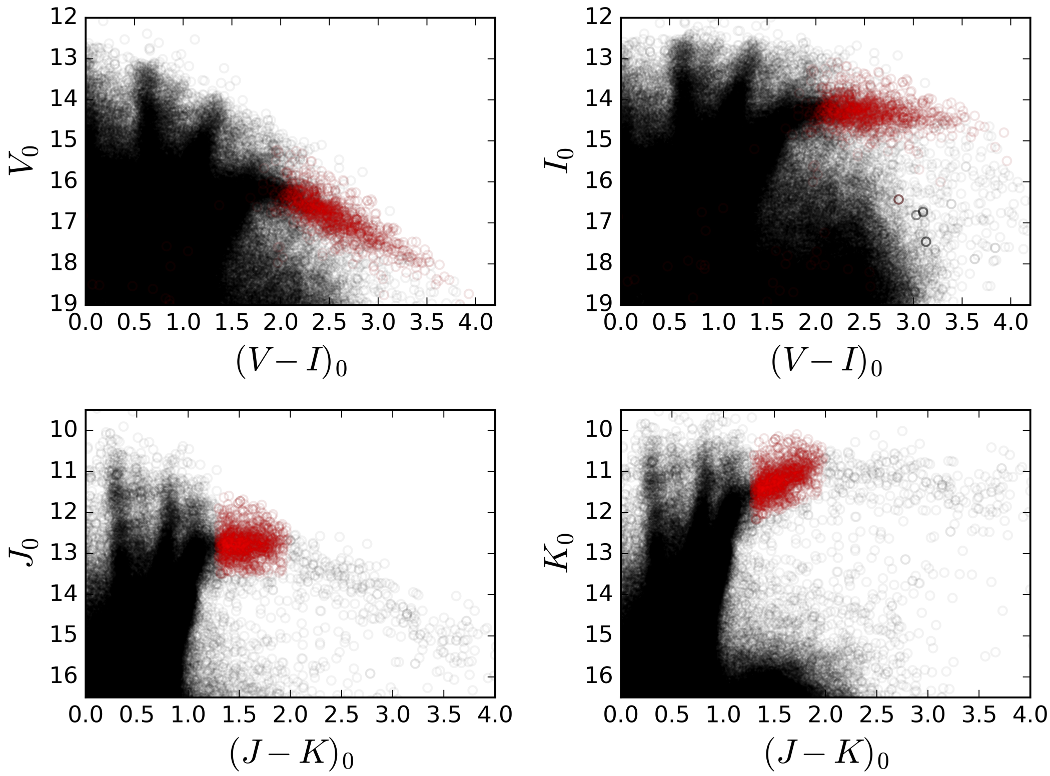

Figure 7: Exemplary color-magnitude diagrams depicting the JAGB samples (in red) for the Small Magellanic Cloud for optical and NIR data, dereddened using the extinction maps of Górski et al. (2020). $V-$ and $I-$band photometry originates from the OGLE-III Photometric Maps of the Small Magellanic Cloud (Udalski et al., 2008b), while the $J-$ and $K-$band photometry from the IRSF Magellanic Clouds Point Source Catalog of Kato et al. (2007). The two catalogs were cross-matched, and the JAGB sample is defined as having $(J-K) \in (1.3, 2.0)$ mag and $J \in (11.5, 14.0)$ mag (as in Figure 12). The advantage of the NIR over optical photometry in the sample's specification is associated with the fact that the JAGB population is far better separated and less contaminated in the NIR CMDs where it is easy to extract carbon star samples using rectangular sample-selection boxes. In the case of optical photometry, one needs to use other criteria (such as narrow-band colors or a spectroscopic survey) to reject M-type dwarfs of similar colors (as in, e.g., Richer et al. 1984). Ripoche et al. (2020) showed that spectroscopic catalogs of carbon stars like those of Raimondo et al. (2005) or Kontizas et al. (2001) correspond well to samples selected using simple color cuts in the J vs. $(J-K)$ CMDs (although they do not reach stars as faint as photometry may reach). The linear least-squares regression fitted for the JAGB sample in the J vs. $(J-K)$ CMD gives $J_0 = (-0.019 \pm 0.059)(J-K)_0 + (12.785 \pm 0.092)$ mag, which shows the assumption of the constant $J-$band magnitude of carbon stars of different colors is justified. However, JAGB samples in the NIR may also be contaminated, especially by the background galaxies, having the same colors but surface densities rising exponentially with apparent magnitudes (e.g., Bershady et al. 1998, Madore et al. 2021). Such contamination would be especially problematic for faint and small samples, and it may introduce positive skewness to the luminosity functions of the JAGB samples.

its distance indicator. Madore & Freedman calibrated their method provisionally and called it simply *the JAGB method* as derived from *Region J* AGB stars. Other publications of Freedman & Madore (2020), Parada et al. (2020), and Lee et al. (2020), which tackled the issue, soon followed. Methods and calibrations presented in these papers differ, mainly because of undertaking numerous arbitrary choices whenever one uses a statistical method that relies on a CMD feature. Freedman & Madore determined JAGB distances to 16 nearby galaxies. They compared their results with TRGB distances and obtained a very good agreement. The authors received the mean difference between JAGB and TRGB moduli of 0.007 mag with the corresponding scatter of 0.08 mag. They also discussed a possible dependence of the absolute magnitude of JAGB on metallicity but provisionally found that there is no such correlation. Ripoche et al. (2020) showed that simple $(J-K) \in (1.4, 2.0)$ color cuts allow retrieving samples of spectroscopically-confirmed carbon stars from catalogs of Kontizas et al. (2001) (LMC, 100% carbon stars retrieved) and Raimondo et al. (2005) (SMC, 98% carbon stars retrieved), thus confirming the claims of Nikolaev & Weinberg.

The task of obtaining the mean $J-$band magnitude of carbon stars from a given population is subject to several different assumptions that may influence the final determination. In my project devoted to distance determinations using statistical analysis of the NIR photometry of carbon stars, I have proposed a new, alternative calibration and method of distance determinations using JAGB. It enables an accurate determination of the mean magnitude of a JAGB sample for a given population using a custom profile of the luminosity function of these stars. I have used it to determine distances to nine galaxies from the local Universe, and compared these with distances obtained by the Araucaria Project using the multi-band PL relations for classical Cepheids - an already well-established method. It resulted in a publication in *The Astrophysical Journal* (Zgirski et al., 2021).

3.2 The new calibration of the JAGB method

In order to estimate the mean absolute magnitude of JAGB in the $J-$band, I took advantage of the very accurate distance determination to the LMC based on detached eclipsing binaries (Pietrzyński et al., 2019), and the recent reddening maps of the Magellanic Clouds (Górski et al., 2020). The NIR photometry in $J-$ and $K-$ bands used for the purpose of the calibration of the method was taken from the publicly available Infrared Survey Facility (IRSF) Magellanic Clouds Point Source Catalog of Kato et al. (2007). That work also gives equations that were required to transform the photometry from the IRSF/SIRIUS into the 2MASS photometric system. Each observing field shown in Figure 8 has been dereddened using the reddening maps of Górski et al. and the corresponding $E(B-V)$ values given there. The color excess was transformed into total extinctions A_J and A_K following the work of Cardelli et al. (1989). I have utilized ratios of total extinction in a given band (given its effective wavelength and the reddening law) to the total reddening in the V band given there. Assuming the reddening law of $R_V = 3.1$, I obtained the following (Table 1) ratios of total-to-selective extinctions - $R_\lambda = \frac{A_\lambda}{E(B-V)}$ for the 2MASS bands (details of that photometric system are given in Cohen et al. 2003):

	$\frac{A_\lambda}{A_V}$	R_λ	$< A_\lambda >_{\mathrm{LMC}}$	$< A_\lambda >_{\mathrm{SMC}}$
$J(\lambda_{eff} = 1.235\ \mu m)$	0.288	0.892	0.124 mag	0.079 mag
$K(\lambda_{eff} = 2.159\ \mu m)$	0.117	0.363	0.050 mag	0.032 mag

Table 1: Ratios of extinctions for 2MASS bands obtained from Cardelli et al. (1989) for the purpose of dereddening the Kato et al. (2007) photometry. Ratios of total-to-selective extinctions R_λ were calculated given the reddening law $R_V = 3.1$. The mean total extinctions for the LMC and the SMC are given just for the reference in the two last columns, as every such field has been dereddened separately based on Górski et al. (2020) extinction maps.

(2020) use the term *the AGB J-band method*.

Both calibrations of Freedman & Madore (2020) and Ripoche et al. (2020) are based on samples of JAGB stars from both Magellanic Clouds. My calibration is founded, more conservatively, on the LMC sample, with the Small Magellanic Cloud (SMC) sample playing only a control role for the calibration. The LMC distance is determined with better accuracy and precision. The LMC sample is also larger and the SMC displays a large spatial span in the line-of-sight direction as reported by, e.g., Graczyk et al. (2020).

When estimating a mean $J-$band magnitude of a given population of JAGB stars, we may choose different statistics. Madore & Freedman (2020), Freedman & Madore (2020), and Lee et al. (2020) use arithmetic means of magnitudes calculated for relatively small intervals of $J-$band magnitudes that define their samples. They use non-uniform criteria of selection of samples. Most sample-selection boxes have their spans along the J axis of, e.g., 0.7 mag, but they apparently depend on a population. The authors generally define the JAGB population as having $(J-K)$ color boundaries of (1.3 and 2.0) mag. However, for some galaxies, they also use CMDs with $(J-H)$ or $(Z-J)$ colors and not strictly defined boundaries of their sample selection boxes (both in the J axis and in the color axis) in order to select their samples. For the calibration of their method in both Magellanic Clouds, they actually use CMDs with different colors for each of the Clouds. It all makes their determinations arbitrary. On the other hand, Ripoche et al. (2020) and Parada et al. (2020) rely on the median value of magnitudes from their samples that have optional cut-offs along the J axis just from the faint side (in the apparent minimum of the luminosity function). Carbon stars from their samples have $(J-K)$ colors from the $(1.4, 2.0)$ mag interval.

In order to obtain a more objective estimation of the mean J magnitude of carbon stars, I have applied a profile fit. The estimation of the mean $J-$band magnitude of the JAGB stars proposed in my work included binning stellar magnitudes from a given sample into histograms and fitting a superposition of a Gaussian and a quadratic function to such empirical luminosity functions. The profile was originally presented by Paczyński & Stanek (1998) for modeling of luminosity functions of samples of the Red Clump stars contaminated with the Red Giant Branch stars. The fitted profile takes the form of:

$$\frac{dn}{dJ} = \frac{N}{\sigma\sqrt{2\pi}} \exp\left[\frac{-(J-<J>)^2}{2\sigma^2}\right] + a(J-<J>)^2 + b(J-<J>) + c \tag{2}$$

where $\frac{dn}{dJ}$ is the number of JAGB stars per $J-$band magnitude interval, N is a scaling factor of the Gaussian component, $<J>$ is the estimated mean $J-$band magnitude of a JAGB population, and σ corresponds to the spread of its luminosities. Such 6-parameter (N, $<J>$, σ, a, b, c) fits were performed using the *curve_fit* procedure of the *SciPy* library (Virtanen et al., 2020) for Python that is based on the non-linear least squares analysis.

While the Gaussian component models the proper, uncontaminated luminosity function of carbon stars, the quadratic component models the contamination of the sample with foreground stars and background galaxies. Additionally, while the Gaussian component is always symmetric, its superposition with the parabolic component may also contribute to the skewness of the modeled luminosity function. The spread of luminosities, denoted by the σ parameter, is a combination of different factors (Weinberg & Nikolaev, 2001):

$$\sigma = \sqrt{\sigma_M^2 + \sigma_{(m-M)}^2 + \sigma_A^2 + \sigma_{ph}^2} \tag{3}$$

where σ_M – the intrinsic spread of the absolute magnitudes of JAGB stars – may be interpreted as the precision of a single carbon star as a standard candle; $\sigma_{(m-M)}$ – the geometric depth[10] of a system associated with different positions of stars in this system along the line of sight (i.e., different distances of stars); σ_A – associated with differential extinction, i.e., the fact that different stars from sample are affected by the extinction of different magnitudes; σ_{ph}

[10] $\sigma_{(m-M)}$ can be easily written in terms of the linear, relative distance spread. By differentiating the defining formula of the distance modulus: $(m-M) = 5log(r) - 5$, where r is the distance in parsecs, we obtain the relation between the absolute geometric depth or uncertainty (spread) of distance modulus and the relative spread of linear distance: $\sigma_{(m-M)} = \frac{2.17}{r}\sigma_r$.

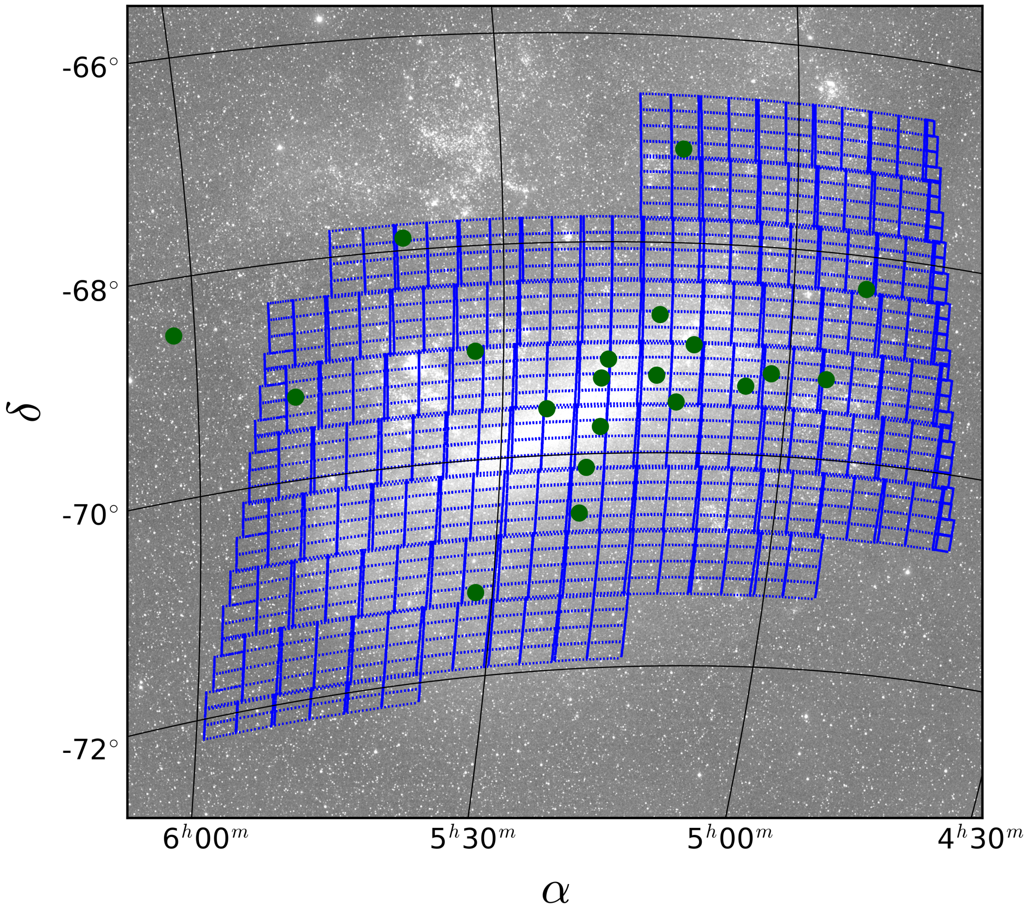

Figure 8: IRSF Magellanic Clouds Point Source Catalog of Kato et al. (2007) observing fields in the LMC - the NIR photometry that has been utilized to calibrate the JAGB method. The location of detached eclipsing binary systems used by Pietrzyński et al. (2019) to determine distance to the LMC with the accuracy of 1% are depicted in green. The background image comes from Udalski et al. (2008a).

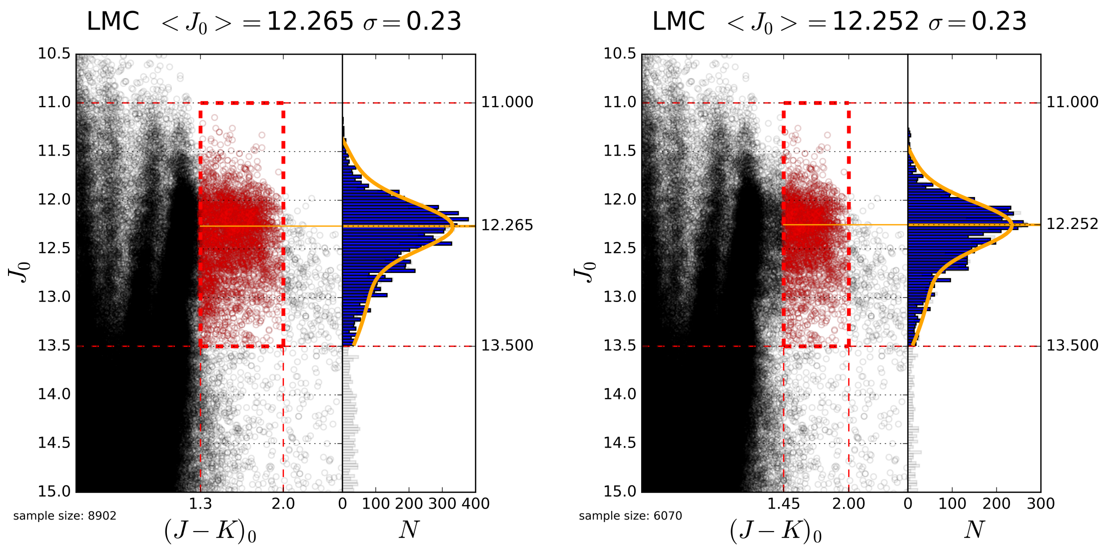

Figure 9: Determinations of mean, dereddened values of $J-$ band magnitudes for the two samples of JAGB stars in the LMC that were selected using different $(J-K)_0$ color (where 0 denotes the dereddened value) ranges give results consistent to about 0.01 mag. Corresponding positions of samples in the CMD produced out of the combined, dereddened IRSF Magellanic Clouds Point Source Catalog photometry are visible to the left of both determinations. The determination founded on the broader color range has been used to calibrate the method.

– the photometric error component of the spread. In practice, it is not an easy task to trace and quantify each component of the total apparent spread of the luminosity function of carbon stars.

In the case of single-epoch photometry, the apparent intrinsic spread of luminosities of carbon stars σ_M is also affected by the fact that virtually all JAGB stars are long-period variables. Some of them are carbon Mira variables, known for their very large amplitudes in the optical bands, they have average peak-to-peak ΔJ amplitudes from between 0.5 and 0.7 mag (Smith et al. 2002, Madore & Freedman 2020). The study of Whitelock et al. (2013) shows, on the example of NGC 6822, that most of the JAGB stars are actually low-amplitude variables having $\Delta K < 0.4$ mag – most of them are probably semi-regular or irregular variables. If, for the sake of simplicity, we assume sinusoidal variability, the variance of the $J-$band magnitude over the variability period will be: $\sigma_{var}^2 = \left\langle \frac{\Delta J^2}{4} sin^2(t) \right\rangle = \frac{\Delta J^2}{8}$. Thus, assuming $\Delta J = 0.5$ mag, we obtain the variability component of the total scatter of luminosities of carbon stars of $\sigma_{var} = \frac{\Delta J}{2\sqrt{2}} = \frac{1}{4\sqrt{2}} = 0.18$ mag, which leaves just 0.09 mag for the variations of mean magnitudes of these stars given the 0.2 mag intrinsic precision of carbon stars claimed by Weinberg & Nikolaev (2001).

Figure 9 shows $< J_0 >$ determinations - the dereddened, mean $J-$band magnitude of carbon stars in the LMC. The two determinations were performed in different $(J-K)_0$ color ranges – $(1.3, 2.0)$ mag and $(1.45, 2.0)$ mag. While the latter will be used further to determine $< J_0 >$ for galaxies contaminated from the bluer side of the sample-selection box, it is the former, broader span of colors that defines our sample that calibrates the method. Both color intervals give results coherent within around 0.01 mag. The box size along the J axis has been consistently set to 2.5 mag. It has been established empirically by searching for box sizes that give stable results (i.e., where changes of the result with changes of the box size are relatively small) for all studied galaxies. Figure 10 compares results obtained with the profile fit, median, and mean. Among those three, the profile fit gives the most stable results that do not depend significantly

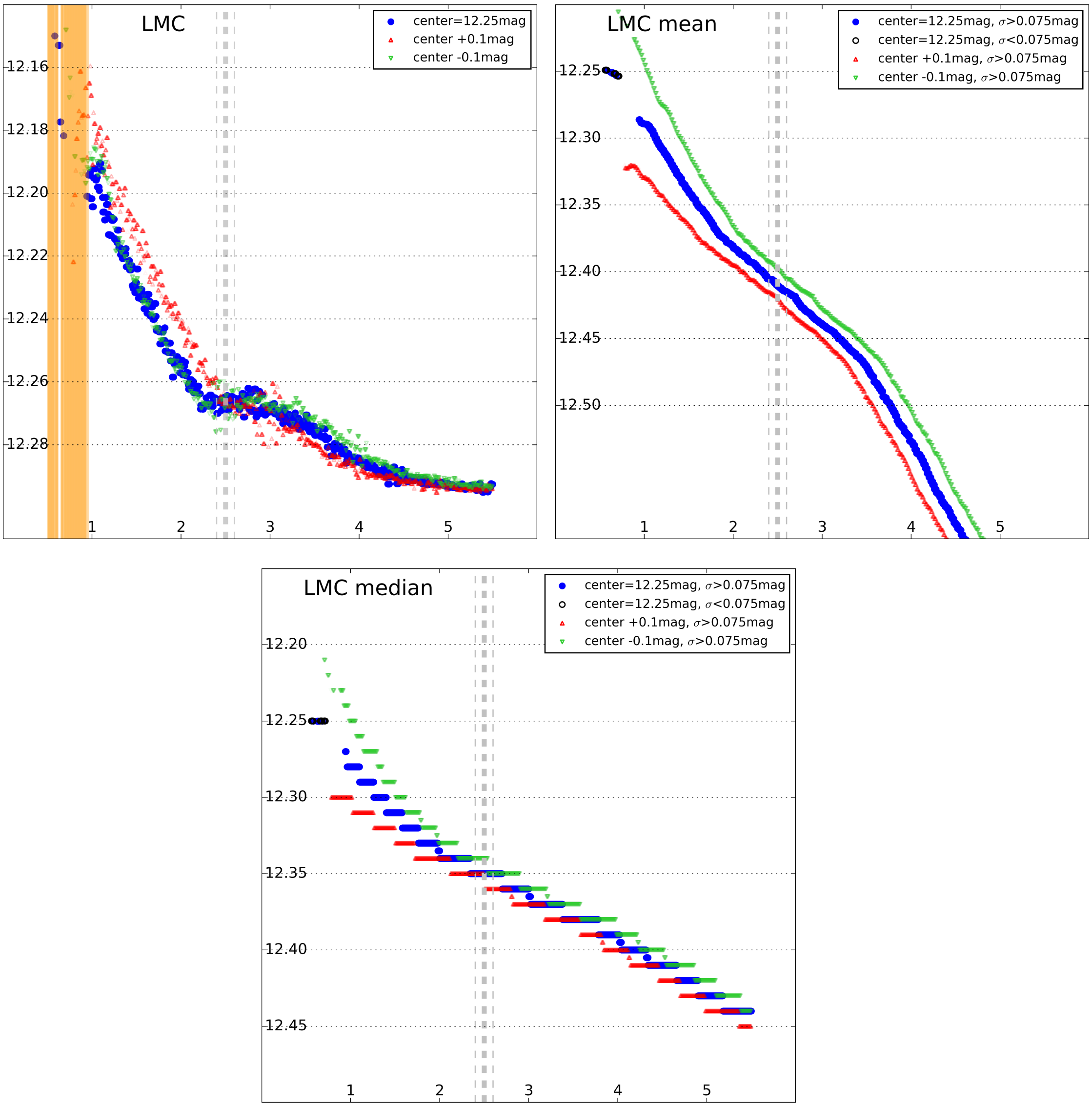

Figure 10: $< J_0 >$ values obtained for three different statistics and their dependence on the sample-selection box size and its center for the LMC. The y-axis and x-axis correspond to $< J_0 >$ (in mag) and the sample-selection box size (also in mag) along the J axis, respectively. The profile fit (upper-left) gives the most stable results that are also little dependent on the position of center of the box. As can be appreciated, the influence of arbitrary choices on our result is significantly weaker when we use the profile fit compared to the two simple statistics – median and arithmetic mean. The vertical dashed line corresponds to the 2.5 mag sample-selection box size, and the thinner surrounding lines correspond to box sizes that differ by ± 0.1 mag. Different colors of points depict results obtained using three different centers of the sample-selection box. Open, black circles denote results that had $\sigma < 0.075$ mag and were rejected. Similar figures (together with determination and diagnostic plots) for all studied galaxies are available at my web page: `https://users.camk.edu.pl/bzgirski/jagb.html`.

on centering of the sample-selection box. It is especially the central magnitude along the J axis that is difficult to choose and researcher may easily shift it by 0.1 mag arbitrarily. Such a shift of the sample-selection box may give results that differ by even 0.05 mag for boxes of the width of 1 mag along the J axis. It immediately introduces a potential distance error of about 2.5%. Thus, the profile fit allows us to minimize the influence of arbitrary choices on the final determination.

The fiducial $< J_0 >$ magnitude of carbon stars from the LMC that will serve for the purpose of the calibration of the method is 12.265 ± 0.010 mag, where the statistical uncertainty has been obtained from bootstrapping[11]. The distribution of simulated results is depicted on the left side of Figure 11, while the right side of that figure represents a breakdown of the fit into the two components and the residual distribution resulting from subtraction of the quadratic component of the fit from the original distribution of magnitudes of JAGB stars. While the residual distribution is not perfectly Gaussian, the least-squares fit gives the most reliable determination of the mean value of $J-$ band magnitude of carbon stars in the sample (which is also not identical to the mode of the distribution which may appear for a given argument due to random fluctuations).

Finally, we calibrate the mean absolute magnitude of JAGB stars by using the accurate LMC distance modulus $\mu_{\rm LMC} = 18.477 \pm 0.004({\rm stat.}) \pm 0.026({\rm syst.})$ mag of Pietrzyński et al. (2019): $\mathbf{M_{LMC} = -6.212 \pm 0.010(stat.) \pm 0.030(syst.)\ mag}$ – with the systematic component corresponding to the total uncertainty of the LMC distance. Ripoche et al. (2020) obtained $M_{R,LMC} = -6.284 \pm 0.004({\rm stat.})$ mag also using the same reddening maps and Madore & Freedman (2020) report $M_{M,LMC} = -6.22 \pm 0.01({\rm stat.}) \pm 0.04({\rm syst.})$ using only Galactic (i.e., foreground) reddening taken from Schlafly & Finkbeiner (2011). Such an approach gives, in principle, worse precision as it neglects differentiation between environmental conditions in different galaxies. Studied carbon stars are affected by intrinsic reddening of mean magnitude depending on their host galaxy. In my work, I have applied total reddenings for the studied galaxies obtained from the multi-band PL relations for classical Cepheids (or from the reddening maps for the Magellanic Clouds of Górski et al.). As thin disk objects, carbon stars should be affected by the same reddening as classical Cepheids. In order to compare my calibration with the absolute magnitude obtained by Madore & Freedman, we need to consider that their value of $A_{J,\rm LMC} = 0.053$ mag differs from the value of foreground + internal extinction presented in Table 1. The remaining 0.071 mag may be subtracted from the absolute magnitude they report to compare it with the value from my work.

Table 2 compares my results with the results of Madore & Freedman (2020) and Ripoche et al. (2020). The three studies are based on photometry from different sources. In the case of my work it is Kato et al. (2007), while Madore & Freedman (2020) relied on Macri et al. (2015), and Ripoche et al. (2020) took advantage of Skrutskie et al. (2006). The anchors used for the purpose of calibrations were the same in the case of the LMC (Pietrzyński et al., 2019). They were different for the SMC as I relied on Graczyk et al. (2020), Madore & Freedman used the Graczyk et al. (2014) distance (the previous version of the detached eclipsing binaries distance), and the Ripoche et al. calibration is based on the Scowcroft et al. (2016) determination (NIR Leavitt law utilized for individual Cepheids in the SMC).

I did not use the JAGB absolute magnitude calibration based on the SMC in further determinations. The studies by Ripoche et al. and Madore & Freedman yield similar absolute magnitudes in the case of the LMC (with the statistical error only in the case of Ripoche et al.). It is worth noticing that the LMC luminosity function of carbon stars is characterized by relatively large positive skewness (Figure 11) thus mean and median must be larger than the mean of the Gaussian component of my fit. This will not be a case for the SMC where the luminosity function is far more symmetric.

[11]Essentially, simulated samples were drawn from the original sample with replacements in number corresponding to the original sample size (for small samples, the number of draws was larger in order to have at least a few hundred simulated results). Then, profile fits were performed for each simulated sample, which resulted in obtaining distributions of possible $< J_0 >$ values.

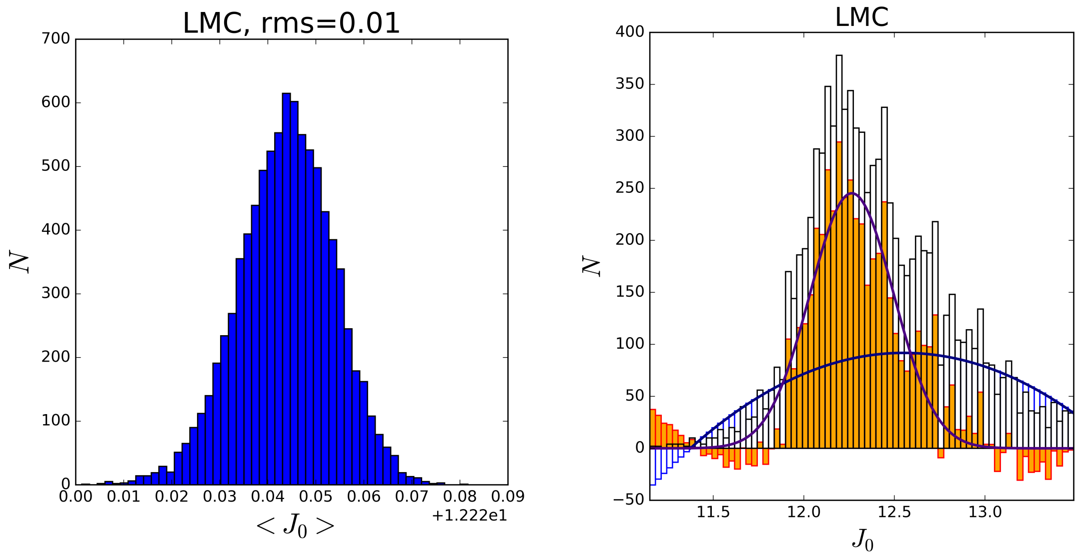

Figure 11: The distribution of simulated results obtained from bootstrapping used to determine the statistical uncertainty of $< J_0 >$ for the LMC (left), together with the two components of the fitted luminosity function and residuals (in orange) of the empirical luminosity function obtained from the subtraction of the quadratic component (blue) from the original distribution of luminosities (black bins).

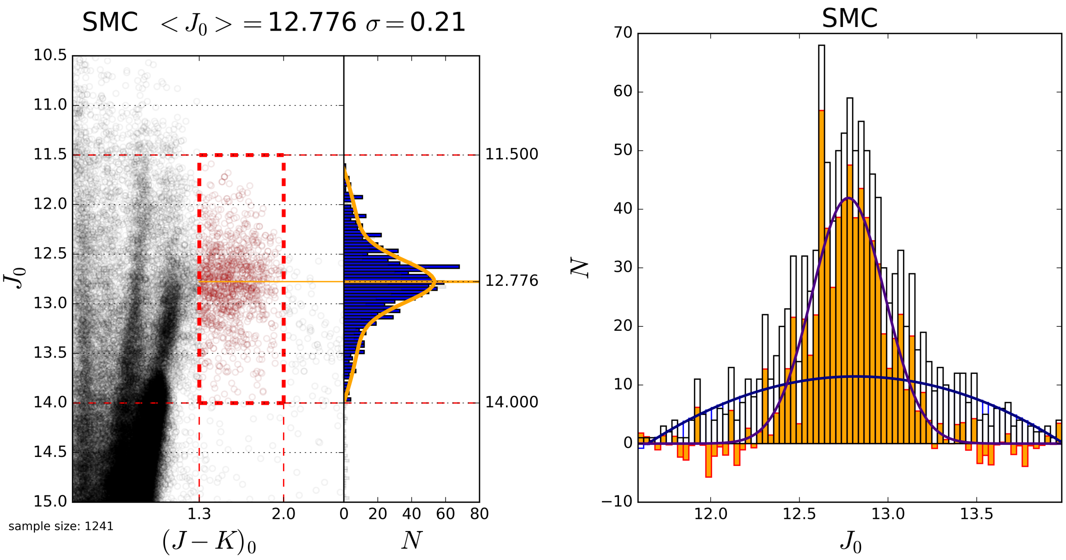

Figure 12: Determination of the mean value of the $J-$band magnitude of carbon stars from the SMC together with the split of the fitted profile into two components. Even though the luminosity function of carbon stars for the SMC is much more symmetric than for the LMC, the obtained mean values of $J-$band luminosities of carbon stars for the two clouds are in very good agreement given distances of the two Clouds.

work	$M_{\rm LMC}$ [mag]	$M_{\rm SMC}$ [mag]	statistic
Zgirski et al. (2021)	$-6.212 \pm 0.010 \pm 0.030$	$-6.202 \pm 0.012 \pm 0.044$	profile fit
Madore & Freedman (2020)	$-6.29 \pm 0.01 \pm 0.04$	$-6.23 \pm 0.01 \pm 0.05$	arith. mean
Ripoche et al. (2020)	-6.284 ± 0.004	-6.160 ± 0.015	median

Table 2: Different values of the absolute $J-$band magnitudes $M_{\rm LMC}$ and $M_{\rm SMC}$ for both Magellanic Clouds with the corresponding statistical and systematic errors. For the sake of comparison, I have additionally dereddened the values from Madore & Freedman as those took into account only the Galactic foreground extinction. For the LMC I applied 0.07 mag, for the SMC 0.05 mag – both values based on Górski et al. 2020. Ripoche et al. report only the statistical component of the error. All three studies use the 2MASS photometric system. Different centrality measures of luminosity functions of carbon stars correspond to various calibrations and definitions of the method and thus they yield absolute $J-$band magnitudes that are not directly comparable.

The first application of the new calibration was used for the SMC distance. It also plays a role in the verification of the reliability of the calibration. The source of the photometry and the dereddening procedure for the SMC were the same as in the case of the LMC. Figure 12 shows the profile fit to the luminosity function of carbon stars from the SMC. The mean value of the $J-$band magnitude of carbon stars from the SMC is $< J_0 >_{\rm SMC} = 12.776$ mag; bootstrapping yields the statistical uncertainty of its determination of 0.012 mag. Assuming the absolute magnitude of JAGB calibrated in the LMC, we obtain the SMC distance modulus $\mu = 18.988 \pm 0.012$(stat.) mag. This is in very good agreement with the recent determination of the SMC distance by Graczyk et al. (2020) using eclipsing binaries $\mu_{\rm SMC-DEB} = 18.977 \pm 0.044$ (total err.) mag, even within the statistical uncertainty of the JAGB determination. On the other hand, we may also obtain the calibration of the absolute magnitude of JAGB assuming the distance of Graczyk et al. (2020). It yields $M_{\rm SMC} = -6.201 \pm 0.012$(stat.)$\pm 0.044$(syst.) mag. Calibrations based on carbon stars from the two Magellanic Clouds give practically the same value of their mean $J-$band magnitude.

It is worth mentioning that while Madore & Freedman (2020) obtain the two quantities that are also in agreement with each other ($M_{\rm LMC} = -6.22 \pm 0.05$ mag, $M_{\rm SMC} = -6.18 \pm 0.06$ mag, total uncertainties), Ripoche et al. (2020) report different values of the absolute magnitude for the two Clouds ($M_{\rm LMC} = -6.284 \pm 0.004$ mag, $M_{\rm SMC} = -6.160 \pm 0.015$ mag, only statistical uncertainties). The authors speculate that the fainter SMC magnitude may be explained by lower metallicity. However, Freedman & Madore established the provisional metallicity-dependence of the JAGB absolute magnitude by comparing their JAGB distances with the corresponding TRGB distances for a sample of galaxies from the Milky Way's neighborhood and obtained -0.03 ± 0.05 mag dex^{-1}. Parada et al. (2020) who rely on the calibrations of Ripoche et al. (2020) go further and determine distances to galaxies based on either the SMC, or the LMC calibration, depending on the skewness of the observed luminosity functions. The authors claim that both star formation history and metallicity contribute to the skewness of the luminosity function, and thus they discriminate between 'SMC-like' and the 'LMC-like' luminosity functions. They use the appropriate calibration to determine distances to galaxies with the corresponding skewness of their luminosity functions. My approach is qualitatively different, as skewness of luminosity functions is modeled through the shifts between the axes of symmetry of the two (symmetric) components of the fitted profile. While the Gaussian component models the JAGB population, the quadratic component takes into account both contamination of the luminosity function and its skewness. Residuals of the luminosity function obtained by subtracting the quadratic component of the fitted profile reproduce the Gaussian profile worse in the case of the more skewed luminosity functions (compare splits into components in Figures 11 & 12). However, our task is to determine the mean value of the Gaussian component relatively well – not necessarily its entire course – and establish it as a standard candle. This task is fulfilled better with the profile fit than with statistics like mean or median that are vulnerable to asymmetries of luminosity functions.

The calibration, and the fiducial mean absolute magnitude of carbon stars in the $J-$ band may serve for the purpose of precision distance determinations to nearby galaxies.

3.3 Distance determinations for a sample of nearby galaxies

During the last two decades, the photometric J and K data were collected specifically for the purpose of distance determinations using multi-band PL relations for classical Cepheids as a part of the Araucaria Project. Distances to such galaxies as NGC 300, NGC 6822, NGC 3109, Wolf-Lundmark-Melotte (WLM), NGC 247, M 33, NGC 7793 were established (Gieren et al. 2005, Gieren et al. 2006, Soszyński et al. 2006, Gieren et al. 2008, Gieren et al. 2009, Gieren et al. 2013, Zgirski et al. 2017). Data were collected using the *PANIC* camera attached to the *Magellan-Baade* telescope at the *Las Campanas Observatory* (NGC 6822, WLM), the *HAWK-I* (NGC 7793, M 33) and *ISAAC* (NGC 3109, NGC 247, NGC 55, NGC 300) instruments installed on the *Very Large Telescope* at the *Cerro Paranal Observatory* of the *European Southern Observatory (ESO)*, and using the *SOFI* camera attached to the *New Technology Telescope* at the *La Silla Observatory* of *ESO* (NGC 6822, WLM).

The method based on the multi-band PL relations for Cepheids allowed not only for distance, but also for independent reddening determinations. These archival data are perfect for the purpose of the statistical analysis of carbon stars as they give a unique chance to compare the currently developed method with the well-established distance determination method based on the Leavitt law. Relying on the same photometry for the purpose of distance determination using the two methods guarantees the minimization of systematic errors that could influence differences between the results obtained with these methods.

All but one published Cepheid distances were anchored to the LMC distance of 18.5 mag. The distance corresponding to NGC 7793 has been anchored to $\mu_{\mathrm{LMC}} = 18.493$ mag (Pietrzyński et al. 2013, 2% accuracy). In order to properly compare the Cepheid distances with those resulting from the JAGB method (anchored to the LMC distance determined with the 1% accuracy – $\mu_{\mathrm{LMC}} = 18.477$ mag - Pietrzyński et al. 2019), I have systematically shifted the Cepheid distance moduli of the studied galaxies accordingly.

As the Araucaria Project NIR photometry of the nearby galaxies is calibrated onto the UKIRT photometric system, I have transformed it onto the 2MASS system to make it compatible with the calibration of the method that is also defined in 2MASS. Carpenter (2001) provided transformation equations between these two photometric systems.

Determinations of the mean values of JAGB $J-$band luminosity functions have been performed using the criteria described in the previous section. Larger samples allowed for a denser binning of J magnitudes of 3 bins per 0.1 mag. The particularly small samples have had their binning set at 1 bin per 0.1 mag (with one exception of the smallest samples of JAGB stars corresponding to the WLM galaxy, where I used 0.7 bins per 0.1 mag). Different binning introduces deviations between the final determinations at the level of a few thousandths of a magnitude, a value which is negligible compared to the statistical error of the determination that is an order of magnitude larger.

Optimally, the method is designed to trace a steady, Gaussian-like change of the 'clear' (i.e., deprived of the contamination that is modeled using the quadratic component) luminosity function of carbon stars. Very narrow, non-physical Gaussian components are not desired. It is especially the case when dealing with a quadratic-like luminosity function with a narrow peak. The profile fits to such functions may lead to unrealistic estimation of the σ parameter then. Such behavior is especially probable for small samples, similar to the one in WLM (the only representative of the discussed class of samples in this work). Determinations based on small samples may be particularly biased by a random fluctuation of the density of stars in the CMD that may produce narrow and prominent peaks in the luminosity function. The Gaussian component tends to pick up such a peak and leaves the residual luminosity function to be covered by the quadratic component. In such a case the determination is still useful (especially when we do not have any better way to deal with the problem) but the corresponding statistical

Galaxy ID	$< J_0 >_{\rm JAGB}$ [mag]	$\delta_{\rm JAGB}$ [mag]	sample size	$E(B-V)$ [mag]	Reddening source
LMC	12.265	0.010	8902	0.139	Górski et al. (2020)
SMC	12.776	0.012	1241	0.089	Górski et al. (2020)
NGC 6822	17.031	0.037	208, 233	0.356	Gieren et al. (2006)
M33	18.356	0.064	616	0.19	Gieren et al. (2013)
WLM	18.742	0.080	85, 99	0.082	Gieren et al. (2008)
NGC 3109	19.305	0.046	274	0.087	Soszyński et al. (2006)
NGC 55	20.145	0.019	1525, 1491	0.127	Gieren et al. (2008)
NGC 300	20.257	0.063	98, 73	0.096	Gieren et al. (2005)
NGC 247	21.194	0.023	1887	0.18	Gieren et al. (2009)
NGC 7793	21.489	0.027	1594	0.08	Zgirski et al. (2017)

Table 3: Summary of the mean values of the $J-$ band magnitude of the Region J Asymptotic Giant Branch (JAGB) stars for all analyzed galaxies. The table contains the mean unreddened magnitudes obtained with the profile fit, and their corresponding statistical uncertainties as obtained from bootstrapping - $< J_0 >_{\rm JAGB}$ and $\delta_{\rm JAGB}$, respectively (in mag). Sizes of samples of carbon stars are denoted in the next column (two values are present when two photometric epochs were available - a simple average of mean $< J_0 >$ was taken then). The table also includes $E(B-V)$ selective extinctions used to deredden the data for each galaxy taken from our previous papers that reported multi-band Cepheid distances. The dereddening for the Magellanic Clouds was done using the Górski et al. (2020) reddening maps based on the $E(B-V)$ grid values. Means of values corresponding to the used fields of Kato et al. (2007) IRSF photometric maps were used (with each photometric field dereddened separately).

uncertainty estimated using bootstrapping will be larger. The obtained σ is of no use in such a case, as it is artificially underestimated (see Figure 13).

Having a well and uniformly defined and calibrated method, determinations of distances for the sample of nearby galaxies are straightforward. All determinations and diagnostic plots for all studied galaxies are available at my web page: `https://users.camk.edu.pl/bzgirski/jagb.html`. I present plots for only a few exemplary cases in the thesis directly. Table 3 presents determinations of mean values of $J-$band magnitudes of carbon stars in a given population.

Statistical uncertainties (i.e., precision) of determinations were estimated using bootstrap simulations by creating distributions of possible $< J_0 >$ results and calculating their standard deviations. Table 3 and Figure 14 give an insight into how the precision of determinations depends on sizes of samples of carbon stars in a given population. One can easily see that for samples having sizes of the order of 10^3, we obtain the expected precision of distance determination of about 1% (~ 0.02 mag), while for samples having slightly less than 100 stars the average precision decreases to around 3% (~ 0.07 mag). As it can be appreciated, the vast majority of these distributions are of a Gaussian-like shape, with one exception of the M 33 galaxy (Figure 15). The distribution of possible values of the mean magnitude is apparently a superposition of the two normal distributions having different standard deviations and mean values here. This is related to the noisy luminosity function which Gaussian component is less distinct than the quadratic component. I have calculated the statistical uncertainty in the previously described way also in this case. Its value, $\delta_{\rm M33} = 0.064$, is much higher than it would arise from a simple interpolation of the sample size - (mostly Gaussian-like) uncertainty relation (Figure 14) where the uncertainty for a sample of the same size would be twice smaller.

The systematic error is, as usual, harder to trace. We may recognize some of its important components - the anchoring distance to the LMC of Pietrzyński et al. (2019) is given with the total uncertainty of 0.03 mag, the calibrating $< J_{0,\rm LMC} >$ determination has the precision of 0.01 mag, and zero points of photometry of the studied galaxies are established with uncertainty up to around 0.04 mag. In total, I estimate the systematic error of my JAGB distance determinations at the level of up to 0.05 mag.

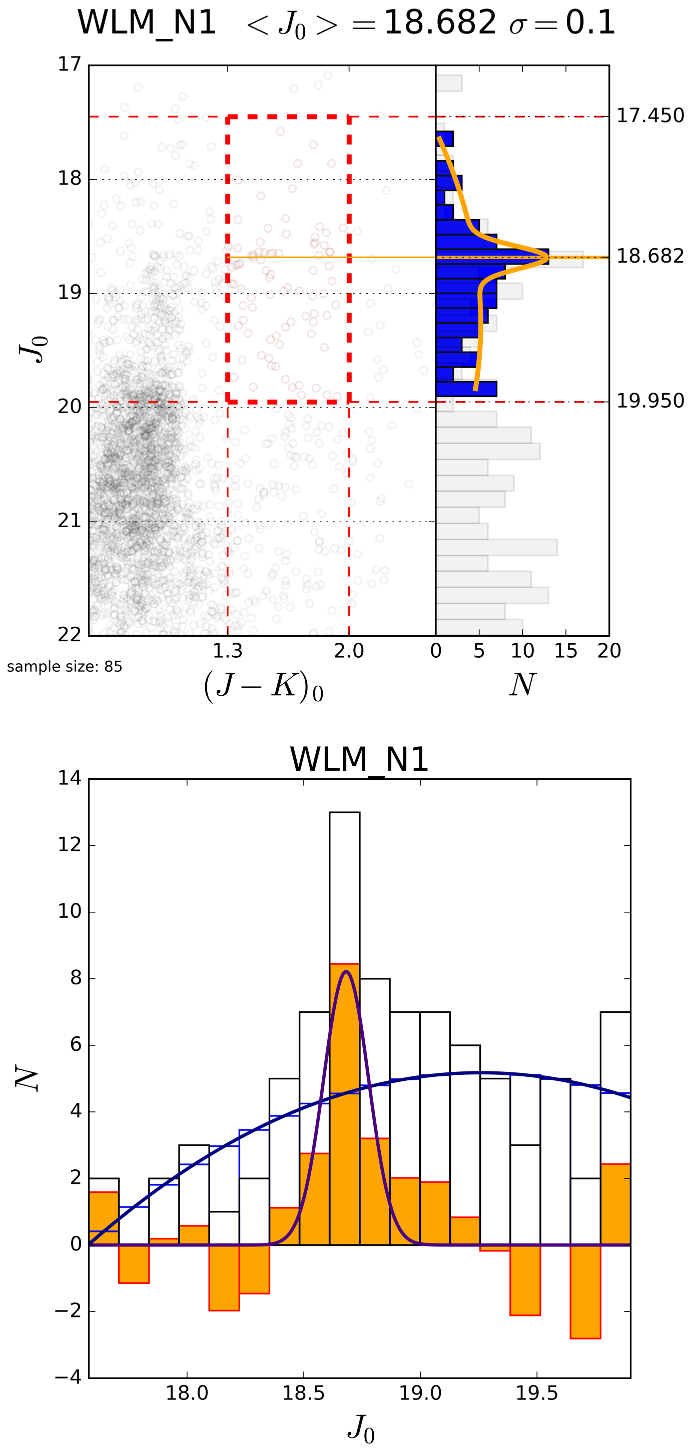

Figure 13: Determination of the mean value of the $J-$band magnitude of carbon stars from the WLM galaxy together with the luminosity function of its carbon stars separated into the two components. The narrow Gaussian component is due to the random fluctuation of the density of carbon stars in the CMD for this particularly small sample. The residual, 'clean' luminosity function obtained by subtracting the quadratic component from the empirical distribution is denoted in orange.

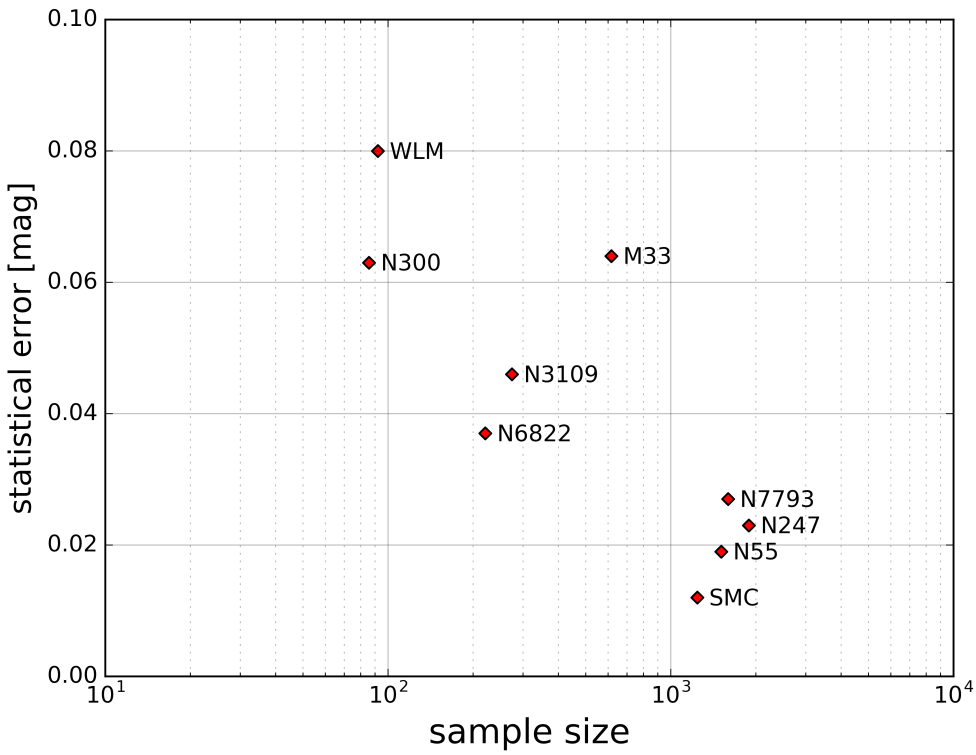

Figure 14: The precision of the JAGB method. Statistical error of $< J_0 >$ determination as a function of sample size for all studied galaxies except the calibrating LMC. Each uncertainty was calculated as rms of distribution of possible outcomes derived using bootstrap simulations. The horizontal axis is in the logarithmic scale. The M 33 sample is peculiar as its distribution of possible outcomes of $< J_0 >$ is not Gaussian, with two prominent peaks.

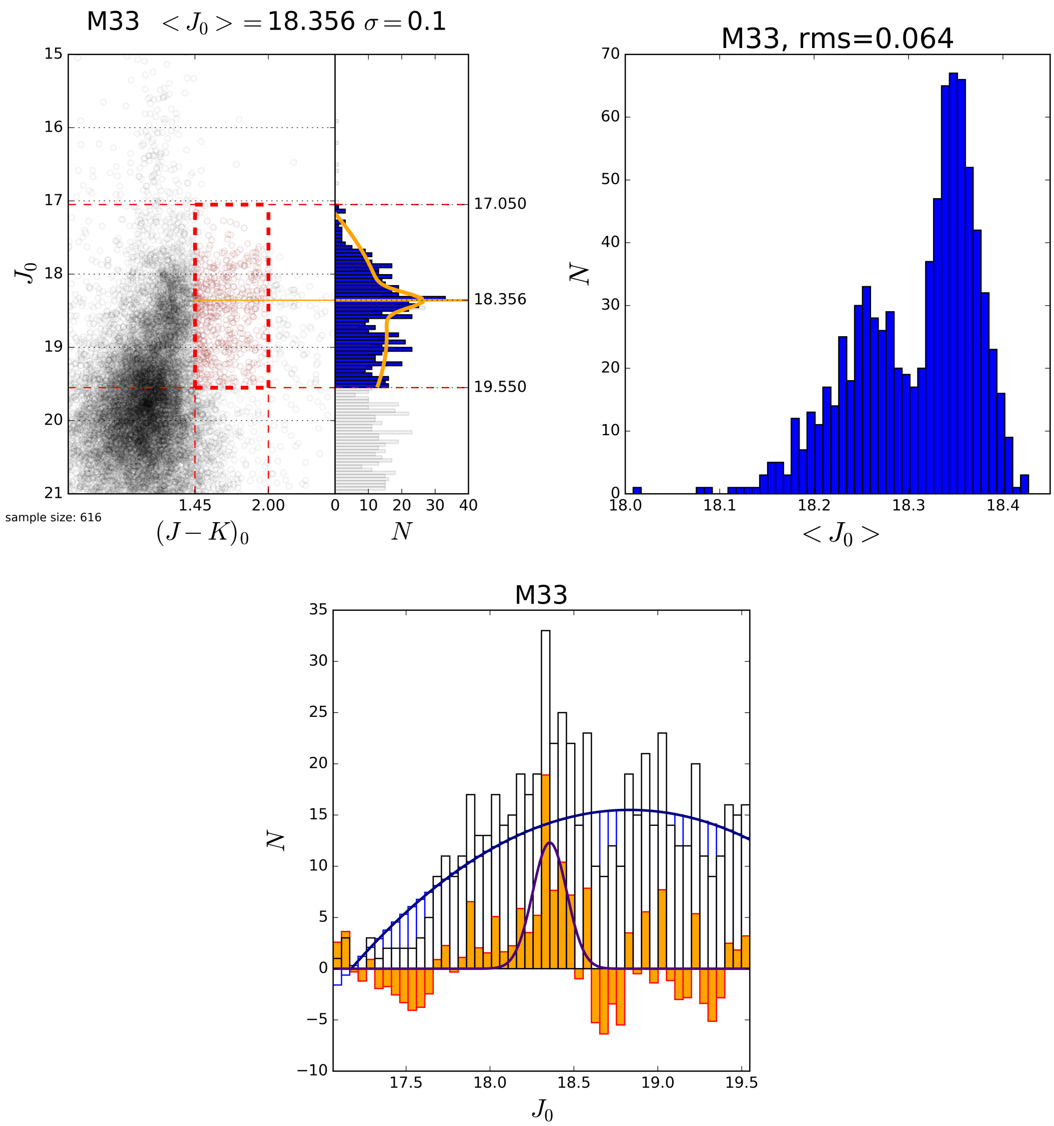

Figure 15: Determination of the mean value of the $J-$band magnitude of carbon stars from M 33 together with the distribution of possible results modeled using bootstrapping, and the luminosity function of its carbon stars split into the two components. The sample corresponding to M 33 is a peculiar and unique case among all studied samples because of its non-Gaussian, non-symmetric distribution of possible $< J_{0,\mathrm{M33}} >$. It is also characterized by a noisy luminosity function with an apparent local minimum, distinct faint continuum, and thus a relatively large quadratic component.

Galaxy ID	$\mu_{0,\mathrm{JAGB}}$ [mag]	$\mu_{0,\mathrm{CEP}}$ [mag]	$\mu_{0,\mathrm{EB}}$ [mag]	δ_{JAGB} [mag]	δ_{CEP} [mag]	δ_{EB} [mag]
SMC	18.988	(...)	18.977	0.012	(...)	0.016
NGC 6822	23.243	23.289	(...)	0.037	0.021	(...)
M33	24.568	24.60	(...)	0.064	0.03	(...)
WLM	24.954	24.901	(...)	0.08	0.042	(...)
NGC 3109	25.517	25.548	(...)	0.046	0.024	(...)
NGC 55	26.357	26.411	(...)	0.019	0.037	(...)
NGC 300	26.469	26.344	(...)	0.063	0.04	(...)
NGC 247	27.406	27.621	(...)	0.023	0.036	(...)
NGC 7793	27.701	27.65	(...)	0.027	0.04	(...)

Table 4: Summary of distance moduli obtained in this work, and their comparison to the corresponding Cepheid distances. Distance moduli resulting from JAGB determinations using the profile fit, determined using the Leavitt law for Cepheids, and their corresponding errors are denoted by $\mu_{0,\mathrm{JAGB}}$, $\mu_{0,\mathrm{CEP}}$, δ_{JAGB}, and δ_{CEP}, respectively (in mag). The table also includes the SMC distance $\mu_{\mathrm{EB}} \pm \delta_{\mathrm{EB}}$ from eclipsing binaries (Graczyk et al., 2020). All uncertainties are statistical. Table adapted from Zgirski et al. (2021).

The ultimate test of the method is a comparison of results it yields with those obtained using Cepheids. Table 4 and Figure 16 compare results obtained using the two methods. The agreement between them is excellent – apart from NGC 247 where the two determinations deviate by more than 0.2 mag. The difference can only be explained by an unrecognized systematic error. However, both determinations were performed using the same photometric data and they are anchored to the same LMC distance. The possible non-vanishing component of the systematic error may be associated with the unusual shape of the luminosity function of carbon stars from this galaxy. Indeed, a prominent faint wing is visible in the luminosity function (Figure 17). The distribution is similar to the one of M 33 and the quadratic component is particularly large because of that. A possible solution may include the assumption of a different profile (e.g., having an exponential instead of the quadratic component). My investigation in this direction has not lead to any definitive solution. Another possible source of error might be associated with crowding. However, after performing determinations for fields of the same galaxy with different source densities, I obtained results that are coherent, given the $J-$band magnitude zero point uncertainty (tests were performed for NGC 7793, NGC 55, and NGC 247). Also, Bresolin et al. (2005) showed that the influence of blending on the distance to NGC 300 using Cepheids should be smaller than 0.04 mag; Cepheids populate similar areas of this galaxy as carbon stars. The reason for the significant deviation between the two methods in the case of NGC 247 is thus unsolved.

Finally, we obtain the mean deviation and rms scatter between the two distance determination methods. After rejecting NGC 247, we obtain a mean difference of 0.01 mag with an rms scatter of 0.06 mag. If we keep the outlying galaxy, the mean deviation is -0.02 mag and the rms scatter increases to 0.09 mag - which still indicates an excellent general agreement between the two methods.

3.4 Summary, prospects and challenges for the future

The statistical method of distance determinations using NIR photometry of carbon stars is a very promising one. Being as bright in the $J-$band as classical Cepheids with periods of around 20 days, JAGB stars provide an excellent tool to determine distances to Supernova host galaxies at distances up to around 50 Mpc. Carbon stars allow checking calibrations of other methods from the cosmic distance ladder and tracing geometrical structures of nearby galaxies.

Just single-epoch photometry is needed for precision determinations of distances, with statistical uncertainties compared to those associated with determinations based on Cepheids. No

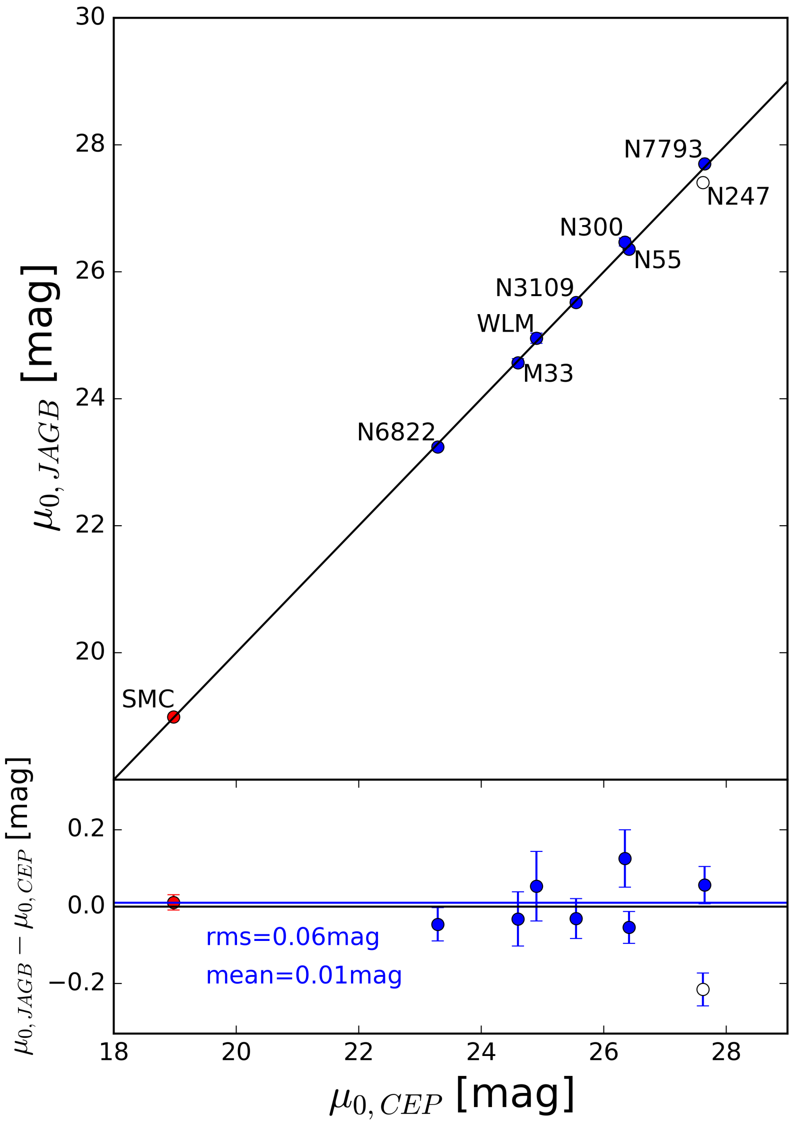

Figure 16: Comparison between distances obtained based on the JAGB and multi-band PL relations for Cepheids. The black line represents 1-1 relations. The lower panel presents differences between the Cepheid distances and the JAGB distances. The red dot corresponding to the SMC is an exception here as it depicts a difference between the JAGB distance and the distance of Graczyk et al. (2020) derived using detached eclipsing binaries.

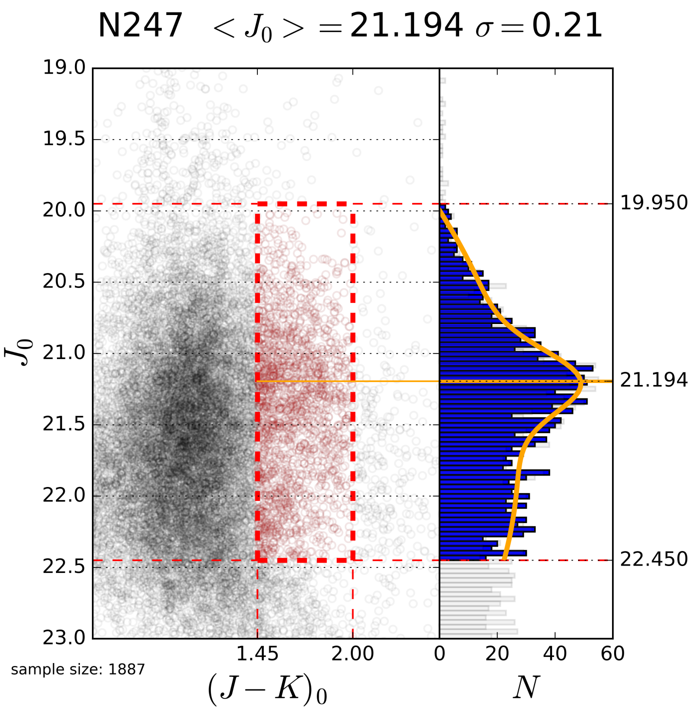

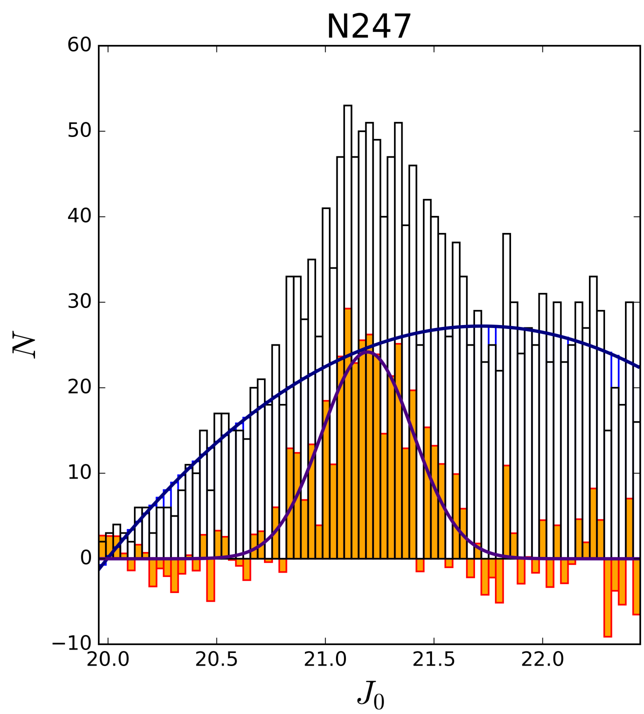

Figure 17: Determination of the mean value of the $J-$band magnitude of carbons stars from NGC 247. The luminosity function of carbon stars from NGC 247 with its two components and the residual distribution (in orange). The prominent contamination from the faint side of the peak is apparent.

period determinations[12] are needed as we are in fact dealing with color-luminosity relations (Weinberg & Nikolaev, 2001).

The calibration of the JAGB method gives very satisfying results that are in agreement with distances obtained using multi-band PL relations for classical Cepheids. Further research can only improve the method. Especially questions like the influence of metallicity or star formation history on absolute magnitudes of carbon stars should be answered. As it is now, the method also relies on external determinations of the reddening. Even though the $K-$band magnitude of carbon stars is no longer constant for different colors (see Figure 7), a smart generalization and extension of the method on the other bands (both NIR and optical) could allow for multi-band solutions, similar to those based on classical Cepheids (e.g., Zgirski et al. 2017), that serve both as distance and reddening determinants. Such a multi-band solution would be qualitatively more challenging for carbon stars.

The method proposed here works for JAGB samples of size large enough to model the course of the luminosity function using the profile fit (having the modeled uncertainty of the mean JAGB magnitude of about 0.07 mag for samples of ~ 100 in size). Statistics like arithmetic mean may be in principle calculated for samples having just a few stars (e.g., Freedman & Madore 2020). Even though in such a case the theoretical statistical uncertainty could take the form of $\delta = \sigma/\sqrt{N}$, which is of the same order as in the case of my method for samples 10 times larger[13]. However, this reasoning does not take into account possible errors committed through the selection of the sample itself. It neglects the non-uniformity of the sample-selection criterion (we should underline especially the value of the center of the sample-selection box that is even more important when the apparent peak of the luminosity function of carbon stars is vague). It also does not take into account errors associated with the contamination with background galaxies which is especially hard to subtract from samples of small sizes. It is even more applicable to samples that correspond to galaxies that lie at the edge of our (present and future) photometric ranges.

Ripoche et al. (2020) and Lee et al. (2021) also studied luminosity functions of carbon stars in our Galaxy using GAIA Data Release 2 (DR2) (Luri et al., 2018) and EDR3 (Bailer-Jones et al., 2021) parallaxes and resulting distances, respectively. While Ripoche et al. obtained $M_{J,MW} = -5.601 \pm 0.026(\text{stat.})$ mag, Lee et al. got $M_{J,MW} = -6.14 \pm 0.05(\text{stat.}) \pm 0.11(\text{syst.})$ mag. The determined σ scatters of the luminosity functions were determined to be of the order of $0.6 - 0.7$ mag. The discrepancy between the two results and the relatively large scatters of both luminosity functions have been attributed to the large parallax errors associated with particularly red and luminous carbon stars. Better Galactic calibrations of carbon stars will be available together with the publication of GAIA DR4 (Lee et al., 2021) that originally was meant to appear in 2022 but was recently postponed to a yet unknown date. Analysis of carbon stars from our Galaxy could be particularly important for the analysis of the luminosity-metallicity dependence for these stars.

The first, provisional, calibration of the method for the F110W filter of the Hubble Space Telescope (HST) was recently published by Madore et al. (2021). The authors calibrated the central[14] absolute magnitude of JAGB in the F110W filter based on archival data and confirmed a good agreement of the method with TRGB[15], estimating that both methods provide the precision of 3%. The calibration may be particularly useful as it allows utilization of the archival data collected using the F110W filter of the HST.

With the advent of the new generation of telescopes such as the *Extremely Large Telescope* and the *James Webb Space Telescope*, the method may reach distances of even $50-60$ Mpc, which would allow determining distances to Supernova host galaxies, and calibrate H_0 independently.

[12] In the case of carbon Miras, which constitute a part of the JAGB population, the standard approach would be to use their PL relations. However, periods of such stars are relatively long. Their determination requires uniform-coverage photometry taken throughout time intervals of more than 100 days.

[13] Taking the fiducial $\sigma = 0.2$ mag from the SMC, we obtain the statistical error $\delta = 0.02$ mag for a sample having 100 stars, and $\delta = 0.06$ mag for 10 stars using this kind of reasoning.

[14] Authors calibrated the absolute magnitude using modal value and determined distances based on arithmetic mean and median values of luminosity functions.

[15] The zero point of that calibration is tied to TRGB distances.

Therefore, carbon stars may help to settle one of the fundamental controversies of modern astronomy - the Hubble tension.

4 Determinations of distances using RR Lyrae stars

4.1 RR Lyrae stars as pulsating variables

RR Lyrae stars constitute one of the best studied variable stars (Bhardwaj, 2020). They were discovered by Wilhelmina Fleming in a Galactic globular cluster M 3 and reported in the work of Pickering (1889). Furthermore, the team of Edward Pickering found many stars of this type in different Galactic globular clusters in the 1890s. It was also Wilhelmina Fleming who discovered the variability of the prototype and the brightest star of the class – the star RR Lyrae in the Lyra constellation that has been apparently indistinguishable from the *cluster-type* variables (Pickering et al., 1901). Bailey (1902) divided these variables into three subclasses – a, b, and c – based on the shapes of their light curves, amplitudes, and periods.

Theoretical advances were achieved in parallel to the observational discoveries. At first, the variability of these stars was explained by eclipses in a binary system, even though their light curves were very different from that of Algol, which was already a confirmed spectroscopic binary in the early 20th century. Martin & Plummer (1915) proposed to explain the variability of the RR Lyrae type stars by pulsations after studying the changes of their radial velocities. Ritter (1879) showed that the pulsation period of an adiabatically-pulsating, homogeneous sphere is inversely proportional to the square root of its density (the *pulsation equation*):

$$P = \frac{Q}{\sqrt{\rho}} \tag{4}$$

where Q is called the *pulsation constant*, P and ρ are the pulsation period and the stellar density, respectively. However, it was Eddington (1918, 1919, 1926) who showed that the adiabatic radial pulsations are adequate to describe the behavior of real stars. The *period-luminosity-color* (PLC) relation results from the pulsation equation when we assume the stellar black-body radiation that yields the applicability of the Stefan-Boltzmann law[16]:

$$\log P + \frac{1}{2}\log g + \log T + 0.1(M_{bol} - M_{bol\odot}) = \log Q' \tag{5}$$

where g is the gravity at the stellar surface, T the effective temperature, M_{bol} the bolometric absolute magnitude, and $M_{bol\odot}$ the solar absolute bolometric magnitude. The stellar color, expressed as a color index, depends on the stellar temperature and gravity.

The model of a radially-pulsating star requires a mechanism that allows to sustain pulsations. The dissipation of energy of pulsations must be balanced by the energy released in the stellar interior and transported through the star by the radiative flux. We distinguish two pulsating mechanisms that are associated with opacity – the κ *mechanism* (dominating) and the γ *mechanism*. The radiative flux is inversely proportional to the opacity (κ). Usually, for the regular bound-free and free-free transitions, the opacity decreases with the rising temperature (Kramers' law, $\kappa \propto T^{-7/2}$): The contraction of a star results in a higher temperature, which yields larger radiative flux across the star that transports more energy from the stellar interior. In the expansion phase, the opposite will happen. Neither energy is accumulated in the contraction phase, nor it is released in the expansion phase. Pulsations cannot be sustained in such a situation. However, the temperature derivative of the opacity switches its sign (the κ mechanism) in stellar layers with the partial ionization of hydrogen or helium; $T \approx 10^4$ K – ionization of hydrogen (H II) and the first ionization of helium (He II), 5×10^4 K – the second ionization of helium (He III). It is associated with the fact that atoms on higher energy levels have smaller energetic distances between the subsequent levels and absorb more radiation. More energy is absorbed because of the ongoing ionization as well. The partially-ionized zone has a larger opacity than the neighboring non-ionized and fully-ionized zones. Gas in the partially-ionized

[16] Given that ρ is the mean stellar density, then $\log \rho = \log g - \log(GR)$ (G - the universal gravitational constant, R - stellar radius). According to the Stefan-Boltzmann law: $\log R = \frac{1}{2}\log L - \frac{1}{2}\log(4\pi\sigma) - 2\log T$ (σ - the Stefan-Boltzmann constant). Additionally, $-2.5\log L/L_\odot = M_{bol} - M_{bol,\odot}$ (L - stellar luminosity).

layer also has a lower value of the adiabatic index (γ) than in the two neighboring layers[17]. Thus, contraction of the star will result in a lower increase of temperature in the partially-ionized zone than in the two adjacent zones, and the opacity change will also be lower there (γ mechanism)[18]. The two mechanisms yield energy accumulation in the partially-ionized zone in the contraction phase and release of energy during the expansion phase. The occurrence of pulsations also depends on the location of the partial ionization layer. It can neither be located too deep (too small oscillation amplitude), nor too shallow (too diluted matter that will not accumulate a sufficient amount of energy) in the stellar interior. Colder M-type stars can pulsate, thanks to the partially-ionized hydrogen, Cepheids and RR Lyrae stars pulsate because of the layer of the partial second ionization of helium. In the case of hot stars, like β Cephei, the increase of opacity is caused by metals. Different stellar populations that pulsate due to the presence of the partial double ionization of the helium layer, occupy the *main instability strip* in the Hertzsprung-Russel diagram. RR Lyrae stars are located at the intersection of the strip with the *horizontal branch* (see Figure 18).

The instability strip provides an additional bound on the theoretical PLC relation.

According to the contemporary look at RR Lyrae stars (Catelan & Smith, 2015), they have masses of $(\sim 0.5-0.8)M_{\odot}$. They are old (with ages above 10 Gyr), metal-poor, helium-burning stars that inhabit the intersection of the horizontal branch and the main instability strip. They trace the Population II and are found in the bulge, halo, and thick disk of the Galaxy as well as in globular clusters. Their temperatures are between ~ 6000 K and ~ 7250 K and they pulsate with periods of $0.2-1$ day.

RR Lyrae stars are nowadays divided into the two main classes depending on the mode of their radial pulsations (Schwarzschild, 1940): RRab (RR0) – the fundamental-mode pulsators and RRc (RR1) – the first-overtone pulsators. While RRab stars exhibit 'saw-like' optical light curves with a very steep ascending branch and often a bump apparent near the minimum, the light curves of RRc are more sinusoidal with typically smaller amplitudes and shorter periods. Rare stars, having both modes excited simultaneously, are known as RRd (RR01). It is still debated whether stars pulsating in the second-overtone (RRe or RR2) really exist or whether they are rather first-overtone stars with very short periods (e.g., Kovács 1998, Catelan 2004b). On the other hand, stars with modes that may be associated with non-radial pulsations (Smolec, 2021) were also reported.

RRab and RRc stars follow different PL relations – the fundamental pulsators are fainter than the first-overtone pulsators for the same pulsation periods. The first-overtone pulsators have, on average, lower periods than RRab stars. Therefore, an important task in the analysis of PL relations of RR Lyrae stars is to properly *fundamentalize* periods of the first-overtone pulsators in order to form uniform relations for *mixed populations* (i.e., including both RRab and RRc stars) that cover the broadest possible span of periods, which would give smaller uncertainties of relation parameters. The widely (e.g., Szewczyk et al. 2008, Karczmarek et al. 2015, Karczmarek et al. 2017b, Muraveva et al. 2018, Cusano et al. 2021) accepted canonical procedure used for the fundamentalization of periods of RRc stars (P_{1O}) is to multiply them by $10^{0.127}$ (Iben 1974, it yields the adopted, fixed ratio of periods of RRc and RRab stars: $\frac{P_{1O}}{P_F} \approx 0.7464$). The ratio $\frac{P_{1O}}{P_F}$ of periods is shown using the *Petersen diagrams* (Petersen, 1973) for RRd stars where it is plotted against the fundamental period P_F (see Figure 19). Not only the ratio is different for each star but also the typical, average value for any two given populations may differ due to environmental effects such as metallicity (Smolec, 2021). Additionally, groups of RRc and RRd stars with peculiar periods ratios were reported (e.g., Netzel & Smolec 2019).

[17] The partially-ionized zone is effectively in a state of the phase transition where more energy is needed to increase its temperature by 1 K because part of the energy is absorbed by ionization. The adiabatic index, also known as the heat capacity ratio, depends on specific heat capacities: $\gamma = \frac{c_p}{c_v} = 1 + \frac{R}{c_v}$ (Mayer's law) where c_p, c_v are the molar specific heat capacities in constant pressure and volume, respectively, and R is the universal gas constant.

[18] While the γ mechanism absolutely requires a zone of partial ionization, the κ mechanism works in any case where the sign of the temperature derivative of opacity changes its sign.

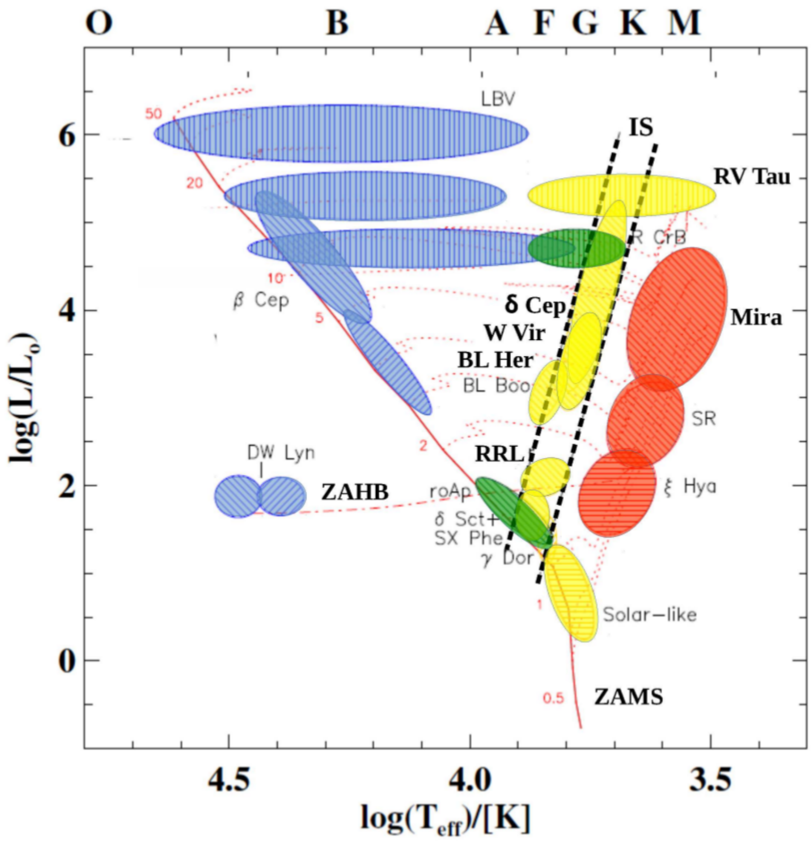

Figure 18: The Hertzsprung-Russel diagram depicting the location of RR Lyrae stars ('RRL') among other populations of pulsating stars. They inhabit the intersection of the instability strip ('IS') and the horizontal branch. The zero-age horizontal branch is denoted with 'ZAHB'. Figure taken from Bhardwaj (2020) (`https://arxiv.org/abs/2006.16262`).

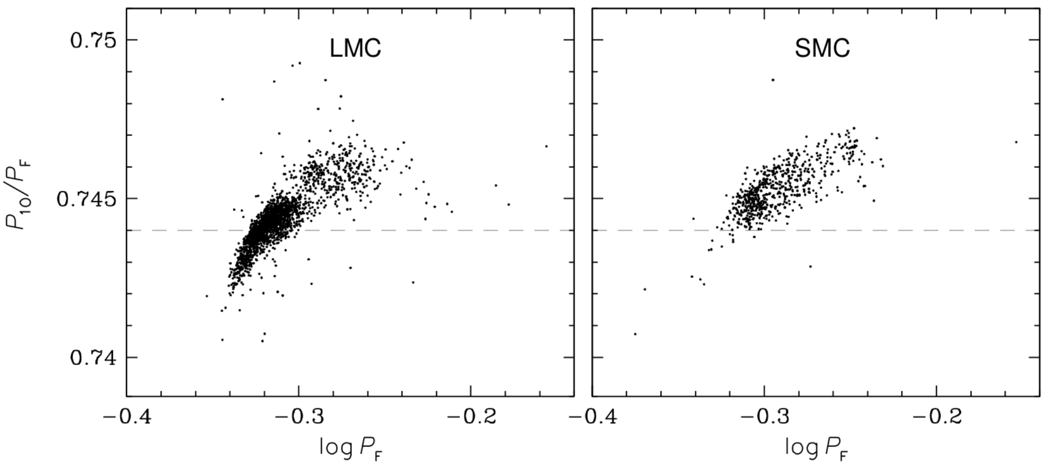

Figure 19: The Petersen diagram for RRd stars from the LMC and the SMC. The typical ratio of first-overtone to fundamental period is slightly different for the two clouds. Image adapted from Soszyński et al. (2016) (`https://arxiv.org/abs/1606.02727`).

Some RR Lyrae variables also experience amplitude modulations with periods longer than those corresponding to the regular pulsation cycle (Blažko, 1907). This so-called *Blazhko effect* has been puzzling for more than a century now. Some observational aspects of the effect may be explained by interactions of the fundamental mode and the 9$^{\text{th}}$ overtone of radial pulsations together with non-radial modes (e.g., Kolláth, Z. 2021). However, the complete explanation of the effect is still missing.

RR Lyrae stars have played a fundamental role in distance determinations since the study of Shapley (1918), who used them to determine distances to a number of globular clusters This contributed to the estimation of the size of the Galaxy and allowed to determine the location of the sun within the Milky Way. The mean V magnitudes of RR Lyrae stars do not depend on their periods. Until the mid-20$^{\text{th}}$ century, it was believed that they did also not depend on metallicity. Oosterhoff (1939) divided the Galactic globular clusters into two types (*Oosterhoff types*) depending on the mean pulsation period of their RR Lyrae stars. Metallicities of clusters started to become available in the 1950s, and soon after that, it turned out that the two Oosterhoff types also correspond to different metallicity groups. Namely, clusters having RR Lyrae stars with longer average periods are more metal-poor (Oosterhoff-II type). Sandage(1958, 1981) showed that stars from this group are more luminous than those from the other one. According to the pulsation equation (4), given constant effective temperature and mass, stars having longer periods, have lower density and thus larger size, which translates into their larger luminosities. Sandage (1990) elaborated these considerations into a linear relationship between the mean $V-$band magnitude of RR Lyrae stars in a given population and its metallicity [Fe/H].

Modern distance determinations using RR Lyrae variables are based on two methods. One of them relies on PL relations that, optionally, may include a dependence on metallicity. This method is used to determine distances to samples of RR Lyrae stars (i.e., systems containing RR Lyrae stars), given the relatively large intrinsic spread of relations. The second, geometrical method of determinations of distances to single pulsating stars, named the Baade-Wesselink method, is based on their radial velocity curves and changes of their angular diameters derived from interferometry or photometry.

I present my calibration of both methods for Galactic RR Lyrae stars based on photometric data from OCA, radial velocities obtained using ESO spectrographs, and GAIA DR3 parallaxes. All NIR magnitudes are calibrated in the 2MASS system unless explicitly stated otherwise.

4.2 Near-infrared period-luminosity(-metallicity) relations for RR Lyrae stars

Longmore et al. (1986) were the first to derive a PL relation for RR Lyrae stars in the $K-$band. The relation follows from bolometric corrections in the NIR, which increase with color. The spread of PL relations in the NIR domain is smaller than for the optical bands. Additionally, amplitudes of RR Lyrae stars are smaller in the NIR. In principle, it allows to estimate their mean magnitudes based on just a few photometric epochs. Influence of extinction is also much lower in the NIR domain. The PLZ relations in the NIR were identified as an excellent tool for distance determinations to systems containing the old stellar population. Their calibration has already been studied by various groups, both theoretical (e.g., Bono et al. 2001, Bono et al. 2003, Catelan et al. 2004c, Marconi et al. 2015) and empirical (e.g., Sollima et al. 2008, Muraveva et al. 2015, Muraveva et al. 2018, Neeley et al. 2019, Cusano et al. 2021).

Even though RR Lyrae stars are much fainter than classical Cepheids, they are excellent standard candles to determine distances to nearby galaxies. In particular, they have been utilized for this purpose by the Araucaria Project as well. Distances to the LMC (Szewczyk et al., 2008), the SMC (Szewczyk et al., 2009), Carina (Karczmarek et al., 2015), and Fornax (Karczmarek et al., 2017b) galaxies were determined using NIR PL relations with additional metallicity corrections, based on some of the calibrations cited above.

In my thesis, I present a new calibration of the JHK PL and PLZ relations for RR Lyrae stars based on the photometry from the IRIS instrument (gathered specifically for this purpose), GAIA EDR3 parallaxes (Gaia Collaboration et al., 2021), and the recent metallicity determinations of the Galactic RR Lyrae stars by Crestani et al. (2021) based on high-resolution spectra. Furthermore, I present new distance determinations to a few nearby galaxies based on the photometric data from the literature and on my calibration.

4.2.1 Calibration of relations for the Galactic RR Lyrae stars

The NIR photometry from my thesis for 28 RR Lyrae at distances up to 1.5 kpc allowed to establish well-covered light curves. Using periods found in the literature (*The International Variable Star Index*, `https://www.aavso.org/vsx/`), I have determined mean magnitudes of these stars fitting (the *curve_fit* procedure of Virtanen et al. 2020) the Fourier series to the phased photometry transformed into flux from magnitudes:

$$F_{\lambda}(\phi) = a_0 + \sum_{i=1}^{N} \left[a_i \sin(2\pi\phi) + b_i \cos(2\pi\phi)\right] \quad (6)$$

where F is the modeled stellar flux in a given band λ for a given phase ϕ, and a_0 is the desired mean flux (offset of the series). Then, the mean magnitude is obtained immediately from the mean flux. The selection of the upper limit N of the sum does not influence the determination of the mean magnitude for N =2, 3, and 4 (typical differences are of the order of few thousandths of a magnitude for different N). I adopted $N = 2$. If there were 5 or less photometric epochs available, I used simple mean of fluxes instead of the Fourier series fit. Figure 20 depicts exemplary light curves together with the determined mean magnitudes.

Statistical errors of mean magnitudes were calculated as the mean uncertainty of magnitude for all epochs divided by the square root of the number of epochs for a given object. For two stars (HY Com & SS Leo) only single comparison stars were used to standardize the photometry. Errors of mean magnitudes were adopted as 0.01 mag in these two cases.

The interstellar reddening was estimated as in Suchomska et al. (2015), i.e., by integrating the reddening and assuming the three-dimensional model of the Milky Way by Drimmel & Spergel (2001), and total galactic reddening in a given direction from Schlafly & Finkbeiner (2011). Table 5 includes all derived mean magnitudes and reddening values. Extinctions corresponding to the three NIR bands were calculated from $E(B-V)$ assuming ratios of total-to-selective extinctions from Cardelli et al. (1989) (as in Table 1, with the additional value $\frac{A_H}{A_V} = 0.180$) and adopting $R_V = 3.1$.

ID	type	$<J>$ [mag]	$<H>$ [mag]	$<K>$ [mag]	P [days]	$E(B-V)$ [mag]
AE Boo	RRc	9.934 ± 0.005	9.759 ± 0.005	9.729 ± 0.005	0.31489	0.023
AN Ser	RRab	10.061 ± 0.005	9.877 ± 0.005	9.786 ± 0.005	0.52207	0.036
BB Eri	RRab	10.543 ± 0.005	10.298 ± 0.005	10.221 ± 0.005	0.56991	0.043
DX Del	RRab	8.901 ± 0.012	8.696 ± 0.013	8.648 ± 0.019	0.47262	0.079
EV Psc	RRc	9.854 ± 0.005	9.662 ± 0.005	9.630 ± 0.005	0.30626	0.030
FW Lup	RRab	7.994 ± 0.005	-	7.718 ± 0.005	0.48417	0.062
HY Com	RRc	9.692 ± 0.010	9.563 ± 0.010	9.426 ± 0.010	0.44859	0.024
IK Hya	RRab	9.088 ± 0.008	8.851 ± 0.005	8.781 ± 0.005	0.65032	0.055
MT Tel	RRc	8.321 ± 0.005	8.148 ± 0.005	8.111 ± 0.005	0.31690	0.034
RR Leo	RRab	10.081 ± 0.008	9.795 ± 0.007	9.768 ± 0.010	0.45240	0.035
RU Psc	RRc	9.347 ± 0.020	9.112 ± 0.020	9.109 ± 0.024	0.39038	0.039
RV Cet	RRab	9.975 ± 0.006	9.774 ± 0.007	9.672 ± 0.005	0.62341	0.027
RX Eri	RRab	8.702 ± 0.005	8.452 ± 0.005	8.358 ± 0.005	0.58725	0.053
RY Col	RRab	10.193 ± 0.025	9.987 ± 0.015	9.913 ± 0.020	0.47884	0.025
SS Leo	RRab	10.212 ± 0.010	9.967 ± 0.010	9.924 ± 0.010	0.62634	0.017
SV Eri	RRab	8.824 ± 0.005	8.630 ± 0.005	8.552 ± 0.005	0.71388	0.078
SX For	RRab	10.163 ± 0.005	9.965 ± 0.005	9.856 ± 0.005	0.60534	0.012
T Sex	RRc	9.347 ± 0.005	9.201 ± 0.005	9.149 ± 0.005	0.32470	0.042
U Lep	RRab	9.725 ± 0.005	9.556 ± 0.005	9.493 ± 0.005	0.58148	0.029
UU Vir	RRab	9.880 ± 0.010	9.562 ± 0.005	9.528 ± 0.005	0.47561	0.016
V467 Cen	RRab	9.522 ± 0.005	9.394 ± 0.005	9.251 ± 0.005	0.55140	0.050
V675 Sgr	RRab	9.281 ± 0.005	9.034 ± 0.005	8.989 ± 0.005	0.64229	0.089
V753 Cen	RRc	9.769 ± 0.005	9.664 ± 0.005	9.608 ± 0.005	0.22135	0.147
V Ind	RRab	9.114 ± 0.005	8.928 ± 0.005	8.875 ± 0.005	0.47960	0.04
WY Ant	RRab	9.835 ± 0.005	9.710 ± 0.005	9.653 ± 0.005	0.57434	0.055
WZ Hya	RRab	9.920 ± 0.005	9.695 ± 0.005	9.630 ± 0.005	0.53772	0.069
X Ari	RRab	8.267 ± 0.005	8.052 ± 0.005	7.903 ± 0.005	0.65118	0.158
XZ Gru	RRab	9.713 ± 0.005	9.440 ± 0.005	9.369 ± 0.005	0.88310	0.010
median					0.52990	0.040

Table 5: Apparent (reddened) mean magnitudes of RR Lyrae stars observed with IRIS in JHK together with their pulsation periods (from AAVSO VSX). Extinctions were estimated using the Milky Way model by Drimmel & Spergel (2001) and the extinction maps from Schlafly & Finkbeiner (2011). Statistical uncertainties are calculated as standard errors of the mean from mean statistical uncertainties of single photometric measurements for a given star. Errors smaller than 0.005 mag were rejected, and this value was fixed instead due to the uncertainty associated with the choice of Fourier series' order. The contribution of the photometric errors to the final uncertainties of the derived parameters of PL and PLZ relations is much smaller than the components related to uncertainties of stellar parallaxes.

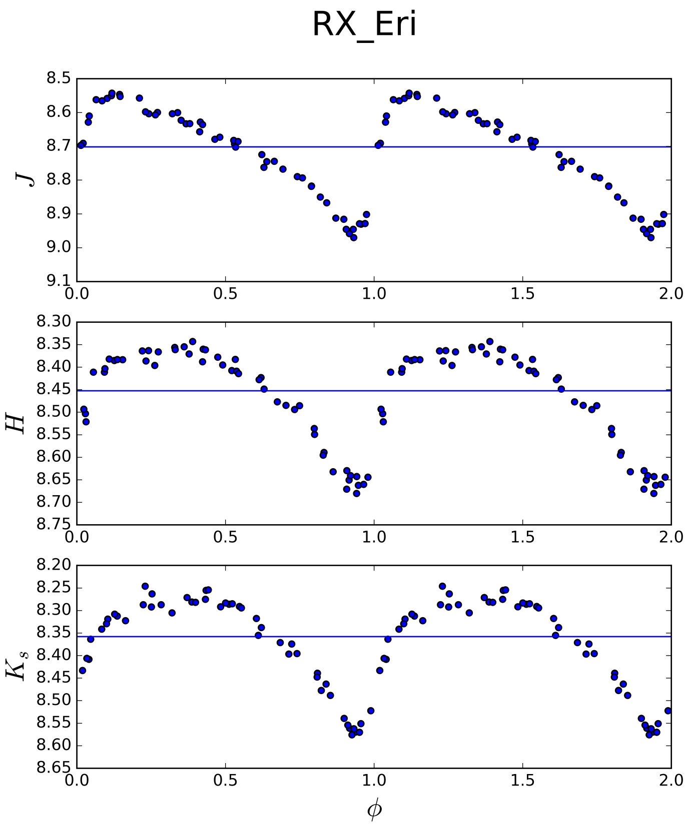

Figure 20: Light curves of RX Eri in JHK obtained from IRIS together with the mean magnitudes determined using the Fourier series fits.

Absolute magnitudes of RR Lyrae stars from my sample were derived from the apparent magnitudes using four different approaches:

- parallaxes are inserted directly into the definition of the distance modulus, yielding the absolute magnitude $M = m + 5 \log \varpi + 5$ (M is the absolute and m the apparent magnitude, ϖ is the parallax in arcsec; a linear least-squares PL fit is applied)
- using distances of Bailer-Jones et al. (2021) derived from GAIA parallaxes using direction-dependent priors on distance (geometric distances), $M = m - 5 \log r + 5$ (r - distance in pc; a linear least-squares PL fit)
- as above, but using distance priors dependent on direction, colors, and apparent magnitudes of stars (photo-geometric distances)
- using the *Astrometry-Based Luminosity* (Arenou & Luri, 1999), a quantity that is directly proportional to the parallax (a non-linear least-squares fit)

Linear least-squares fits were performed using *linregress* and non-linear least-squares fits using the *curve_fit* functions of SciPy (Virtanen et al., 2020). I used parallaxes from GAIA EDR3 (Gaia Collaboration et al., 2021) after applying corrections of Lindegren et al. (2021). Bailer-Jones et al. (2021) already took into account these corrections. Parallaxes with the renormalized unit weight error for astrometry $ruwe > 1.4$ and the level of asymmetry of a source in the GAIA image $ipd\_gof\_harmonic\_amplitude > 0.1$ in order to avoid resolved binaries

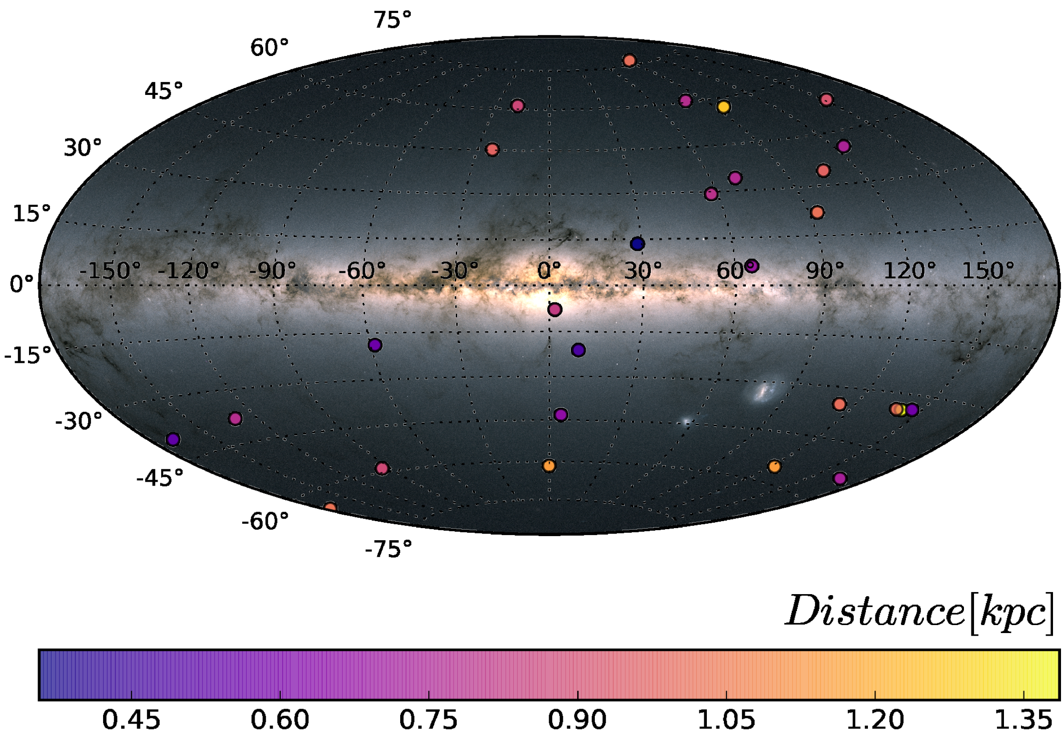

Figure 21: Location of 28 RR Lyrae stars in the Galactic coordinate system used to establish PLZ relations; their distances from GAIA EDR3 are indicated by colors. Due to the location of IRIS near the Tropic of Capricorn there is an inhomogeneity in the distribution of sources on the largest scale. Background image *'The colour of the sky from Gaia's Early Data Release 3'*: `https://www.esa.int/ESA_Multimedia/Images/2020/12/The_colour_of_the_sky_from_Gaia_s_Early_Data_Release_3`.

(Fabricius et al., 2021). No star was rejected after applying this criterion.

In cases of linear fits, I simply fit a PL relation:

$$M_\lambda(P) = a(\log P - \log P_0) + b \tag{7}$$

where λ denotes dependence on the photometric band, P is period in days, P_0 is the pivot period value chosen to minimize uncertainties of the fitted b (the intersection) and also minimize the correlation between the intersection b and the slope a. I have selected $\log P_0 = -0.25$, which is close to the median for the whole studied sample of RR Lyrae.

We assume a Gaussian distributions of parallax errors. Instead of fitting a relation between the absolute magnitude derived from parallaxes and periods, we may use a quantity that is directly proportional to the parallax - the *Astrometry-Based Luminosity* (ABL, Arenou & Luri 1999):

$$a_\lambda := 10^{0.2M_\lambda} = \varpi 10^{\frac{m_\lambda+5}{5}} \tag{8}$$

Such an approach, recently applied by Breuval et al. (2021) for PL relations for classical Cepheids derived from GAIA EDR3 parallaxes, has the advantage of minimizing the Lutz-Kelker bias. Its uncertainty, dominated by the parallax component, is practically symmetric. The ABL is an *asymptotically unbiased estimator* as the higher number of stars used for the fit allows obtaining better precision of the mean values derived using it. Assuming the linear relation between the absolute magnitude and logarithm of the pulsation period, I fit the relation:

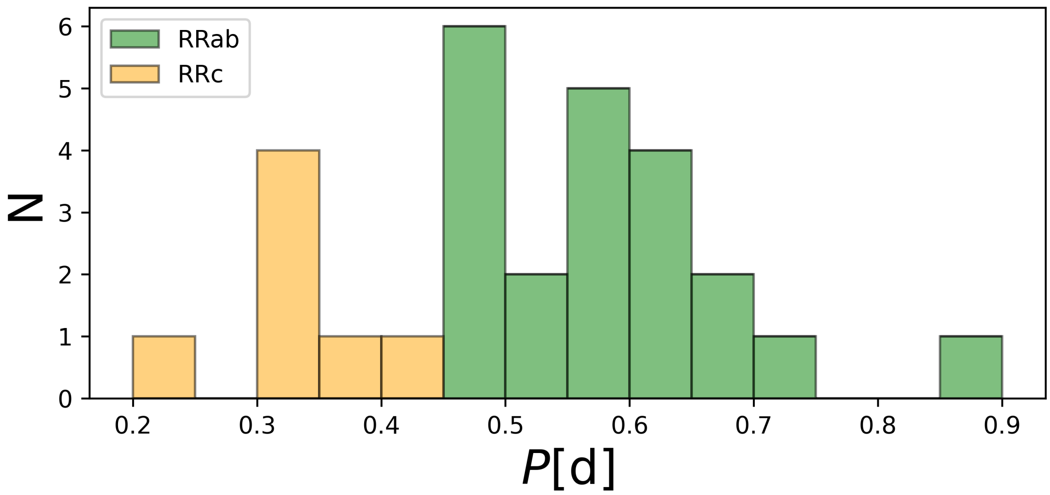

Figure 22: The distribution of pulsation periods of all stars from my sample. P is in days.

$$a_\lambda(P) = 10^{0.2[a(\log P - \log P_0)+b]} \tag{9}$$

Table 6 includes slopes and intersections of PL relations established using the four methods. JHK relations were obtained using dereddened photometry and W_{JK} relations using original apparent magnitudes that were not dereddened. While results obtained from linear fits give practically the same results, the ABL usually yields expected values of parameters that deviate from them slightly (but not significantly in the statistical sense, given the uncertainties of fits). Figures 23 and 24 show PL relations fitted using photo-geometric distances of Bailer-Jones et al. (linear fit) and the ABL (exponential fit), respectively. 28 stars were used to establish PL relations in the J,$K-$bands and in the W_{JK} Wesenheit index[19]. In the case of the $H-$band, 27 stars were used (without FW Lup whose IRIS H photometry is not available due to its too large brightness and the fact that the IRIS camera is most sensitive in this band). Fits are divided into three subsamples of the Galactic RR Lyrae stars: RRab and RRc (with fundamentalized periods) type stars, and a sample corresponding to the mixed population (RRab+RRc). Periods of RRc stars were fundamentalized so that logarithms of their periods were shifted by +0.127 following Iben (1974). All approaches give results that are in very good agreement with each other. The studied stars lie at distances up to 1.5 kpc and their GAIA parallaxes are sufficiently precise so that the simplest approach gives results that agree with those obtained from more sophisticated procedures.

One can easily see (Figures 23 and 24) that RRab and RRc samples follow slightly different PL relations. While in the case of the $J-$band it can be argued that these relations have even a different slope, all RRc relations are shifted towards brighter magnitudes (or lower periods) compared to RRab relations. This can be associated with the adopted non-optimal period fundamentalization shift value. Therefore, one should be careful when using fiducial PL relations for the mixed population. It is also visible through the rms scatter of residuals of the fits for a mixed population compared to those derived separately for each of the populations (written in Figures 23 and 24). On the other hand, the fit based on the mixed population provides lower uncertainties of the derived parameters (Table 6) because of the larger span of periods used in the fit. This will be also the case for relations that include metallicity.

[19]The Wesenheit index, originally introduced by Madore (1982) for optical bands, is a linear combination of a magnitude and color that is reddening-free. In this case: $W_{JK} = K - 0.69(J - K)$. The vector [0.69, 1] is parallel to the reddening vector $[E(J-K), A_K]$ in the K vs. $(J-K)$ CMD. Thus, the extinction in K is compensated by the subtraction of reddening for $(J-K)$ color that is multiplied by the ratio of total-to-selective extinction $A_K/E(J-K)$.

Although two points corresponding to the RRab stars UU Vir and XZ Gru are outliers in the PL relation for the $J-$band, there is no reason to reject them. UU Vir has a large parallax error, and XZ Gru has the longest pulsation period among all studied stars. Their deviation from the fitted relation is smaller at longer wavelengths and, especially, in the reddening-free W_{JK} Wesenheit index, which suggests that their reddening may be underestimated. The formal $E(B-V)$ errors given in Schlafly & Finkbeiner (2011) (recalibration of Schlegel et al. 1998) are only 0.0004 mag for UU Vir and 0.0006 mag for XZ Gru.

The uncertainties of the fitted parameters are the errors of the slope and the intersection of the linear least-squares fits. In the case of the non-linear fit, they are estimated using the Levenberg-Marquardt algorithm (Virtanen et al., 2020). Error bars corresponding to points in Figures 23 and 24 are associated with parallax and statistical photometric errors only (where the parallax error is the dominating component). The uncertainties of reddening (uncertainties reported in the literature are usually underestimated) are not included in the error budget. The influence of extinction is minimized in the NIR domain (mean extinction values for stars from my sample are 0.046 mag, 0.029 mag, and 0.019 mag for J, H, and K, respectively). I traced the propagation of quantified uncertainties and their influence on the uncertainties of the fitted parameters using Monte Carlo simulations. Figure 25 depicts the propagation and the influence of photometric and parallax errors on the uncertainties of the fitted components independently for the Wesenheit W_{JK} index. The influence of photometric uncertainties is negligible compared to the influence of parallax errors. The propagation of these two error components does not recreate real uncertainties of the parameters mostly because physical properties of RR Lyrae stars having the same pulsation periods are in general different due to the finite width of the instability strip. Therefore, I adopted uncertainties obtained in the fitting process. The zero point uncertainty of the IRIS photometry (0.002 mag) is negligible compared to the uncertainties of the intersections of the PL relations (≥ 0.02 mag).

Although all methods of the establishment of PL relations give consistent, almost identical results with very similar uncertainties (especially for the three approaches based on linear least-squares fits), it is the photo-geometric distance of Bailer-Jones et al. and the linear least-squares fit that formally yield the lowest values for the uncertainties of the fitted parameters. I will further use it to establish PLZ relations. I will also use the ABL fit for the purpose of comparison. Table 7 contains the GAIA EDR3 parallaxes, photo-geometric distances (Bailer-Jones et al.), and metallicities of Crestani et al. (2021) for stars from my sample.

PLZ relations have a form similar to that of PL relations, with one additional term:

$$M_\lambda\left(P, [Fe/H]\right) = a(\log P - \log P_0) + b + c\left([Fe/H] - [Fe/H]_0\right) \tag{10}$$

where c is the additional fitted metallicity parameter and $[Fe/H]_0$ is the pivot metallicity value that I selected as -1.5 dex. This value is close to the median metallicity of -1.62 dex of the sample.

Alternatively, one may also generalize the ABL to include the metallicity dependence:

$$a_\lambda(P, [Fe/H]) = 10^{0.2\left[a(\log P - \log P_0) + b + c\left([Fe/H] - [Fe/H]_0\right)\right]} \tag{11}$$

In order to fit planes to three-dimensional data sets, I have used once again the *curve_fit* procedure based on the Levenberg–Marquardt least-squares algorithm that provides uncertainties for the three fitted parameters.

Table 8 includes fitted parameters of PLZ relations together with their uncertainties. Samples of 23 stars were used in the case of J and K and the W_{JK} index, while 22 stars were used for the $H-$ band. Obviously, results obtained using both the photo-geometric distances and the ABL approach are virtually identical. The parameters of relations obtained for the mixed population have smaller uncertainties than those corresponding to the population of fundamental pulsators. Figure 27 depicts the three-dimensional PLZ space with the fitted relation for an exemplary case of the $K-$band. In a two-dimensional plane, it is better to visualize the fit by plotting residuals. Figures 28 & 29 include residuals of fits plotted against metallicities

		parallax		geometric distance		photo-geometric distance		Astrometry-Based Luminosity	
band	population	a	b	a	b	a	b	a	b
J	RRab+RRc	-2.52 ± 0.30	-0.164 ± 0.028	-2.52 ± 0.31	-0.164 ± 0.029	-2.53 ± 0.30	-0.165 ± 0.028	-2.41 ± 0.30	-0.155 ± 0.031
	RRab	-3.45 ± 0.39	-0.121 ± 0.027	-3.46 ± 0.39	-0.120 ± 0.027	-3.43 ± 0.38	-0.124 ± 0.027	-3.64 ± 0.42	-0.117 ± 0.027
	RRc	-2.48 ± 0.47	-0.270 ± 0.066	2.47 ± 0.47	-0.271 ± 0.067	-2.45 ± 0.46	-0.262 ± 0.066	-2.49 ± 0.45	-0.269 ± 0.072
H	RRab+RRc	-2.70 ± 0.26	-0.361 ± 0.024	-2.70 ± 0.26	-0.362 ± 0.024	-2.71 ± 0.25	-0.362 ± 0.024	-2.64 ± 0.25	-0.356 ± 0.026
	RRab	-3.40 ± 0.35	-0.325 ± 0.024	-3.41 ± 0.35	-0.325 ± 0.024	-3.38 ± 0.34	-0.328 ± 0.024	-3.48 ± 0.37	-0.322 ± 0.024
	RRc	-2.78 ± 0.47	-0.452 ± 0.066	-2.76 ± 0.47	-0.452 ± 0.067	-2.75 ± 0.47	-0.444 ± 0.066	-2.88 ± 0.45	-0.463 ± 0.072
K	RRab+RRc	-2.91 ± 0.25	-0.418 ± 0.023	-2.91 ± 0.25	-0.418 ± 0.023	-2.92 ± 0.24	-0.419 ± 0.022	-2.83 ± 0.24	-0.412 ± 0.025
	RRab	-3.59 ± 0.31	-0.384 ± 0.022	-3.61 ± 0.31	-0.384 ± 0.022	-3.58 ± 0.30	-0.387 ± 0.021	-3.72 ± 0.33	-0.382 ± 0.021
	RRc	-3.00 ± 0.46	-0.516 ± 0.065	-2.99 ± 0.47	-0.517 ± 0.067	-2.97 ± 0.46	-0.508 ± 0.065	-3.05 ± 0.44	-0.520 ± 0.072
W_{JK}	RRab+RRc	-3.18 ± 0.22	-0.594 ± 0.021	-3.18 ± 0.23	-0.594 ± 0.021	-3.19 ± 0.22	-0.595 ± 0.020	-3.14 ± 0.21	-0.590 ± 0.023
	RRab	-3.69 ± 0.29	-0.566 ± 0.020	-3.71 ± 0.29	-0.565 ± 0.020	-3.68 ± 0.28	-0.569 ± 0.019	-3.78 ± 0.31	-0.564 ± 0.020
	RRc	-3.36 ± 0.46	-0.686 ± 0.066	-3.34 ± 0.48	-0.687 ± 0.068	-3.33 ± 0.47	-0.678 ± 0.066	-3.44 ± 0.44	-0.694 ± 0.073

Table 6: Different ways to fit the parameters a (slope) and b (intersection) of PL relations for Galactic RR Lyrae stars. Parallax denotes the first case mentioned in the text, i.e., distance moduli obtained directly from parallaxes. Geometric and photo-geometric distances from Bailer-Jones et al. (2021) correspond to relations based on distances derived direction-dependent priors only and additionally assuming a dependence of absolute magnitudes on apparent magnitudes and colors of stars in the Milky Way, respectively. The last two columns contain parameters fitted through the ABL (Arenou & Luri, 1999) using a non-linear least-squares procedure. Rows are divided into different bands, with $W_{JK} = K - 0.69(J - K)$ being the Wesenheit index. All relations are fitted using the pivot logarithm of a period value of -0.25. Relations are also given for different populations of RR Lyrae stars. Intersections of relations for RRc and the mixed population RRab+RRc are fitted after the fundamentalization of the first-overtone pulsators' periods. Relations are calibrated in the 2MASS system (Cohen et al., 2003). The IRIS $K-$band corresponds here to the 2MASS K_S-band.

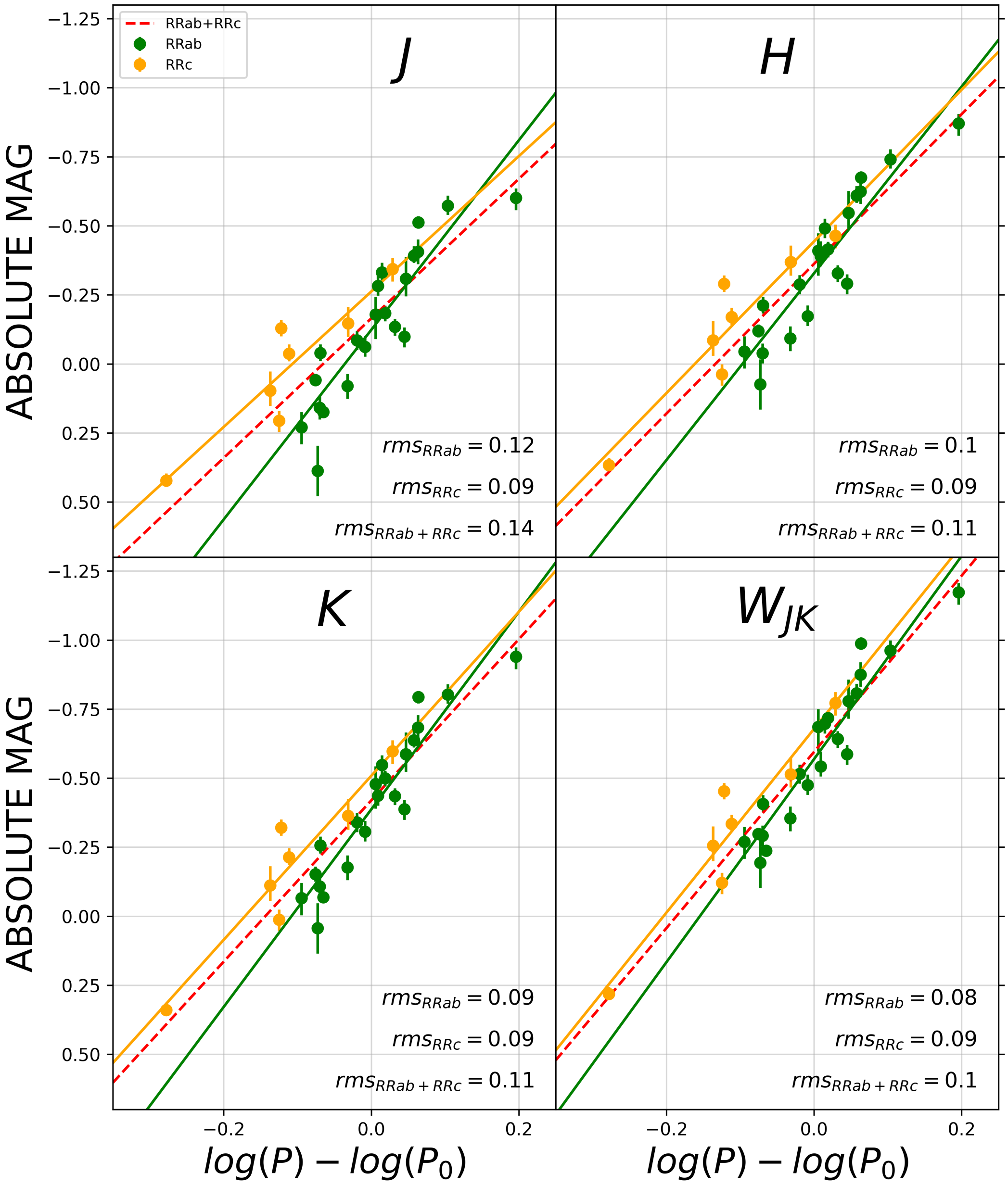

Figure 23: PL relations in JHK and the W_{JK} index based on photo-geometric distances of Bailer-Jones et al. (2021). RRab stars and the corresponding relation are denoted in green. RRc stars with fundamentalized periods and their relation are marked in orange. The red dashed line depicts the relation for the mixed population of all stars. Non-symmetric error bars (Bailer-Jones et al. give upper and lower 1σ distances) of absolute magnitudes correspond to a propagation of the parallax error (dominating) and of the photometric error: $\sigma_M = \sqrt{\left(5\frac{\sigma_r}{r ln 10}\right)^2 + \sigma_m^2}$ with ln being the natural logarithm.

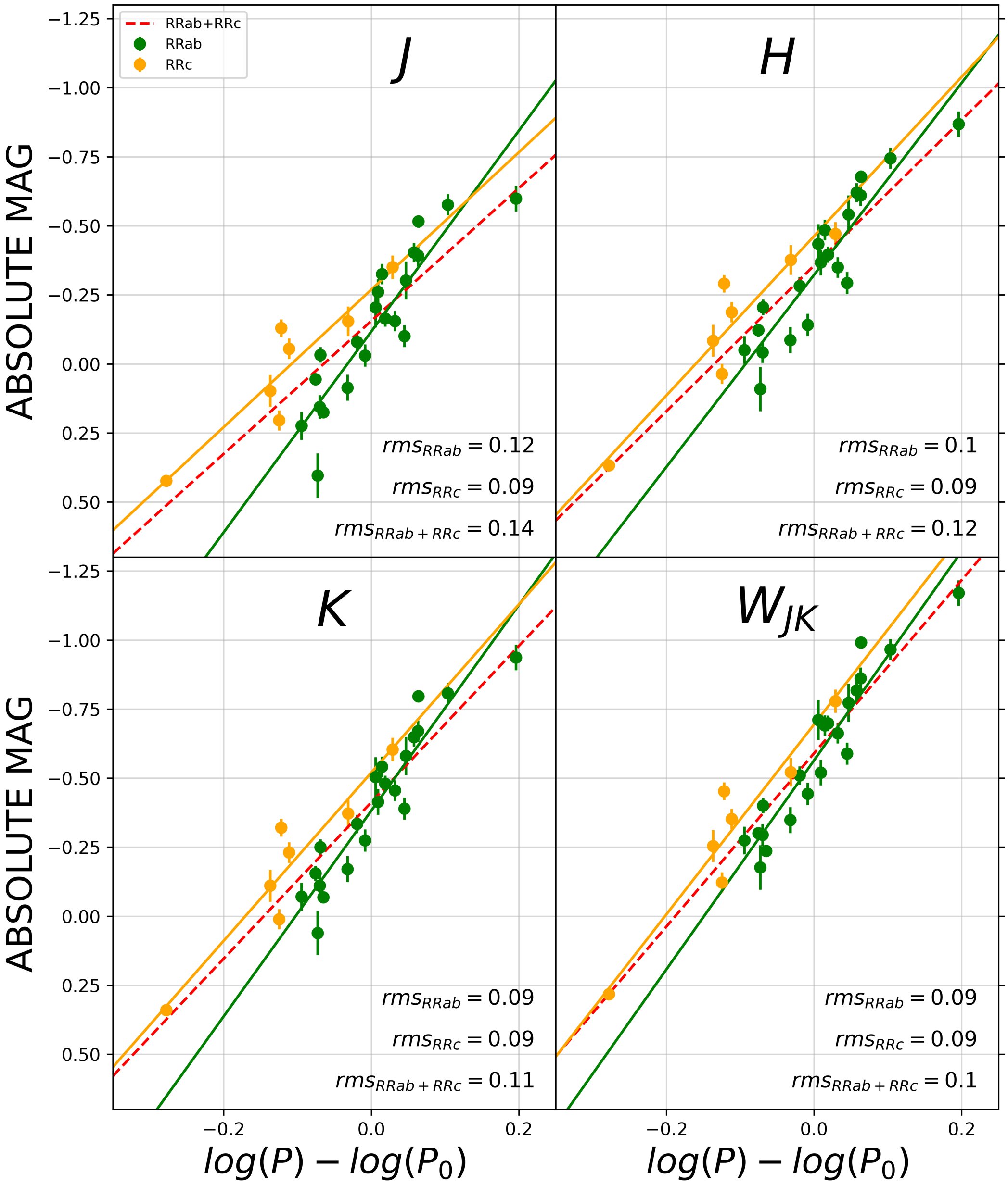

Figure 24: Same as Figure 23 but fitted using the ABL. The error bars of absolute magnitudes correspond to the propagation of the parallax error (dominating) and of the photometric error: $\sigma_M = \sqrt{\left(5\frac{\sigma_\varpi}{\varpi ln10}\right)^2 + \sigma_m^2}$ with ln being the natural logarithm.

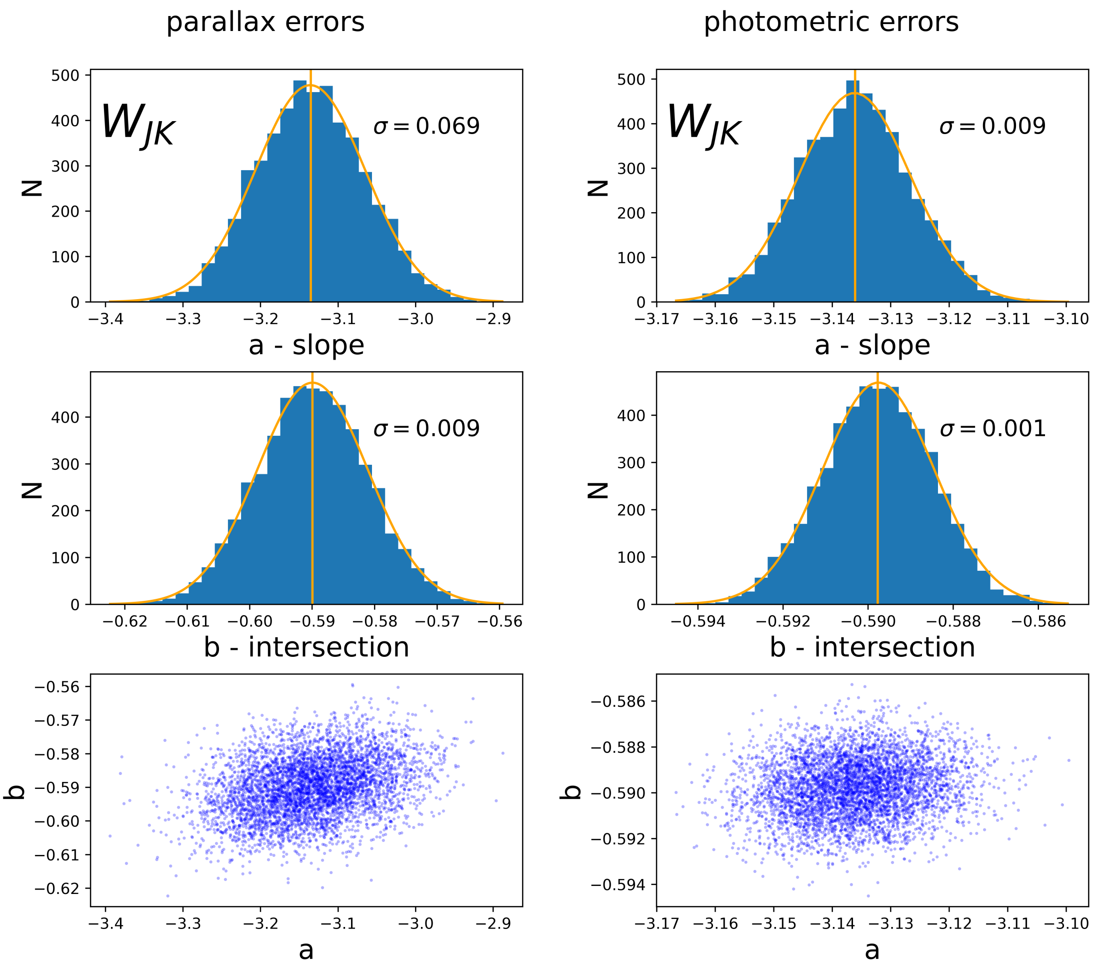

Figure 25: Monte Carlo simulations of the independent influences of photometric and parallax errors as the specific components of uncertainties of the fitted parameters. The distributions depict the most probable values of parameters while varying the parallax and the apparent Wesenheit index value for each star, assuming Gaussian distributions of parallax and magnitude. In both cases, the fits were performed 5000 times for randomly drawn magnitudes and parallaxes. The total error is the square root of the sum of squares of all components. The contribution of the photometric error to the total error budget is negligible compared to the parallax error. The real uncertainties of fitted parameters are larger, mostly due to the intrinsic spread of RR Lyrae stars in the instability strip.

ID	type	ϖ [mas]	r (photo-geo) [pc]	[Fe/H] [dex]
AE Boo	RRc	1.143 ± 0.019	874^{+14}_{-16}	-1.62 ± 0.08
AN Ser	RRab	1.026 ± 0.022	976^{+19}_{-20}	0.05 ± 0.10
BB Eri	RRab	0.722 ± 0.024	1370^{+40}_{-56}	-1.66 ± 0.040
DX Del	RRab	1.758 ± 0.015	567^{+5}_{-4}	-0.19 ± 0.050
EV Psc	RRc	1.133 ± 0.03	883^{+28}_{-22}	–
FW Lup	RRab	2.800 ± 0.017	357^{+2}_{-2}	-0.17 ± 0.02
HY Com	RRc	0.990 ± 0.019	1006^{+18}_{-20}	-1.75 ± 0.02
IK Hya	RRab	1.299 ± 0.023	774^{+16}_{-15}	-2.54 ± 0.08
MT Tel	RRc	2.070 ± 0.030	482^{+6}_{-6}	-2.58 ± 0.14
RR Leo	RRab	1.084 ± 0.025	920^{+23}_{-25}	-1.58 ± 0.08
RU Psc	RRc	1.278 ± 0.029	779^{+20}_{-16}	–
RV Cet	RRab	0.976 ± 0.018	1023^{+15}_{-17}	-1.5 ± 0.02
RX Eri	RRab	1.723 ± 0.023	585^{+7}_{-7}	-1.45 ± 0.15
RY Col	RRab	0.993 ± 0.016	1005^{+14}_{-15}	-1.21 ± 0.02
SS Leo	RRab	0.795 ± 0.025	1261^{+45}_{-36}	-1.8 ± 0.10
SV Eri	RRab	1.361 ± 0.024	733^{+12}_{-10}	-2.22 ± 0.02
SX For	RRab	0.868 ± 0.015	1141^{+14}_{-16}	-2.2 ± 0.02
T Sex	RRc	1.340 ± 0.023	740^{+11}_{-9}	-1.52 ± 0.03
U Lep	RRab	0.989 ± 0.017	1014^{+16}_{-16}	-1.81 ± 0.17
UU Vir	RRab	1.281 ± 0.047	786^{+32}_{-33}	–
V467 Cen	RRab	1.255 ± 0.023	808^{+14}_{-13}	–
V675 Sgr	RRab	1.199 ± 0.019	829^{+13}_{-9}	-2.47 ± 0.02
V753 Cen	RRc	1.436 ± 0.014	696^{+8}_{-5}	-0.56 ± 0.04
V Ind	RRab	1.506 ± 0.019	666^{+9}_{-8}	-1.62 ± 0.01
WY Ant	RRab	0.979 ± 0.021	1032^{+25}_{-16}	-1.6 ± 0.15
WZ Hya	RRab	1.029 ± 0.016	974^{+15}_{-15}	-1.48 ± 0.02
X Ari	RRab	1.869 ± 0.019	534^{+5}_{-5}	-2.53 ± 0.08
XZ Gru	RRab	0.870 ± 0.018	1150^{+17}_{-23}	–
median		1.28	874	-1.62

Table 7: Parallaxes ϖ from GAIA EDR3 (Gaia Collaboration et al., 2021) for Galactic RR Lyrae stars from my sample corrected with the Lindegren et al. (2021) corrections. Photo-geometric distances r were taken from Bailer-Jones et al. (2021), metallicities [Fe/H] come from Crestani et al. (2021).

		photo-geometric distance				Astrometry-Based Luminosity			
band	population	a	b	c	rms	a	b	c	rms
J	RRab+RRc	-2.04 ± 0.30	-0.160 ± 0.024	0.125 ± 0.035	0.099	-1.94 ± 0.27	-0.155 ± 0.025	0.123 ± 0.033	0.097
	RRab	-3.09 ± 0.56	-0.147 ± 0.022	0.070 ± 0.042	0.087	-3.09 ± 0.51	-0.145 ± 0.022	0.067 ± 0.037	0.083
H	RRab+RRc	-2.28 ± 0.24	-0.348 ± 0.020	0.120 ± 0.030	0.079	-2.24 ± 0.22	-0.346 ± 0.020	0.118 ± 0.029	0.078
	RRab	-2.84 ± 0.49	-0.343 ± 0.021	0.084 ± 0.039	0.076	-2.80 ± 0.46	-0.342 ± 0.020	0.083 ± 0.036	0.074
K	RRab+RRc	-2.50 ± 0.23	-0.412 ± 0.018	0.116 ± 0.027	0.076	-2.44 ± 0.20	-0.410 ± 0.019	0.115 ± 0.025	0.075
	RRab	-3.10 ± 0.43	-0.404 ± 0.017	0.080 ± 0.037	0.066	-3.09 ± 0.39	-0.402 ± 0.017	0.078 ± 0.029	0.065
W_{JK}	RRab+RRc	-2.81 ± 0.21	-0.587 ± 0.017	0.110 ± 0.024	0.069	-2.79 ± 0.18	-0.586 ± 0.018	0.110 ± 0.023	0.070
	RRab	-3.11 ± 0.41	-0.581 ± 0.016	0.087 ± 0.031	0.064	-3.10 ± 0.38	-0.580 ± 0.016	0.085 ± 0.027	0.064

Table 8: Parameters of PLZ relations for RR Lyrae stars from the solar neighborhood obtained from photo-geometric distances of Bailer-Jones et al. (2021) and using a linear fit and the GAIA EDR3 parallaxes (corrected according to Lindegren et al. 2021) through the ABL fit. The fitted parameters are as follows: a is the period slope, b the intersection, and c is the metallicity slope; the rms of each fit is given in mag. The relations are fitted using the pivot logarithm of pulsation period -0.25 and the pivot metallicity of -1.5 dex to minimize intersection uncertainties. Relations corresponding to the mixed population RRab+RRc are fitted after the fundamentalization of the first-overtone pulsator periods. The relations are calibrated in the 2MASS system (Cohen et al., 2003). The IRIS $K-$band corresponds here to the 2MASS K_S–band.

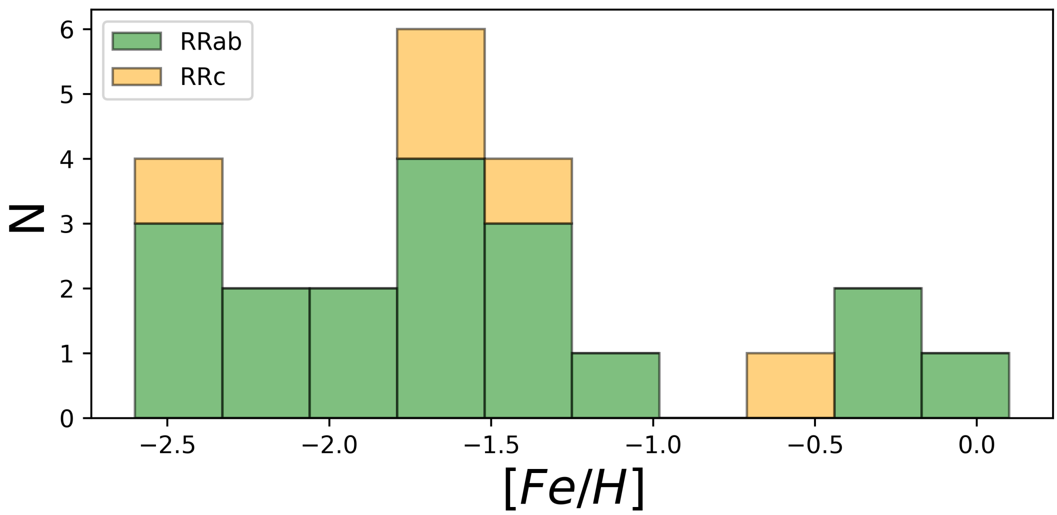

Figure 26: The distribution of metallicities for stars from my sample. Metallicities were adopted from Crestani et al. (2021).

with periods denoted using color maps. The fitted relations indicate smaller metallicity dependence than in the theoretical works of Bono et al. (2001) (0.17 mag/dex in K), Catelan et al. (2004c) $(0.17-0.19)$ mag/dex for JHK), and Marconi et al. (2015) $(0.15-0.18$ mag/dex for JK, with lower values corresponding to the RRc stars). However, given the uncertainties of ~ 0.03 mag/dex, as seen in Table 8, they are still in agreement at least for the mixed population RRab+RRc. Metallicity terms found by me for the population of fundamental pulsators are smaller but they agree with those determined for the mixed population. On the other hand, empirical calibrations usually give smaller dependence on metallicity[20], in a very good agreement with values reported in this work. Sollima et al. (2006) obtained (0.08 ± 0.11) mag/dex for the $K-$band. Muraveva et al. (2015) got (0.03 ± 0.07) mag/dex for the LMC, explaining the especially low parameter value by a narrow span of metallicities of RR Lyrae stars in that galaxy. They reported (0.07 ± 0.04) mag/dex for the Galactic RR Lyrae stars in the same work. Cusano et al. (2021), who utilized the photometry of the *Vista Magellanic Cloud Survey (VMC)*, report the effect of 0.095 ± 0.004 mag/dex and 0.121 ± 0.004 mag/dex for the mixed and the RRab populations in J (and virtually the same in the $K-$ band), respectively.

In addition to the reported statistical uncertainties of PL and PLZ relation intersections, we are also dealing with their systematic uncertainties associated mainly with the uncertainty of the zero points of GAIA EDR3 parallaxes. I will discuss this issue to another subsection.

In the following subsection, I will compare my calibrations with those obtained previously by others. I will also determine distances to a few nearby galaxies using photometry available in the literature.

4.2.2 Comparison with other calibrations

When it comes to accurate distance determinations using PL or PLZ relations for RR Lyrae stars (or pulsating stars in general), the most important challenge is to define accurately the zero point of a calibration. It is especially challenging to estimate the uncertainty of the zero point of calibration that is associated with the elusive systematic errors. This is why we should compare our calibrations with others, especially those obtained using independent, alternative methods. In this subsection, I am comparing my results with calibrations derived in the last

[20]Calibrations without distinction between populations of fundamental and first-overtone pulsators are given for the mixed population of RRab+RRc with the applied fundamentalization procedure based on Iben (1974).

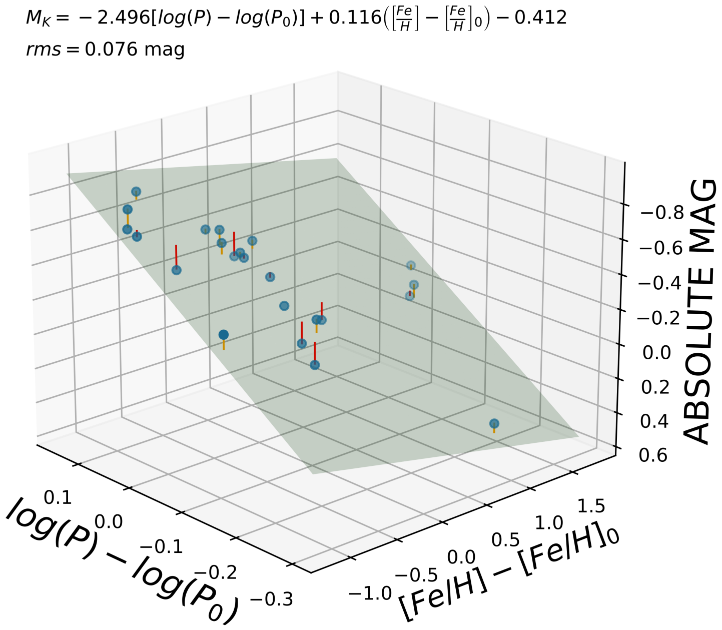

Figure 27: An example of a plane fit; the PLZ relation for the mixed population (RRab+RRc) in the $K-$band is based on the photo-geometric distances of Bailer-Jones et al.

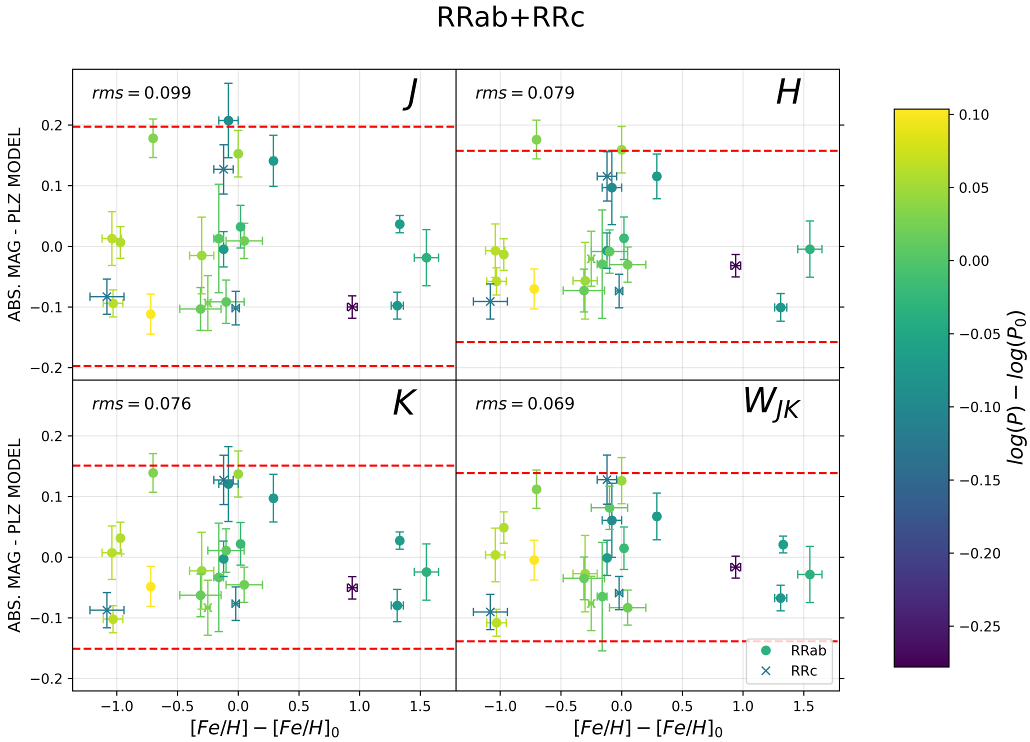

Figure 28: Residuals of plane fits for three bands and the Wesenheit index for the mixed population (RRab+RRc). Dashed lines denote the $2\times$ rms deviation from the model; $\log P_0 = -0.25$ and $[\mathrm{Fe/H}]_0 = -1.5$. RRab are depicted as dots, RRc as crosses.

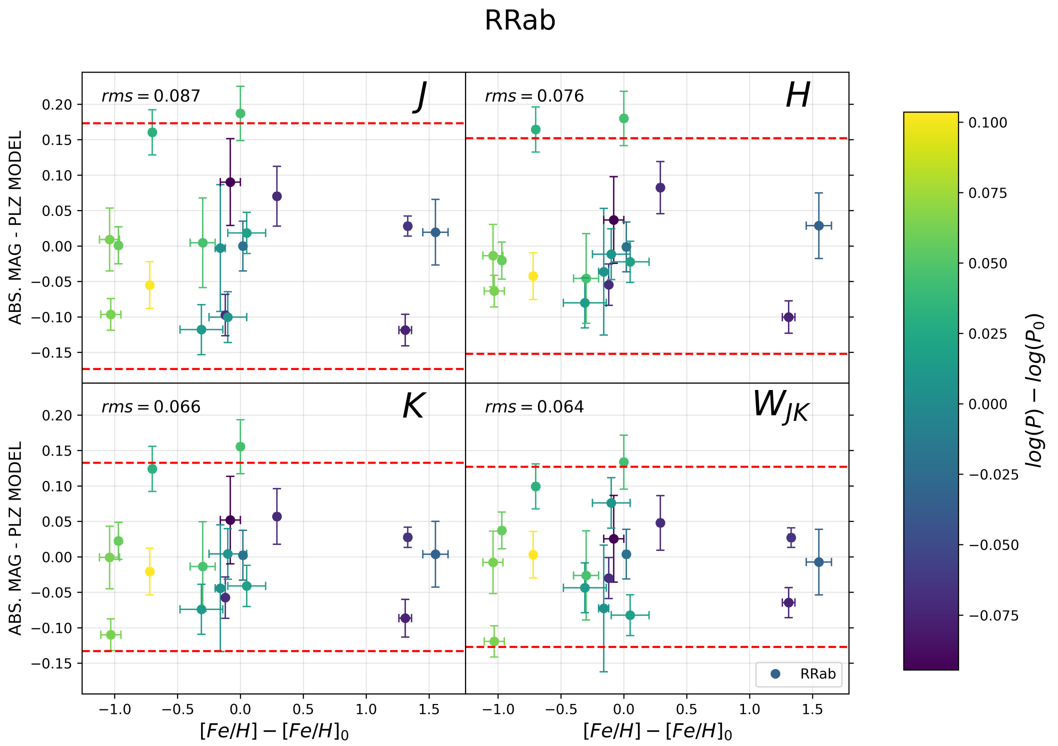

Figure 29: Same as Figure 28 but for the population of fundamental pulsators (RRab).

years (Muraveva et al. 2015, Muraveva et al. 2018, Neeley et al. 2019 Cusano et al. 2021). Indirectly, I am comparing my calibration with the older calibrations from the first decade of the century (Bono et al. 2001, Catelan et al. 2004c, Sollima et al. 2008), as they were utilized, as a part of the Araucaria Project, for distance determinations to the Magellanic Clouds (Szewczyk et al. 2008, Szewczyk et al. 2009) and the Fornax and the Carina galaxies (Karczmarek et al. 2015, Karczmarek et al. 2017b) using RR Lyrae PLZ relations (see the next subsection).

Muraveva et al. (2015) established RR Lyrae PLZ relations for the LMC in the VISTA K_S–band[21] using the VMC photometry of 70 stars from Cioni et al. (2011). They tied them with two different anchors. The first one was the very accurate 2% distance to the LMC by Pietrzyński et al. (2013). In an alternative approach, they assumed the same period and metallicity slopes of the relations as in the LMC and performed a one-parameter fit to 4 Galactic RR Lyrae stars having trigonometric parallaxes determined at the HST (*Hubble Space Telescope*) by Benedict et al. (2011). Those two zero points do not agree with each other, which may be caused by the difficulties of the complex analysis of relative parallaxes from the HST. The relation of Muraveva et al. (2015) based on the anchoring distance of Pietrzyński et al. (2013) is as follows:

$$M_{K_S}(-2.73 \pm 0.25)\log P + (0.03 \pm 0.07)[Fe/H] - (1.06 \pm 0.01) \quad (12)$$

while the zero point based on the parallaxes of 4 stars by Benedict et al. (2011) is (-1.25 ± 0.06) mag instead.

At first, we notice that both the period and the metallicity slope are in agreement with

[21] My $K-$band relations are calibrated onto the 2MASS K_S–band that is shifted by just about $3-4$ mmag from VISTA K_S for the typical color of RR Lyrae stars (Muraveva et al., 2015). For the formal agreement, I am still converting my photometry to the VISTA system using the transformation equations given at `http://casu.ast.cam.ac.uk/surveys-projects/vista/technical/photometric-properties` (González-Fernández et al., 2018).

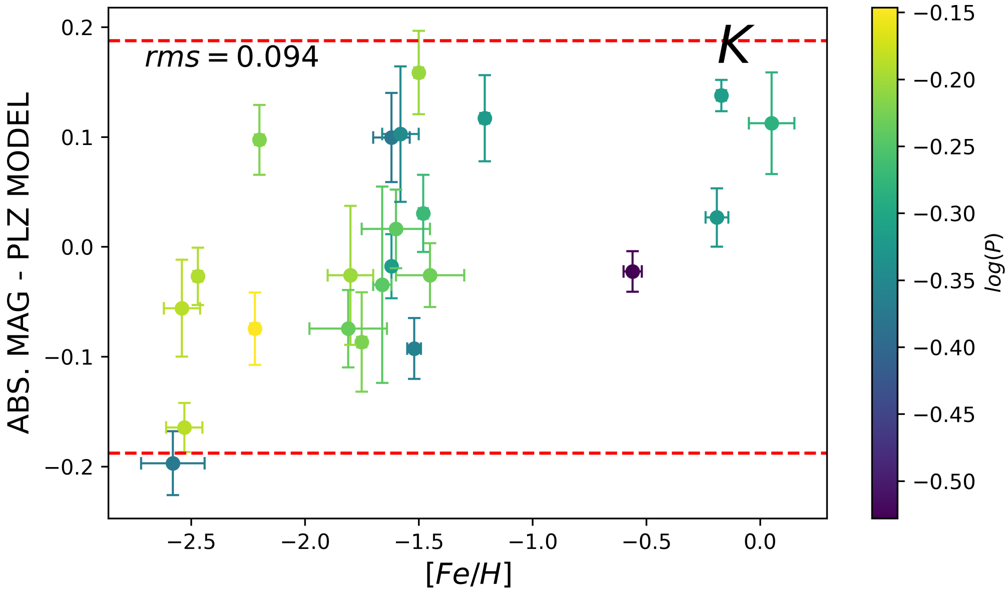

Figure 30: Residuals of the fit of the zero point of the PLZ relation for the mixed population of RR Lyrae stars, given the LMC slopes by Muraveva et al. (2015) and the photo-geometric distances of stars from my sample. The metallicity dependence is still visible due to the exceptionally low metallicity slope value found by Muraveva et al. for RR Lyrae stars in the LMC.

those derived in the present study for the $K-$band and the mixed population. Although the dependence from metallicity is much smaller in the case of the calibration of Muraveva et al. (0.03 ± 0.07 dex/mag vs. 0.115 ± 0.025 dex/mag, see Table 8), the distribution of the differences between the two may be considered a Gaussian with a mean value of 0.085 dex/mag and a spread of 0.074 dex/mag. In this sense, the results are consistent within 1.15σ. In order to compare zero points of our calibrations, I am fixing both slopes and perform a fit of one parameter once again. The value I obtain is in very good agreement with the calibration of Muraveva et al. based on the distance to the LMC of Pietrzyński et al. (2013). The ABL fit yields (-1.055 ± 0.020) mag while the fit based on the photo geometric distances gives (-1.063 ± 0.020) mag. Besides the remarkable agreement of these zero points with the LMC-anchored calibration of Muraveva et al., the two types of fit give extremely similar results when it comes to the determination of the zero points of the PLZ relations. I will stick to the fits based on the photo-geometric distances only from now on. Figure 30 depicts residuals of the fit based on the photo-geometric distances.

Muraveva et al. (2015) also presented another calibration based on 23 Galactic RR Lyrae stars that were used for studies with respect to the Baade-Wesselink (B-W) method (Jones et al. 1988b, 1992, Fernley et al. 1990b, Liu & Janes 1990a, Cacciari et al. 1992, Skillen et al. 1993, Fernley 1994). They took the photometry and the reddening from Fernley et al. (1998). Absolute magnitudes of 23 stars (the same sample size as mine) were derived using the B-W method with the fixed value of $p = 1.38$. The assumed p value makes the zero point of these absolute magnitudes arbitrary, as no robust calibration of $p-$ factors for RR Lyrae stars was performed. Even though the relation is calibrated in the Johnson photometric system, authors underline the average difference with the 2MASS K_s–band of the order of 0.03 mag while the B-W-based absolute magnitudes have uncertainties of $0.15 - 0.25$ mag. The Galactic relation of Muraveva et al. (2015):

$$M_K = (-2.53 \pm 0.36) \log P + (0.07 \pm 0.04)[Fe/H] - (0.95 \pm 0.14) \tag{13}$$

The metallicity dependence is slightly larger now and in better agreement with the value

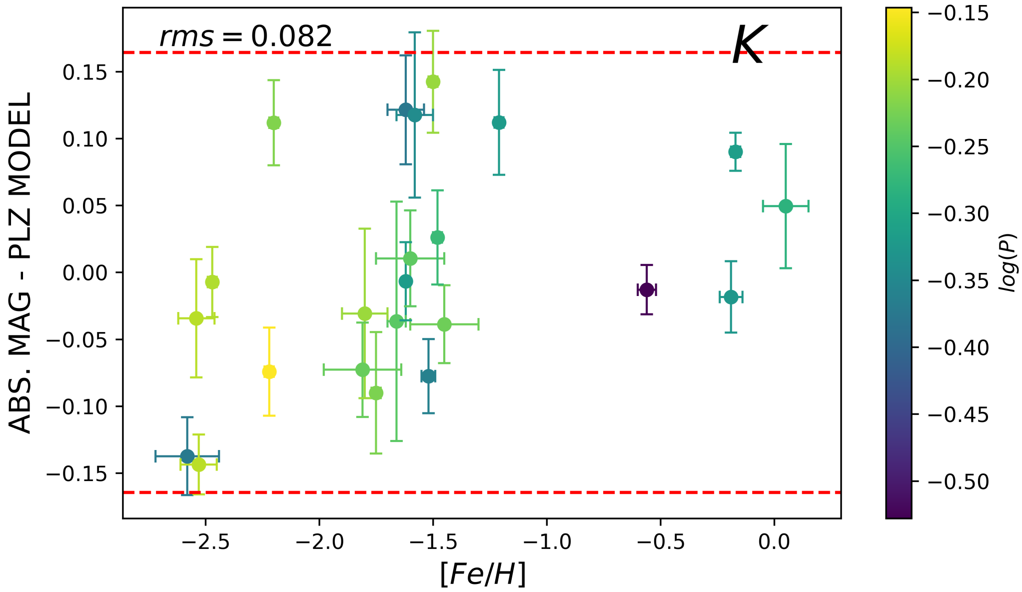

Figure 31: Same as Figure 30 but with the Galactic slopes from Muraveva et al. (2015) that were based on a sample of RR Lyrae stars whose distances were determined by the Baade-Wesselink method.

derived in this work. However, the zero point uncertainty is much larger compared to the LMC calibration. Figure 31 presents residuals of the PLZ relation fit for the mixed population of RR Lyrae stars from my sample with slopes fixed from the Galactic calibration of Muraveva et al. (2015). The fitted zero point 0.944 ± 0.018 mag is also in excellent agreement despite the low precision of the Galactic calibration based on the B-W distances.

In their later work, Muraveva et al. (2018) included the zero point of the PLZ relation based on the GAIA DR2 parallaxes. They used Bayesian modeling, with the parallax offset being the model's parameter. The authors found a systematic offset of the GAIA DR2 parallaxes of -0.054 mas in the case of the PLZ relation for the $K-$band derived from a sample of 400 stars from the Milky Way. The adopted metallicities of various quality came from different methods. All these constraints resulted in a distance modulus for the LMC (using the same sample of RR Lyrae stars from the LMC as in Muraveva et al. 2015) of $\mu_{\rm LMC} = 18.55 \pm 0.11$ mag. Their relation (2MASS system) takes the following form:

$$M_{K_S} = (-2.58 \pm 0.20) \log P + (0.17 \pm 0.03)[Fe/H] - (0.84 \pm 0.09) \tag{14}$$

The metallicity dependence is even larger in this case but still in agreement with the value obtained here. After fixing the period and the metallicity slopes in my fit, I obtain a zero point value of -0.802 ± 0.019 which is consistent with the zero point of Muraveva et al. (2018).

In the following work, that presents PL and PLZ relations for RR Lyrae stars based on GAIA DR2 parallaxes, Neeley et al. (2019) used the photometry of 55 stars from our Galaxy gathered for the *Carnegie RR Lyrae Program*. The authors obtained a rather large scatter of residuals of their fits ~ 0.2 mag, which they identify as possibly due to unaccounted uncertainties or systematics. The work includes a variety of different PL, PLZ, PW, and PWZ relations (including Wesenheit indices instead of luminosity in a given band) obtained using weighted least-squares fits[22]. The results (2MASS photometric system) of Neeley et al. (2019) are as follows:

[22]The authors also use a Bayesian approach and a 'robust' analysis (including the weighting of points based on the scatter of the fit) but find no significant differences between different methods.

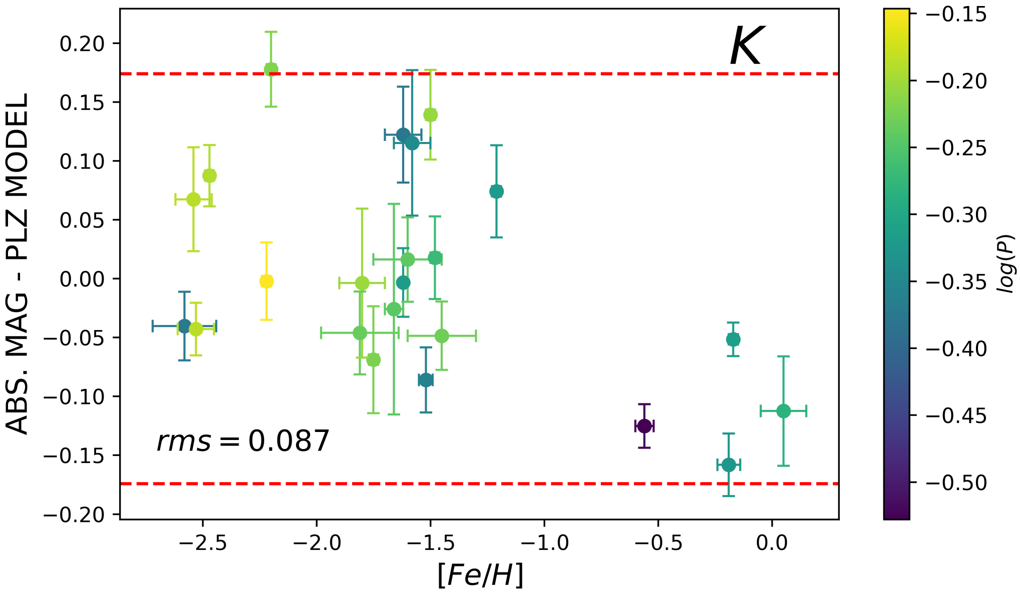

Figure 32: Residuals of the zero point fits using slopes for the PLZ relation for 400 stars from the Milky Way in the $K-$band from Muraveva et al. (2018). The relatively large, unaccounted dependence on the metallicity is apparent.

$$M_J = (-1.91 \pm 0.29)(\log P + 0.3) + (0.20 \pm 0.03)([Fe/H] + 1.36) - (0.14 \pm 0.02) \quad (15)$$

$$M_H = (-2.40 \pm 0.29)(\log P + 0.3) + (0.17 \pm 0.03)([Fe/H] + 1.36) - (0.31 \pm 0.02) \quad (16)$$

$$M_K = (-2.45 \pm 0.28)(\log P + 0.3) + (0.17 \pm 0.03)([Fe/H] + 1.36) - (0.37 \pm 0.02) \quad (17)$$

$$W_{JK} = (-2.91 \pm 0.30)(\log P + 0.3) + (0.15 \pm 0.03)([Fe/H] + 1.36) - (0.53 \pm 0.02) \quad (18)$$

Especially the period slopes here are in good agreement with my derivations while the metallicity slopes are systematically larger but still consistent within the uncertainties. As Neeley et al. show in their Figure 9, all fitted parameters, slopes and the zero point (intersection) of PLZ relations depend monotonically on the zero point offset of GAIA DR2 parallaxes; this may be investigated using quasars and may range from -0.030 mas to -0.056 mas (Arenou et al., 2018)[23]. The authors adopt a smaller offset (in terms of the absolute value) than Muraveva et al. (2018), i.e., -0.03 mas, which is the same as in Bailer-Jones et al. (2018).

It is also worth to notice that Neeley et al. compared distances obtained from simple inversion of parallaxes with those reported by Bailer-Jones et al. (2018) and found no differences for stars at distances at least up to about 1.5 kpc (their Figure 2). This is another proof for the direct applicability of parallaxes in order to calculate absolute magnitudes of RR Lyrae stars from the solar neighborhood. It is coherent with virtually no differences between relations obtained from parallaxes and those that are based on geometric and photo-geometric distances of Bailer-Jones et al. (2021) (see Table 6).

Using the same pivot period and metallicity ($\log P_0 = -0.3$ and $[Fe/H]_0 = -1.36$) as Neeley et al. and fixing slopes obtained by them, I get zero point values of -0.029 ± 0.024, -0.200 ± 0.019, -0.261 ± 0.018, and -0.420 ± 0.016 for J, H, K, and W_{JK}, respectively. The zero points of my relations are systematically larger by about 0.11 mag. Figure 33 depicts

[23]Arenou et al. (2018) report an offset of (0.056 ± 0.005) mas for RR Lyrae stars – a value which is consistent with the result of Muraveva et al. (2018). Neeley et al. note that it is not possible to set such an offset for RR Lyrae stars without assuming a PL relation.

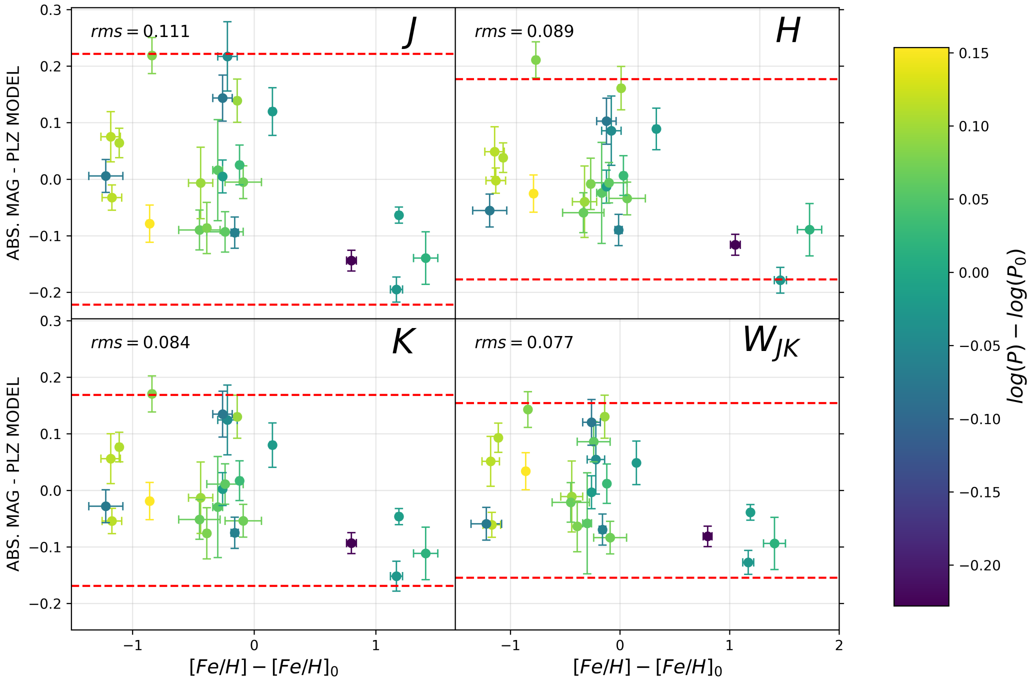

Figure 33: Residuals of the fits of zero points of PLZ relations using slopes from Neeley et al. (2019). The dependence on metallicity is similar to that reported by Muraveva et al. (2018). The fits yield zero points that are about 0.11 mag larger than those reported by Neeley et al. (see text). In this case, $\log P_0 = -0.3$ and $[Fe/H]_0 = -1.36$.

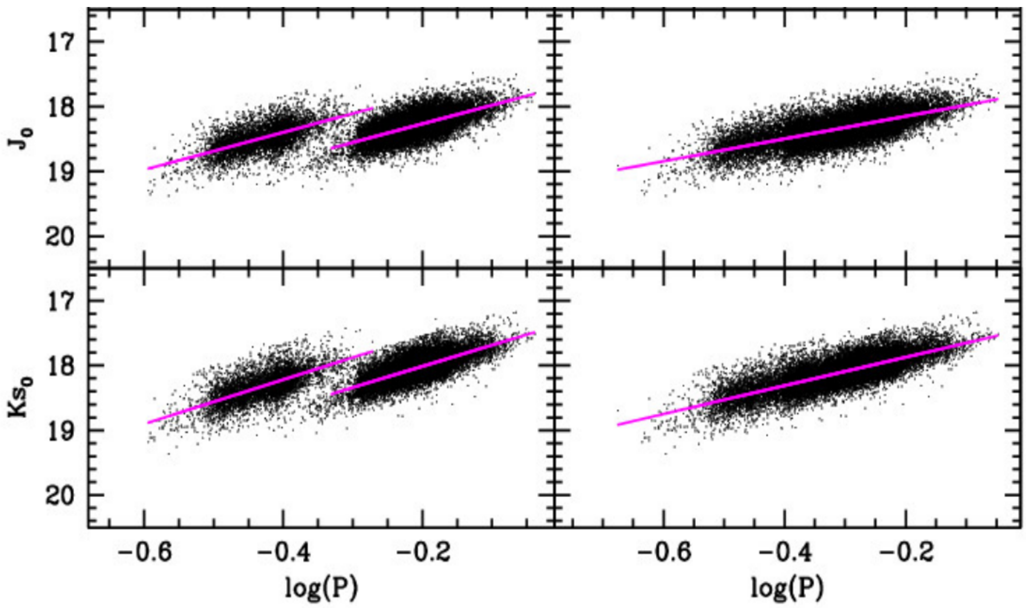

Figure 34: PL relations for J and K_S from Cusano et al. (2021). The plot on the left includes separate relations for RRab and RRc stars, while the plot on the right depicts the global relation with RRc having their periods fundamentalized. The non-optimal alignment of points corresponding to stars from the two populations is apparent. Figure taken from: `https://arxiv.org/abs/2103.15492`.

residuals of these fits. Interestingly, the authors report that calibrations based on the adoption of a parallax offset of -0.06 mas yield an LMC distance that is 0.1 mag smaller than without an offset. However, one must keep in mind that Neeley et al. used GAIA DR2 parallaxes and my research is based on EDR3. The parallax zero points (and their corrections) for different data releases are different: The parallax zero points and uncertainties published in the EDR3 are improved compared to DR2.

Another calibration takes advantage of the VMC photometry of RR Lyrae stars from the LMC. Cusano et al. (2021) established PL and PLZ relations based on 22 thousand stars; the measurements were taken in, i.a., J and K and comprised a mixed population – among them almost 17,000 fundamental pulsators). What is especially striking in those relations is the question of fundamentalization of periods of the first-overtone pulsators (the accepted $+0.127$ shift of logarithms of periods). Relations for the mixed population have a significantly smaller slope compared to relations for the two populations separately (where the slope values are very similar). It is especially visible in Figures 6 & 7 from that paper: fundamentalized RRc stars do not follow the same relations as RRab. They are still more luminous, which flattens the *global* relation for the mixed population and slightly increases its intersection (Figure 34). It shows that such a situation of a non-optimal alignment of points corresponding to stars from the two populations can introduce a bias. RRc stars also form different fractions of different samples[24] of mixed populations. The distributions of periods of RRc and RRab stars vary from sample to sample. Thus, the weight and impact of the first-overtone pulsators on the final values of fitted parameters also differ between different samples. The dependence of the 'fundamentalization shift' on the environmental conditions, typically determined for the double-

[24] When it comes to PLZ relations, the ratio of numbers of RRc to RRab in my sample – 5/18 (28%) – is slightly different from that of Cusano et al. (2021), which is $\sim 5,000/13,000$ (38%) for JK bands. In Muraveva et al. (2015) (the Galactic sample) it is 2/21 (10%) and in Muraveva et al. (2018) it is 35/366 (10%). I have not found the relevant information explicitly in Neeley et al. (2019) but one can derive it from their plots – the corresponding ratio is around 17/38 (44%).

band	population	slope	μ_{LMC} [mag]	δ_{stat} [mag]	δ_{VMC} [mag]	δ_{LMC} [mag]	rms [mag]
J	RRab+RRc	−2.00	**18.453**	0.028	0.004	0.028	0.15
	RRab	−2.50	**18.454**	0.030	0.005	0.030	0.13
	RRc	−2.53	**18.465**	0.037	0.022	0.043	0.09
K	RRab+RRc	−2.53	**18.473**	0.022	0.004	0.023	0.12
	RRab	−2.84	**18.462**	0.024	0.005	0.024	0.11
	RRc	−2.98	**18.442**	0.037	0.023	0.044	0.09
W_{JK}	RRab+RRc	−2.888	**18.500**	0.020	0.004	0.020	0.10
	RRab	−3.075	**18.492**	0.021	0.006	0.022	0.09
	RRc	−2.289	**18.514**	0.038	0.055	0.067	0.09

Table 9: LMC distance moduli $\mu_{\text{LMC}} \pm \delta_{\text{LMC}}$. δ_{stat} is a statistical error of the fit of the zero point of the relation while δ_{LMC} is a superposition of errors of fits of intersections, $\delta_{\text{LMC}} = \sqrt{\delta^2_{\text{stat}} + \delta^2_{\text{VMC}}}$, where δ_{VMC} is the uncertainty of zero point of the fiducial relation reported by Cusano et al. 2021. δ_{VMC} is one of the systematic errors that is involved in the determination. Obviously, it is usually negligible compared to δ_{stat}; however, this is not the case for RRc stars. The distance moduli were obtained as the differences between intersections of PL relations from fits with fixed slopes taken from Cusano et al. (2021) and LMC intersections given there. The canonical LMC distance of Pietrzyński et al. (2019) is $\mu_{\text{LMC}} = (18.477 \pm 0.004 \pm 0.026)$ mag.

band	population	period slope	metallicity slope	μ_{LMC} [mag]	δ_{stat} [mag]	δ_{VMC} [mag]	δ_{LMC} [mag]	rms [mag]
J	RRab+RRc	−1.91	0.095	**18.456**	0.022	0.007	0.023	0.103
	RRab	−2.45	0.121	**18.465**	0.022	0.008	0.024	0.091
K	RRab+RRc	−2.41	0.096	**18.473**	0.016	0.007	0.018	0.078
	RRab	−2.80	0.114	**18.479**	0.017	0.008	0.019	0.069
W_{JK}	RRab+RRc	−2.810	0.094	**18.497**	0.015	0.008	0.017	0.070
	RRab	−3.033	0.111	**18.502**	0.016	0.009	0.018	0.065

Table 10: Same as Table 9 but based on PLZ relations with the metallicity slope fixed additionally.

mode RRd stars, makes it difficult to calibrate for extragalactic stars properly. In a sense, it makes the global relations containing a relatively large number of first-overtone pulsators non-comparable (especially when it comes to values of individual parameters) with those having just a few. However, these are zero points, i.e., intersections of relations, that affect the distance determinations most severely. Even if slopes of different relations are slightly different, we may fix their values based on given fiducial relations.

Figure 35 depicts PL relations for my sample of RR Lyraes with slopes adopted from Cusano et al. (2021). Intersections are fitted separately for RRab, RRc, and RRab+RRc samples. Slope of the relation for RRab in $J-$ band barely agrees with the one from the free fit (-2.50 ± 0.02 v.s. -3.45 ± 0.39). On the other hand, RRc stars follow relations with fixed slopes pretty well. Intersections obtained using fits with fixed slopes serve for distance determinations. Namely, the LMC distance modulus is the difference between intersection value reported in Cusano et al. (2021) and the intersection obtained through the fit. As Cusano et al. (2021) give relations for the non-fundamentalized RRc, I have 'fundamentalized' intersections of these relations by subtracting 0.127× slope(RRc), which is consistent with the fundamentalization procedure in their study and in the present work. In the case of PLZ relations, I have additionally fixed metallicity slopes at the values reported by Cusano et al. (2021). In this sense, I have been shifting a plane rather than a line for the purpose of distance determination. Even though it is not guaranteed that the geometric center of the eclipsing systems from Pietrzyński et

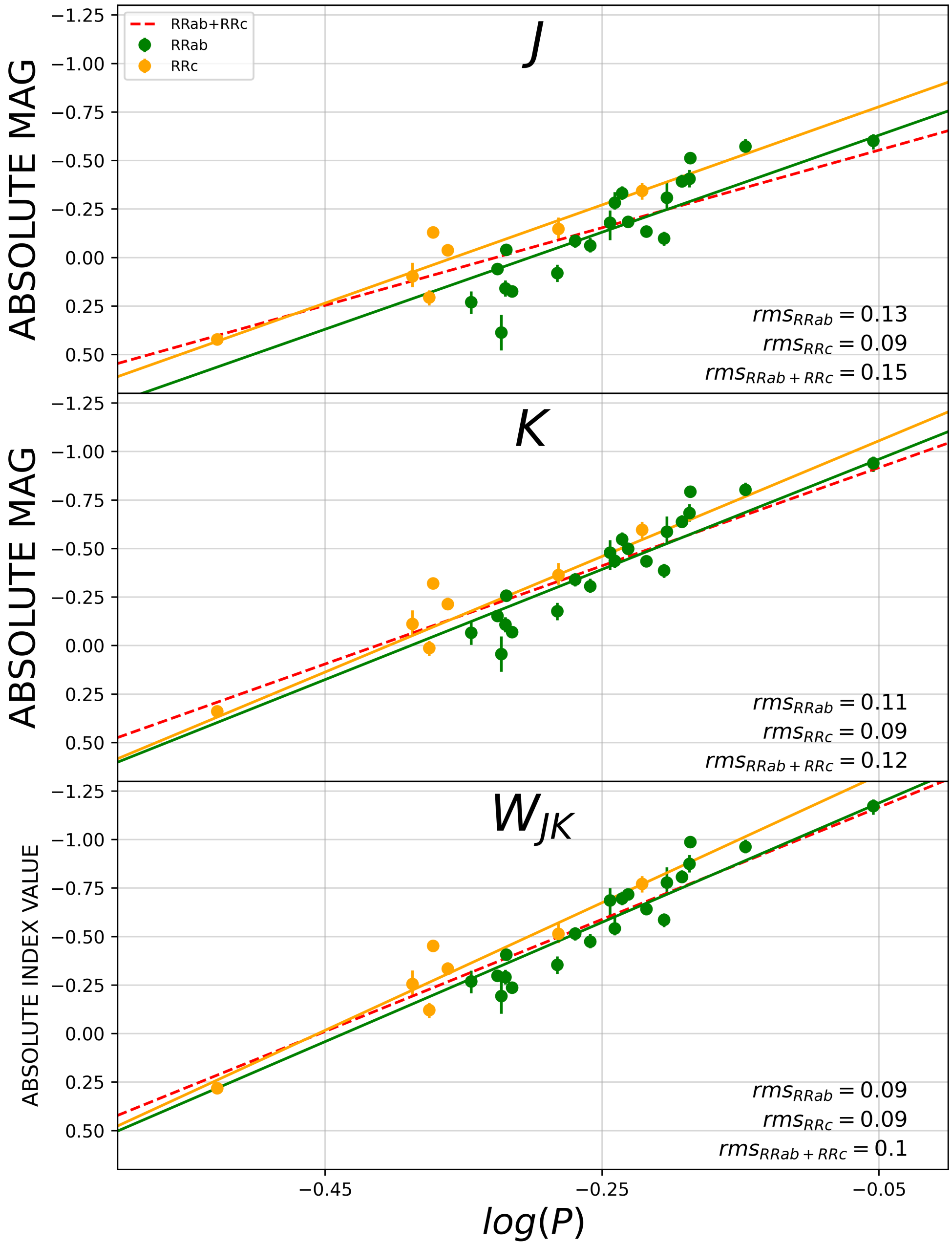

Figure 35: PL relations for RR Lyrae stars from my sample obtained by fitting the intersections with the slopes from Cusano et al. (2021)

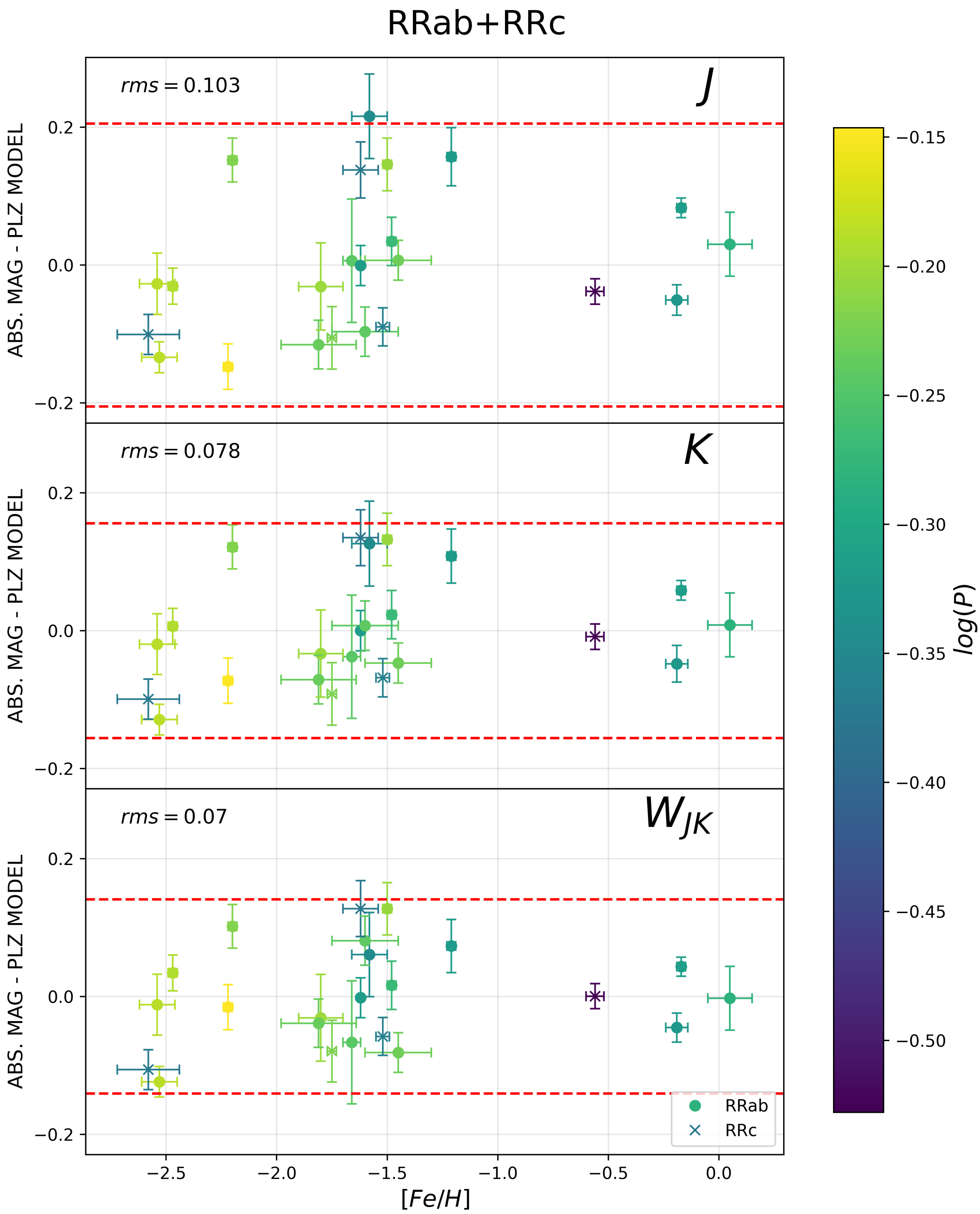

Figure 36: Residuals of fits of zero points of PLZ relations to my sample of Galactic RR Lyrae stars with both period and metallicity slopes taken from Cusano et al. (2021) for the mixed population of fundamental and first-overtone pulsators.

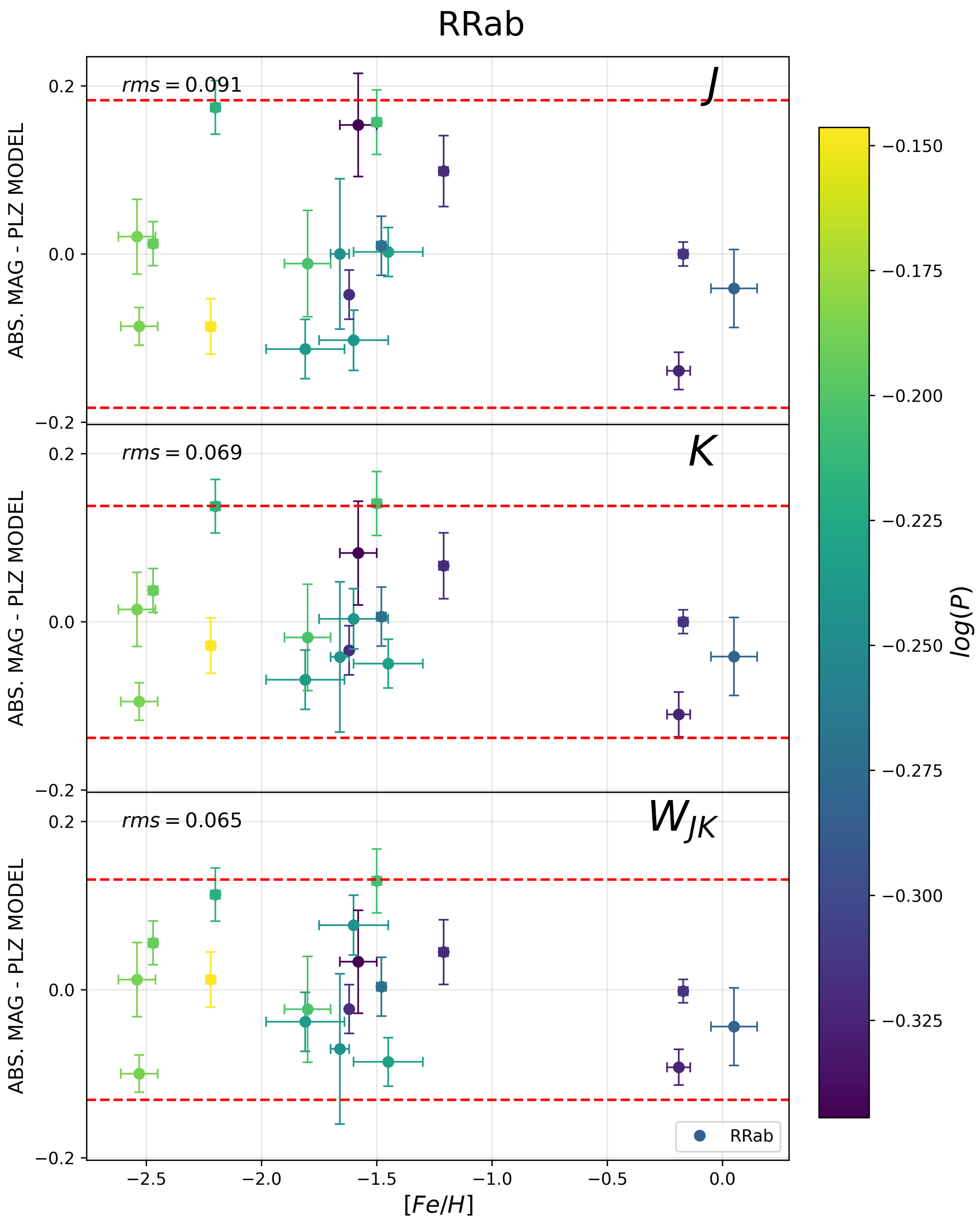

Figure 37: As in Figure 36 but just for the fundamental pulsators.

al. (2019) is identical to the geometric center of the population of RR Lyrae stars in the LMC, we can see that results, summarized in Tables 9 & 10 (where LMC distance moduli are given depending on photometric band or, alternatively, the W_{JK} index, and population of RR Lyraes), are in extremely good agreement with the canonical distance from eclipsing binaries of $\mu_{\mathrm{LMC}} = 18.477 \pm 0.004 \pm 0.026\,\mathrm{mag}$. It seems that neither the use of different populations of RR Lyrae stars nor the inclusion of the metallicity dependence changes the value of the distance in this case. All determinations, based both on PL and PLZ relations, are in agreement given the small statistical uncertainties of the zero point fits. However, as expected, uncertainties and rms of residuals are smaller in the case of PLZ relations .

4.2.3 Determinations of distances to four nearby galaxies

The final test of my calibrations is the determination of distances to four galaxies, which had already been studied within the Araucaria Project. NIR photometry of RR Lyrae stars from the LMC, SMC, and from the Carina and Fornax galaxies is available in papers by Szewczyk et al. (2008), Szewczyk et al. (2009), Karczmarek et al. (2015), and Karczmarek et al. (2017b). Original distances reported in these papers were based on calibrations of the PLZ relations in K for RR Lyrae stars by Bono et al. (2003), Catelan et al. (2004c), Sollima et al. (2008); Catelan et al. supplemented additionally a calibration for the $J-$band. Carina also had its distance determined using Dékány et al. (2013) calibration for the $K-$ band, which yields virtually the same distance modulus as the Catelan et al. (2004c) calibration for the same band.

There are no individual metallicity determinations for the RR Lyrae stars in these galaxies. Therefore, we rather assume a mean metallicity of a given galaxy, perform a linear fit of the PL relation with the period slope fixed, and treat the metallicity component as a correction of the zero point. I will compare this approach with the simpler PL fit without taking into account the metallicity component[25]. Given that my PLZ relations are calibrated with the pivot metallicity value of $[Fe/H]_0 = -1.5\,\mathrm{dex}$, we can immediately estimate the influence of metallicity on my determinations, adopting the same metallicities for the galaxies as in the aforementioned papers. The metallicity correction is simply a metallicity slope multiplied by $[Fe/H] - [Fe/H]_0$. These differences take the values of $0.02\,\mathrm{dex}$, $-0.2\,\mathrm{dex}$, $-0.22\,\mathrm{dex}$, and $-0.1\,\mathrm{dex}$ for the LMC, the SMC, Carina, and Fornax, respectively. Given the metallicity slope of $0.1\,\mathrm{mag/dex}$, these values translate into $0.002\,\mathrm{mag}$, $-0.02\,\mathrm{mag}$, $-0.022\,\mathrm{mag}$, and $-0.01\,\mathrm{mag}$ metallicity corrections that are very small and at most comparable to the statistical errors.

All original determinations were performed for J and K. Szewczyk et al. (2008) also provide $K-$band mean magnitudes that were determined using light curve templates of Jones et al. (1996) in addition to the averaged magnitudes of the stars. For comparison, I have also fitted relations based on the Wesenheit index (that were not included in the original papers).

Szewczyk et al. provided already dereddened photometry of RR Lyrae stars from the Magellanic Clouds using reddening maps of Udalski et al. 1999a, 1999b. Karczmarek et al. reported original apparent magnitudes. I have dereddened the photometry of RR Lyrae stars published by Karczmarek et al. using the same $E(B-V)$ values as in the corresponding papers, i.e., $E(B-V)_{\mathrm{CARINA}} = 0.06\,\mathrm{mag}$ and $E(B-V)_{\mathrm{FORNAX}} = 0.021\,\mathrm{mag}$. Wesenheit indices for stars from Fornax and Carina were calculated from the apparent J and K magnitudes while in the case of the LMC and the SMC they were formed using the dereddened magnitudes. As the Araucaria Project NIR photometry has been calibrated onto the UKIRT system, I have used the transformation equations of Carpenter (2001) in order to transform it onto the 2MASS system.

Tables 11-18 include the derived distances together with their uncertainties depending on the photometric band and population of pulsators. Figures 38-41 present fitted PL relations for each photometric band (and the W_{JK} index) and for each population of RR Lyrae stars separately. The reported distances are accompanied by statistical errors δ_{stat} of fits of intersections of PL

[25] In principle, PL and PLZ relations also have different period slopes and zero points, so one cannot simply think of a fiducial PL relation as a fiducial PLZ relation without the metallicity component. The comparison between the two approaches is thus not associated merely with the 'metallicity correction' but comprehensive.

band	population	μ_{LMC} [mag]	δ_{stat} [mag]	δ_{MW} [mag]	δ_{LMC} [mag]	rms [mag]
J	RRab+RRc	**18.450**	0.034	0.028	0.044	0.27
	RRab	**18.450**	0.039	0.027	0.047	0.28
	RRc	18.389	0.067	0.066	0.094	0.20
K	RRab+RRc	**18.447**	0.028	0.022	0.036	0.22
	RRab	**18.450**	0.031	0.021	0.037	0.22
	RRc	18.381	0.053	0.065	0.084	0.16
K_t	RRab+RRc	**18.440**	0.026	0.022	0.034	0.21
	RRab	**18.440**	0.029	0.022	0.036	0.21
	RRc	18.381	0.051	0.065	0.082	0.15
W_{JK}	RRab+RRc	**18.445**	0.030	0.020	0.037	0.24
	RRab	**18.451**	0.034	0.019	0.039	0.25
	RRc	18.376	0.057	0.066	0.087	0.17

Table 11: LMC distance moduli μ_{LMC} together with a superposition of uncertainties of intersections of fits: $\delta_{\text{LMC}} = \sqrt{\delta_{\text{stat}}^2 + \delta_{\text{MW}}^2}$, where δ_{stat} is the statistical uncertainty of the zero point. δ_{MW} is the uncertainty of the fiducial zero point from the Milky Way determined in the present work. It is one of the systematic errors that is involved in the determination. The distance moduli are obtained as differences between the intersections of the PL relations based on fits with fixed slopes and LMC intersections. The canonical LMC distance of Pietrzyński et al. (2019) is $\mu_{\text{LMC}} = (18.477 \pm 0.004 \pm 0.026)$ mag. K_t denotes the relation where average $K-$band magnitudes were determined using templates frpm Szewczyk et al. (2008), thus establishing a more precise relation.

band	population	μ_{LMC} [mag]	δ_{stat} [mag]	δ_{MW} [mag]	δ_{LMC} [mag]	rms [mag]
J	RRab+RRc	**18.446**	0.034	0.024	0.041	0.27
	RRab	**18.468**	0.038	0.022	0.044	0.28
K	RRab+RRc	**18.441**	0.028	0.018	0.033	0.22
	RRab	**18.460**	0.030	0.017	0.035	0.22
K_t	RRab+RRc	**18.434**	0.026	0.018	0.032	0.20
	RRab	**18.450**	0.028	0.017	0.033	0.20
W_{JK}	RRab+RRc	**18.438**	0.031	0.017	0.035	0.24
	RRab	**18.454**	0.034	0.016	0.038	0.25

Table 12: Same as Table 11 but based on PLZ relations.

band	population	μ_{SMC} [mag]	δ_{stat} [mag]	δ_{MW} [mag]	δ_{SMC} [mag]	rms [mag]
J	RRab+RRc	**18.781**	0.03	0.028	0.041	0.17
	RRab	**18.757**	0.031	0.027	0.041	0.17
	RRc	18.894	0.122	0.066	0.139	0.17
K	RRab+RRc	**18.796**	0.027	0.022	0.035	0.15
	RRab	**18.770**	0.029	0.021	0.036	0.16
	RRc	18.948	0.069	0.065	0.095	0.10
W_{JK}	RRab+RRc	**18.807**	0.030	0.020	0.036	0.17
	RRab	**18.780**	0.033	0.019	0.038	0.18
	RRc	18.985	0.032	0.066	0.073	0.05

Table 13: SMC distance moduli based on PL relations. The canonical distance to SMC by Graczyk et al. (2020) based on eclipsing binaries is $\mu_{\mathrm{SMC}} = (18.977 \pm 0.016 \pm 0.028)$ mag. Note: only 3 RRc stars from the SMC were used in these determinations, making determinations only based on RRc stars rather unreliable.

band	population	μ_{SMC} [mag]	δ_{stat} [mag]	δ_{MW} [mag]	δ_{SMC} [mag]	rms [mag]
J	RRab+RRc	**18.796**	0.031	0.024	0.039	0.18
	RRab	**18.787**	0.031	0.022	0.038	0.17
K	RRab+RRc	**18.808**	0.027	0.018	0.033	0.16
	RRab	**18.794**	0.028	0.017	0.033	0.16
W_{JK}	RRab+RRc	**18.817**	0.031	0.017	0.035	0.18
	RRab	**18.799**	0.032	0.016	0.036	0.18

Table 14: Same as Table 13 but based on PLZ relations.

band	population	μ_{CARINA} [mag]	δ_{stat} [mag]	δ_{MW} [mag]	δ_{CARINA} [mag]	rms [mag]
J	RRab+RRc	**19.916**	0.021	0.028	0.035	0.12
	RRab	**19.933**	0.023	0.027	0.036	0.12
	RRc	19.928	0.061	0.066	0.090	0.11
K	RRab+RRc	**19.904**	0.016	0.022	0.027	0.09
	RRab	**19.911**	0.020	0.021	0.029	0.10
	RRc	19.943	0.024	0.065	0.069	0.04
W_{JK}	RRab+RRc	**19.896**	0.016	0.020	0.026	0.09
	RRab	**19.897**	0.019	0.019	0.027	0.10
	RRc	19.954	0.010	0.066	0.067	0.02

Table 15: Carina distance moduli based on PL relations. Note: only 4 RRc stars from Carina were used in these determinations, making determinations only based on RRc stars rather unreliable.

band	population	μ_{CARINA} [mag]	δ_{stat} [mag]	δ_{MW} [mag]	δ_{CARINA} [mag]	rms [mag]
J	RRab+RRc	**19.921**	0.02	0.024	0.031	0.11
	RRab	**19.954**	0.022	0.022	0.031	0.12
K	RRab+RRc	**19.908**	0.015	0.018	0.024	0.09
	RRab	**19.922**	0.018	0.017	0.025	0.1
W_{JK}	RRab+RRc	**19.899**	0.015	0.017	0.023	0.09
	RRab	**19.899**	0.018	0.016	0.024	0.09

Table 16: Same as Table 15 but based on PLZ relations.

band	population	μ_{FORNAX} [mag]	δ_{stat} [mag]	δ_{MW} [mag]	δ_{FORNAX} [mag]	rms [mag]
J	RRab+RRc	**20.606**	0.015	0.028	0.032	0.13
	RRab	**20.601**	0.016	0.027	0.031	0.13
	RRc	20.574	0.035	0.066	0.075	0.11
K	RRab+RRc	**20.601**	0.013	0.022	0.026	0.11
	RRab	**20.600**	0.013	0.021	0.025	0.11
	RRc	20.561	0.028	0.065	0.071	0.09
W_{JK}	RRab+RRc	**20.599**	0.014	0.020	0.024	0.12
	RRab	**20.601**	0.014	0.019	0.024	0.11
	RRc	20.552	0.032	0.066	0.073	0.1

Table 17: Fornax distance moduli based on PL relations.

band	population	μ_{FORNAX} [mag]	δ_{stat} [mag]	δ_{MW} [mag]	δ_{FORNAX} [mag]	rms [mag]
J	RRab+RRc	**20.611**	0.015	0.024	0.028	0.13
	RRab	**20.625**	0.015	0.022	0.027	0.12
K	RRab+RRc	**20.604**	0.013	0.018	0.022	0.11
	RRab	**20.618**	0.013	0.017	0.021	0.10
W_{JK}	RRab+RRc	**20.601**	0.013	0.017	0.022	0.12
	RRab	**20.613**	0.014	0.016	0.021	0.11

Table 18: Same as Table 17 but based on PLZ relations.

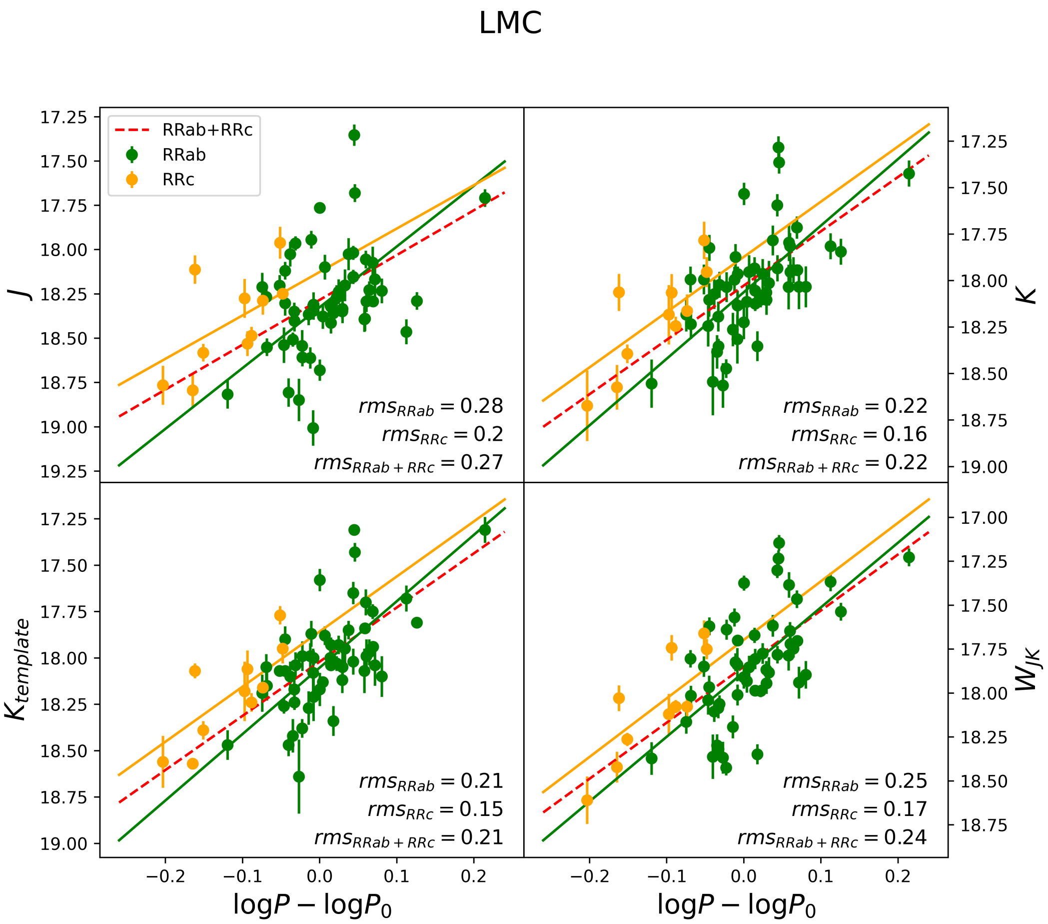

Figure 38: PL relations for RR Lyrae stars from the LMC (Szewczyk et al., 2008) fitted with slopes fixed and taken from the corresponding relations for Milky Way RR Lyrae stars derived in this work.

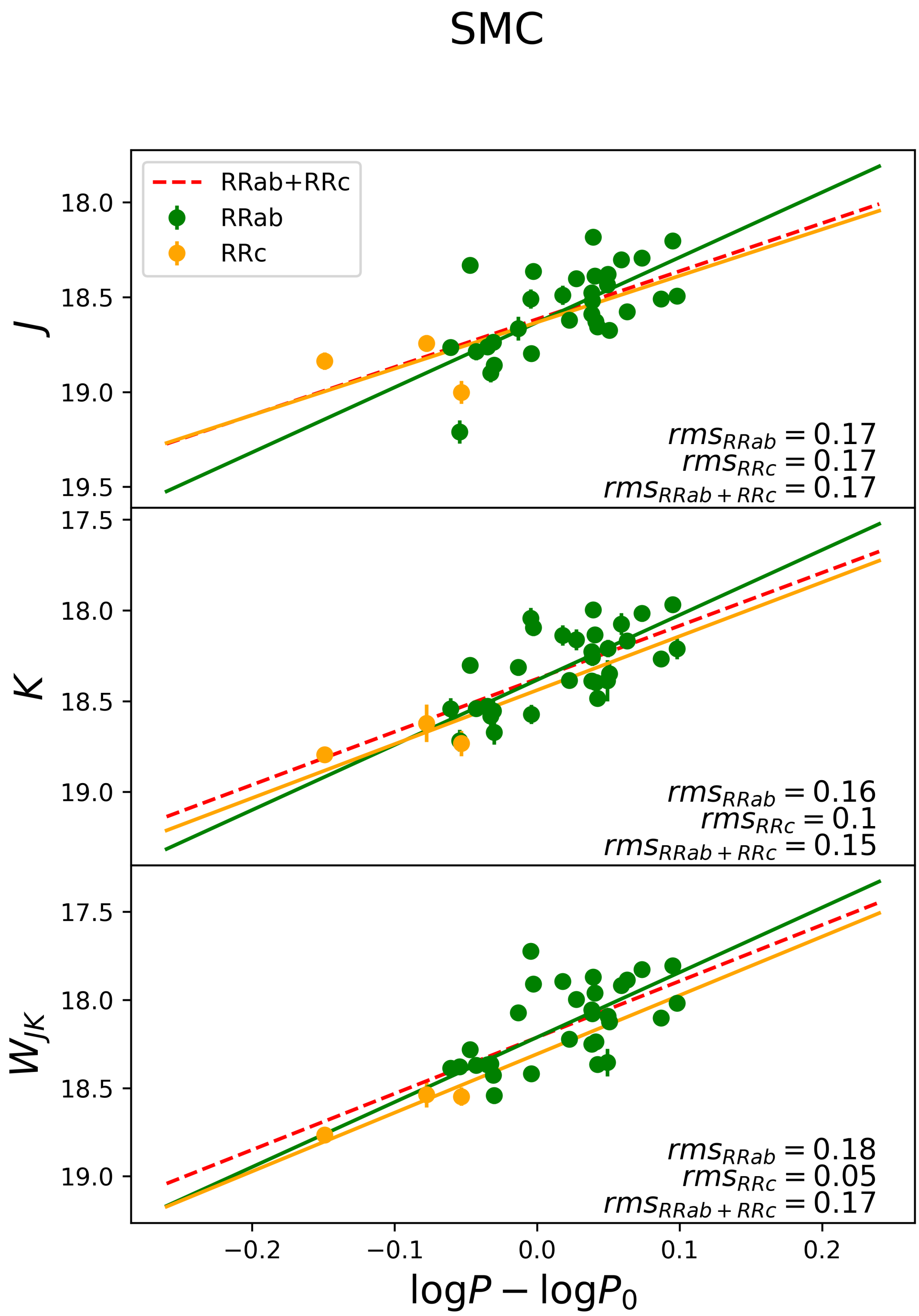

Figure 39: PL relations for RR Lyrae stars from the SMC (Szewczyk et al., 2009) fitted with slopes fixed and taken from the corresponding relations for Milky Way RR Lyrae stars derived in this work.

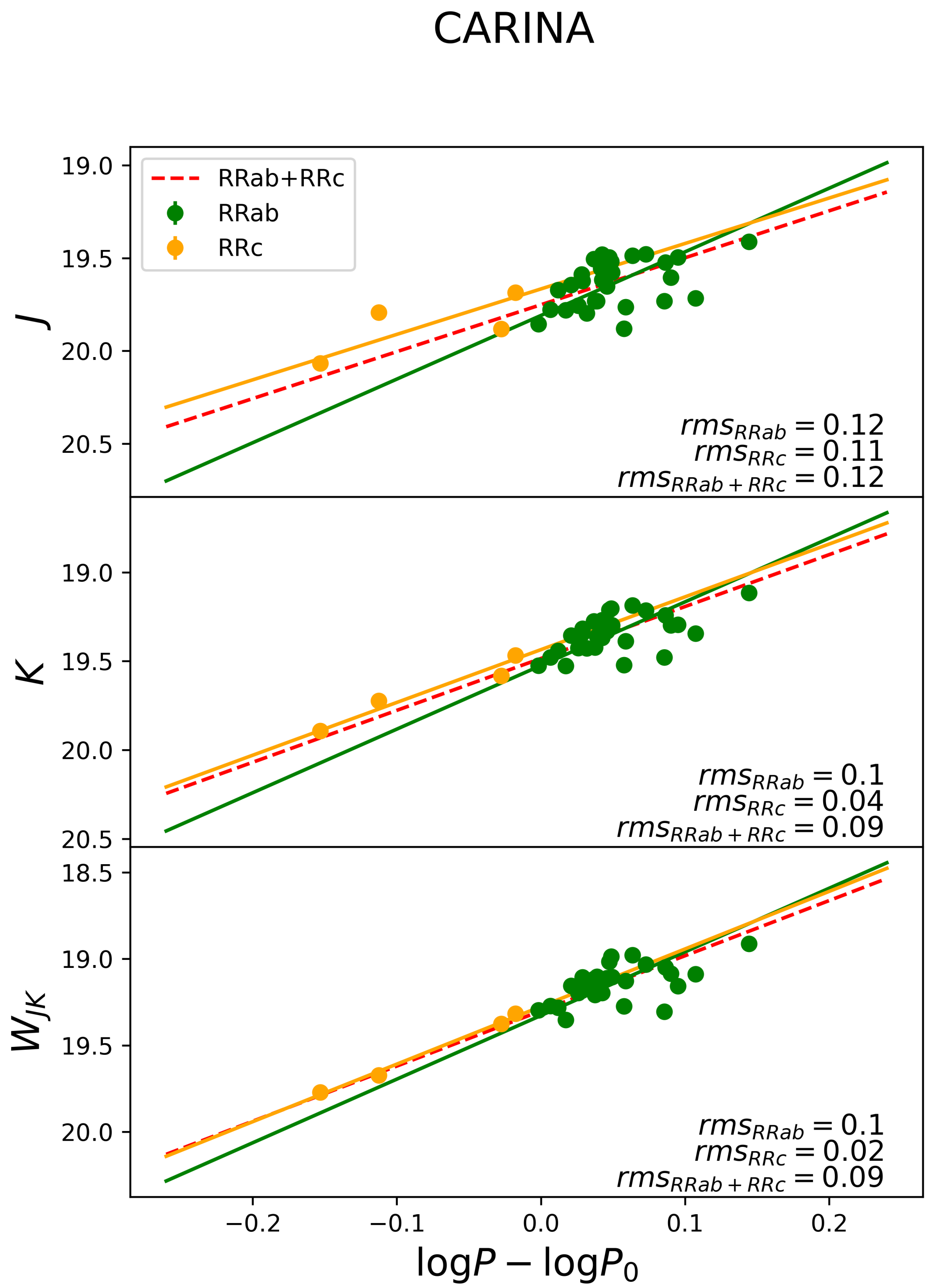

Figure 40: PL relations for RR Lyrae stars from the Carina galaxy (Karczmarek et al., 2015) fitted with slopes fixed and taken from the corresponding relations for Milky Way RR Lyrae stars derived in this work.

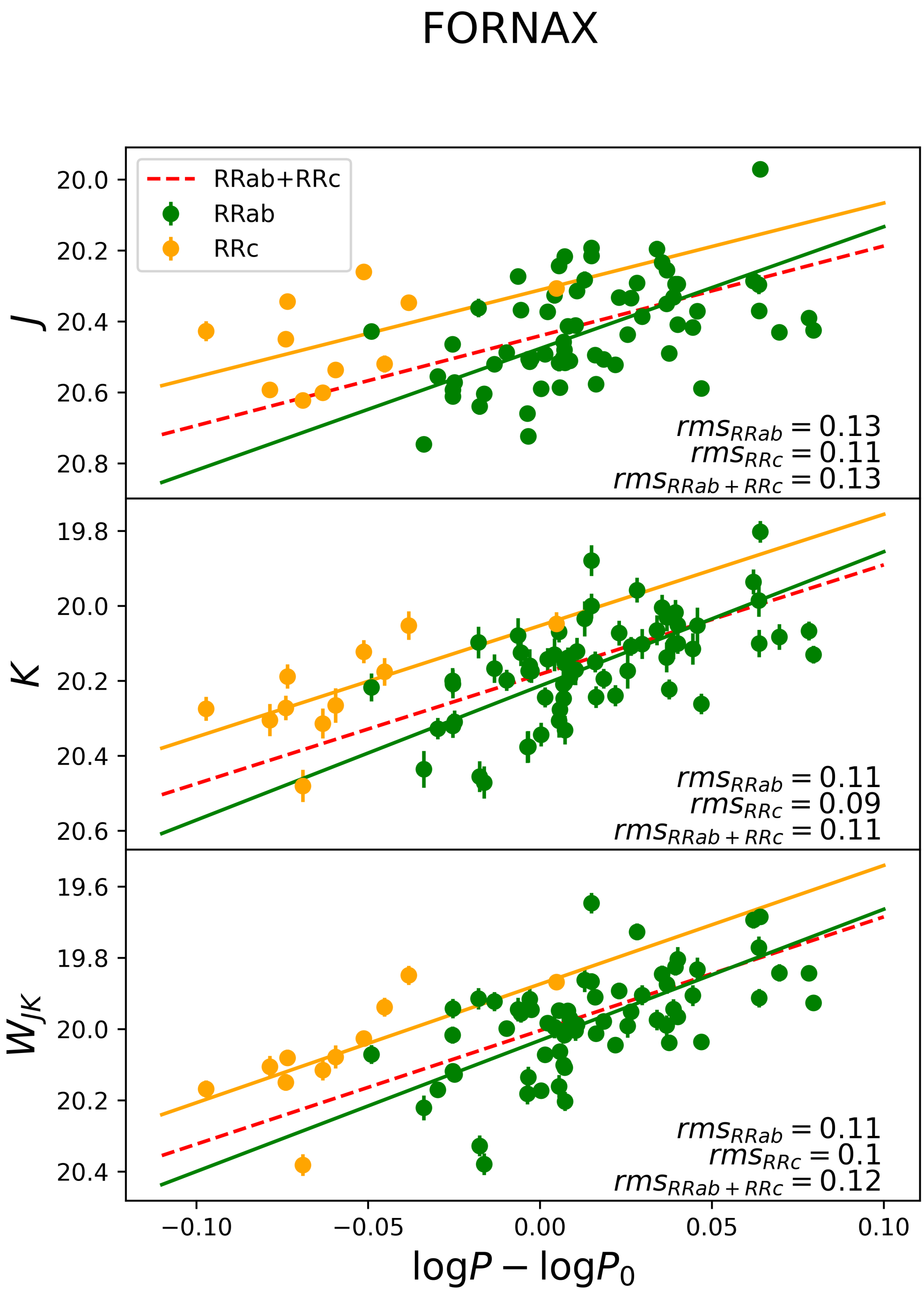

Figure 41: PL relations for RR Lyrae stars from the Fornax galaxy (Karczmarek et al., 2017b) fitted with slopes fixed and taken from the corresponding relations for Milky Way RR Lyrae stars derived in this work.

relations. The corresponding errors δ_{MW} for the fiducial relations play here a role as one of the components of systematic uncertainty. We immediately notice that distances based on RRc stars only have relatively low precision. Usually, the number of these stars is much lower than that of RRab stars. For comparison, I decided to present these distances, too. Keeping in mind that in order to determine a distance, we fit only the intersection of a relation, we may perform such a fit even for just a few stars. The apparent problem with determinations based on such a small number of stars is that the span of their luminosities does not reliably represent the distribution of luminosities resulting from the uniform coverage of the instability strip. Fiducial relations should optimally include stars that cover the strip randomly but, given their relatively large numbers, also uniformly. My fiducial PL relations for RRc stars are based only on 7 objects so they should be treated with caution. On the other hand, with the relatively large uncertainty of their zero points of about 0.065 mag, determinations based on them should still agree with determinations based on relations for RRab stars and the mixed population.

Generally, distances from PL relations are in excellent agreement with those obtained from PLZ relations. The metallicity effect does not seem to play an important role in determining distances to galaxies with metallicities similar to the typical metallicity of a star from the calibrating sample. Likewise, the dependence of NIR absolute magnitudes of RR Lyrae stars on metallicity is small. The divergence between results obtained using PL and PLZ relations is similar to that between results obtained using the mixed population and just fundamental pulsators. Poor fundamentalization of periods of RRc stars does not alter determinations in a significant way.

The sample of RR Lyrae stars from the LMC includes 53 RRab and 10 RRc stars. Distances obtained for the LMC using fiducial relations for RRab and RRab+RRc described in this work are in very good agreement with the canonical value of Pietrzyński et al. (2019). Szewczyk et al. (2008) reports distances between 18.56 ± 0.03 mag (stat. err.) and 18.62 ± 0.03 mag (stat. err.), depending on the used calibration. Finally, they report an average distance of $\mu_{\mathrm{LMC}} = 18.58 \pm 0.03 \pm 0.11$ that agrees with values presented in Tables 11 & 12 only with a large systematic error. The difference between the result of Szewczyk et al. and my results is around 0.13 mag. RRc stars yield systematically smaller distances. This is not a question of the fundamentalization of their periods as this process is exactly the same as for my calibrating sample. Given the large uncertainties of these determinations, they are still in agreement with those based on the two remaining populations. However, a question related to the fundamentalization of periods is the apparent deviation of RRc stars from the PL relation formed by the fundamental pulsators. Again, fundamentalized RRc stars are brighter as if they would follow the same relation as RRab stars.

The SMC sample includes 31 RRab stars and just 3 RRc stars. The distances obtained from RRab and RRab+RRc yield values that are inconsistent with the distance based on eclipsing binaries determined by Graczyk et al. (2020), as they are smaller by about 0.2 mag. It also means that the difference of distance moduli for RR Lyrae stars from the Magellanic Clouds is ~ 0.33 mag. This value is similar to that by Neeley et al. (2019) who found ~ 0.37 mag. On the other hand, it is quite discrepant with the difference of distances of 0.5 mag resulting from the two studies regarding the eclipsing binaries in the Clouds[26]. The SMC is known to be an extended system along the line-of-sight (e.g., Jacyszyn-Dobrzeniecka et al. 2016, Jacyszyn-Dobrzeniecka et al. 2017, Graczyk et al. 2020). The geometric center of the observed sample of RR Lyrae stars in a given system may not coincide with the geometric center of eclipsing binaries used to determine the distance to that system. Szewczyk et al. (2009) derived distances to the SMC between 18.965 ± 0.161 mag and 19.002 ± 0.165 mag (tot. err.) with an average value of $\mu_{\mathrm{SMC}} = 18.97 \pm 0.03 \pm 0.12$, This is exceptionally close to the value of Graczyk et al. but differs again by about 0.2 mag from the estimates in the present work. The determinations based on RRc stars are closer to the canonical value from Graczyk et al..

Similar discrepancies with the original determinations are observed for Carina (29 RRab

[26] Graczyk et al. (2014) fitted a normal distribution to 17 distance differences $\Delta\mu = \mu_{\mathrm{SMC}} - \mu_{\mathrm{LMC}}$ determined using different methods (their Table 11 and Figure 9). They obtained $\Delta\mu = 0.458 \pm 0.068$ mag.

method	$\mu_{\rm SMC} - \mu_{\rm LMC}$ [mag]	$\mu_{\rm C} - \mu_{\rm LMC}$ [mag]	$\mu_{\rm F} - \mu_{\rm LMC}$ [mag]
RC	0.47 ± 0.02	1.67 ± 0.02	2.36 ± 0.02
PLZ RR Lyrae[27]	0.39 ± 0.04	1.54 ± 0.03	2.24 ± 0.03
this work[28]	0.33 ± 0.05	1.47 ± 0.04	2.16 ± 0.04

Table 19: Distance differences between SMC, Carina, Fornax and the LMC for different methods. The first row results from $K-$band photometry of the red clump (RC) of Pietrzyński et al. (2003). Below there are differences of RR Lyrae distances from Szewczyk et al. and Karczmarek et al. based on PLZ relations from Bono et al. (2003), Sollima et al. (2008), Catelan et al. (2004c), and Dékány et al. (2013). The last row contains distance differences obtained in this work resulting from PLZ relations after taking into account just RRab stars and average distance moduli based on $J-$ and $K-$bands. Uncertainties are just superpositions of statistical uncertainties of distances corresponding to the LMC and to a given object.

and 4 RRc stars) and Fornax (66 RRab and 11 RRc stars). Karczmarek et al. (2015) reported distances between $20.078 \pm 0.016 \pm 0.090$ mag and $20.142 \pm 0.016 \pm 0.110$ mag for Carina, with the average value of $\mu_{\rm CARINA} = 20.118 \pm 0.017 \pm 0.11$ mag. In the case of Fornax, Karczmarek et al. (2017b) found distances between $20.787 \pm 0.013 \pm 0.116$ mag and $20.837 \pm 0.015 \pm 0.083$ mag with the average distance modulus of $\mu_{\rm FORNAX} = 20.818 \pm 0.015 \pm 0.116$ mag. Both average distances are about 0.2 mag larger than values resulting from calibrations based on parallaxes based on GAIA EDR3 presented in this work.

Pietrzyński et al. (2003) obtained a distance to Carina of $\mu_{\rm CARINA} = 20.165 \pm 0.015$ mag and to Fornax of $\mu_{\rm FORNAX} = 20.858 \pm 0.013$ mag (statistical errors) using $K-$band photometry of red clump (RC) stars. Systematic uncertainties corresponding to the red clump distances are unknown. Thus, it is hard to compare them with RR Lyrae distances resulting from my calibration.

Pietrzyński et al. (2009) reported the following distances based on J and K photometry of the TRGB: $\mu_{{\rm CARINA},J} = 20.09 \pm 0.03 \pm 0.12$ mag, $\mu_{{\rm CARINA},K} = 20.13 \pm 0.04 \pm 0.14$ mag, $\mu_{{\rm FORNAX},J} = 20.84 \pm 0.03 \pm 0.12$ mag, and $\mu_{{\rm FORNAX},K} = 20.84 \pm 0.04 \pm 0.14$ mag. Only large systematic uncertainties allow for an agreement of these values with my results.

Interestingly, the distances obtained by Pietrzyński et al. (2003) from $K-$band photometry of the red clump are different from those resulting from PLZ relations for RR Lyrae stars. Table 19 contains differences of distances between the LMC and the SMC, Carina, and Fornax. Even though I am using the photometry of RR Lyrae stars published by Szewczyk et al. and Karczmarek et al., the differences I obtain are different from those originally reported by these authors, but still in agreement within the statistical uncertainties. The original distances were based on $K-$band PLZ relations of Bono et al. (2003), Sollima et al. (2008), and J and K relations of Catelan et al. (2004c) (with the Carina distance additionally based on the Dékány et al. 2013 relation for the $K-$ band); distances resulting from different calibrations were averaged.

On the other hand, Mackey & Gilmore (2003) found a mean distance of Fornax of $\mu_{\rm FORNAX} = 20.66 \pm 0.03 \pm 0.15$ mag based on the $V-$band magnitude of RR Lyrae stars. It is in agreement with my result within the statistical uncertainty. The authors determined distances to four globular clusters in the galaxy and reported its relatively large depth along the line of sight. The distance moduli of the clusters were determined between 20.58 and 20.74 mag with statistical uncertainties of 0.05 mag. These distances are based on the calibration of the absolute $V-$band magnitude of RR Lyrae stars from Chaboyer (1999) that is based on the Hipparchos parallaxes.

The substantial systematic uncertainty that affects distance determinations, besides $\delta_{\rm MW}$, is associated with the uncertainty of the mean metallicity of samples. Adopting a conservative value of ± 0.25 dex and a metallicity slope of ~ 0.1 mag/dex, we obtain an uncertainty of 0.025 mag that should be added quadratically to the reported uncertainties. When it comes to the uncertainty associated with the reddening, determinations based on the Wesenheit index play a control role here. Distances based on both $J-$ and $K-$bands are in good agreement with those resulting from W_{JK}. Systematic errors of the PL and PLZ relation zero points arising from the calibration of the IRIS photometry onto the 2MASS system using comparison stars from the 2MASS catalog are estimated to be 0.002 mag (Wielgórski et al., 2021). This is the error of the mean calculated by comparing magnitudes of a control set of constant stars obtained from calibrated IRIS photometry with their catalog values. The systematic photometric error is negligible compared to other uncertainties in this case. Another systematic uncertainty that is especially vague and hard to estimate is connected to the uncertainty of the zero point of the GAIA EDR3 parallaxes.

4.2.4 On the parallax zero point and its influence on calibrations

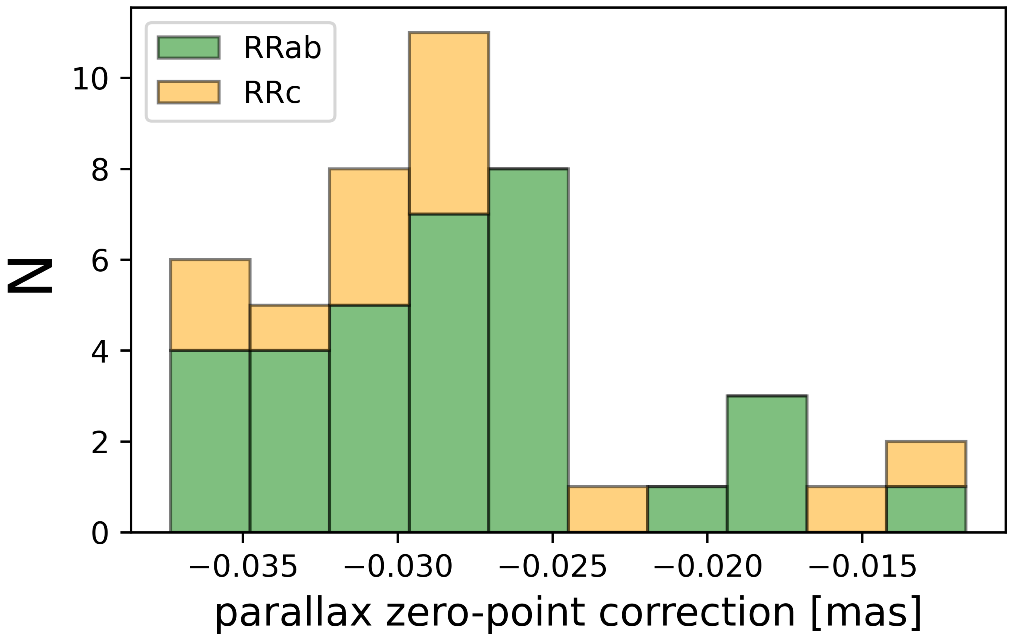

Figure 42: Corrections of Lindegren et al. (2021) for objects from my calibrating sample.

A proper calibration of the GAIA EDR3 parallaxes is pivotal for any calibration of distance indicators. It is a complex issue as the parallax zero point depends on different variables such as the stellar color, magnitude, or position of an object in the celestial sphere. The original GAIA EDR3 parallaxes used for the purpose of calibrations presented in this work were corrected using the Lindegren et al. (2021) corrections. The same corrections were used in the Bailer-Jones et al. (2021) study in order to derive geometric and photo-geometric distances. They were estimated for single objects based on distant quasars and LMC sources that provided a fixed reference frame. However, in the case of bright stars ($G < 13$ mag, where G is the GAIA photometric band, all RR Lyraes from my sample have $G \sim 9-11.5$ mag); the authors had to use binaries with similar parallaxes but different colors and magnitudes. Given such *physical pairs* and using known biases for fainter sources, they were allowed to estimate biases for brighter companions and subsequently obtained a correcting relation for bright sources. Figure 42 depicts the distribution of corrections of Lindegren et al. for objects from my calibrating sample. The median value of corrections is -0.029 mas[29].

Figure 43, inspired by the analysis done by Neeley et al. (2019), depicts a relationship between parallax systematic shift, relative to parallaxes corrected using the Lindegren et al.

[29]Such negative corrections were subtracted from the original GAIA EDR3 parallaxes, so that parallaxes became larger and the resulting distances smaller.

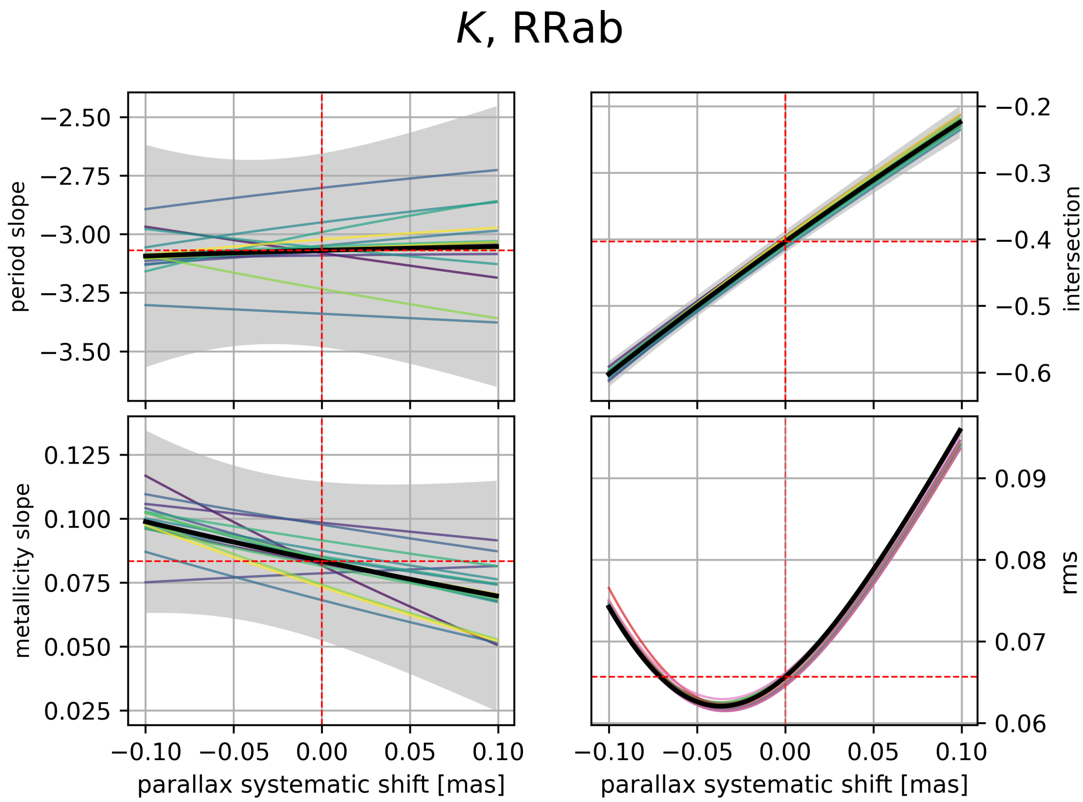

Figure 43: Dependence of PLZ parameters from the systematic parallax shift relative to parallaxes corrected according to Lindegren et al. (2021). Thick black lines denote fits using the whole sample of RRab. Thinner colored lines correspond to jackknife resampling, where one star from the sample was rejected for the purpose of each fit. The gray zone denotes the 1σ uncertainty of each parameter. The red dashed lines correspond to the values of parameters realized in the fit using the Lindegren et al. parallax corrections and the whole sample of RRab.

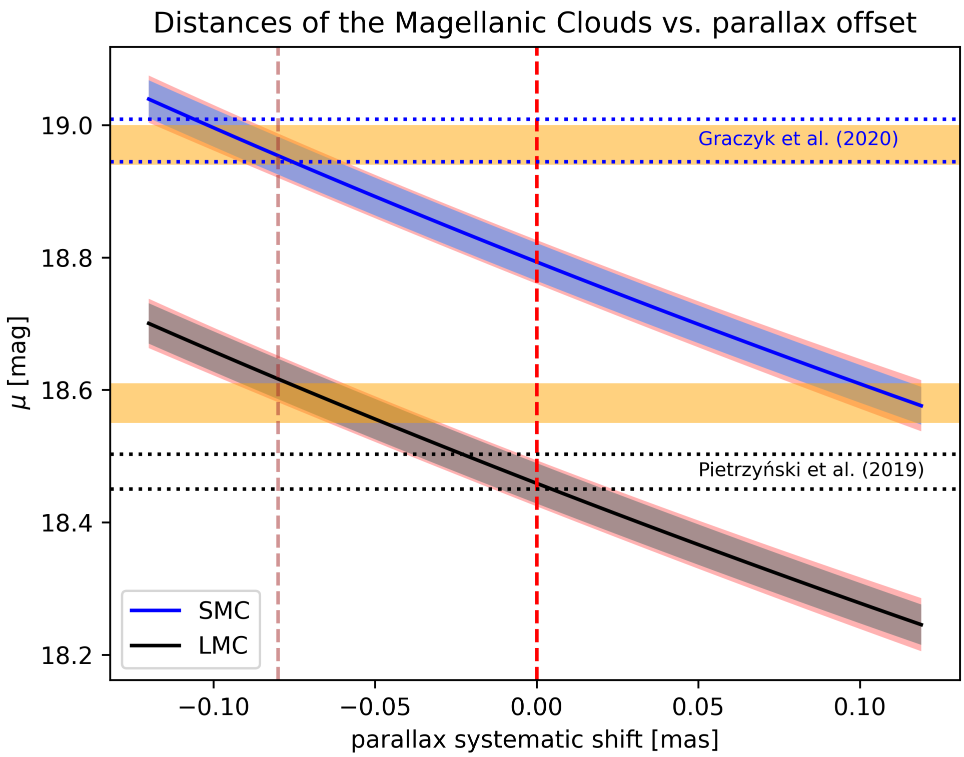

Figure 44: Dependences of distances to each of the Magellanic Clouds ($K-$ band, RRab stars) from the systematic parallax offset, relative to GAIA EDR3 parallaxes with Lindegren et al. (2021) corrections, based on photometry of RR Lyrae stars from the LMC and the SMC from Szewczyk et al. (2008) and Szewczyk et al. (2009). Zone around each of the relations corresponds to the statistical error δ_{stat}. Superpositions of uncertainties of fiducial intersections of PLZ relation and their LMC and SMC counterparts, $\delta_{\rm LMC}$, $\delta_{\rm SMC} = \sqrt{\delta^2_{\rm MW} + \delta^2_{stat}}$, are denoted using rose-colored areas - they do not differ much from the statistical errors. Canonical distances of Pietrzyński et al. (2019) and Graczyk et al. (2020) within their 1σ total errors are given for comparison. Orange zones denote original results of Szewczyk et al. within their statistical uncertainties. These determinations would be in agreement with my calibrations if GAIA parallaxes were shifted by -0.08 mas.

(2021) corrections, and parameters of PLZ relation for the example of $K-$band and the RRab population. Other cases look very similar. One can clearly see that the rms of the fit has a minimum; it depends on the band and the used population of RR Lyrae. Colored lines correspond to fits with one star rejected (the jackknife resampling); they all lie within the 1σ zone of the line corresponding to fits based on the whole sample.

Figure 44 presents the relation between the parallax offset and the distances to the Magellanic Clouds ($K-$band, fundamental pulsators only) together with the comparison of the canonical distances obtained using eclipsing binaries and original distances reported by Szewczyk et al.. Differences of distance moduli between the two Clouds are constant for all parallax shifts, as expected. The original distance moduli of Szewczyk et al. would be in agreement with my calibrations of PLZ relations after applying a -0.08 mas systematic parallax shift. In any case, distance differences between the SMC and the LMC obtained from RR Lyrae stars differ from those obtained from eclipsing binaries.

Lindegren et al. (2021) estimate the uncertainty of parallax corrections of a few μas (microarcseconds). After assuming the conservative error of $10\,\mu as$, we obtain a parallax component of the systematic uncertainty of the zero point of my calibration of around 0.02 mag. This is the dominating component of the total systematic uncertainty for the zero point of PL and PLZ relations. The combination of the above uncertainty with the metallicity error (~ 0.025 mag) and the statistical uncertainty of intersection of the PL(Z) relation (~ 0.025 mag) yields the total systematic uncertainty of the distance of 0.04 mag.

4.3 The Baade-Wesselink method for RR Lyrae stars

The Baade-Wesselink (B-W) method (Baade 1926, Wesselink 1946) appeared as an idea for testing the pulsation hypothesis and for determining the mean radii of classical Cepheids. The method also allows to determine geometrical distances to single, radially pulsating stars. The inference is based on changes of the stellar metric radius and its angular diameter:

$$\theta(\phi) = \frac{2R(\phi)}{r} = \frac{2\left[R_0 + \Delta R(\phi)\right]}{r} = 2\varpi\left[R_0 + \Delta R(\phi)\right] \tag{19}$$

where θ is the angular diameter of a star for a given pulsation phase ϕ; R is the metric radius of the star, r is its distance, and ϖ is the corresponding parallax. R_0 is the radius of the pulsator corresponding to (arbitrarily chosen) $\phi = 0$ while ΔR corresponds to its variations in time.

Determinations of the angular diameter may be carried out directly through interferometry or using a previously-calibrated surface brightness-color relation (SBCR) that allows for the derivation of stellar angular diameter from the color and $V-$band magnitude of the star. The latter is a far more economical approach as photometry is more accessible and less demanding instrumentally than interferometry.

On the other hand, changes of stellar radius can be tracked through integration of radial velocity curve obtained using spectroscopy:

$$\Delta R(\phi) = -\int p\left[v_r(\phi) - v_{r,0}\right] d\phi \tag{20}$$

where $v_r(\phi)$ is the radial velocity of the object measured using spectroscopy, $v_{0,r}$ is its systemic (average) radial velocity obtained from integrating the radial velocity over the whole phase; p is a *projection factor*[30], also known as the *p-factor*. It is a parameter, whose calibration is crucial for this method of distance determinations. The factor plays a normalization role, taking into account mostly geometrical effects, limb darkening but also velocity gradients in the stellar atmosphere (Nardetto et al., 2017). Figure 45 presents a qualitative depiction of the reason for normalization of the integral of the apparent radial velocity of a star to properly determine variations of its radius. The derived values of $p-$factors depend on many arbitrary

[30] In my considerations, I will assume that p does not depend on the pulsation phase.

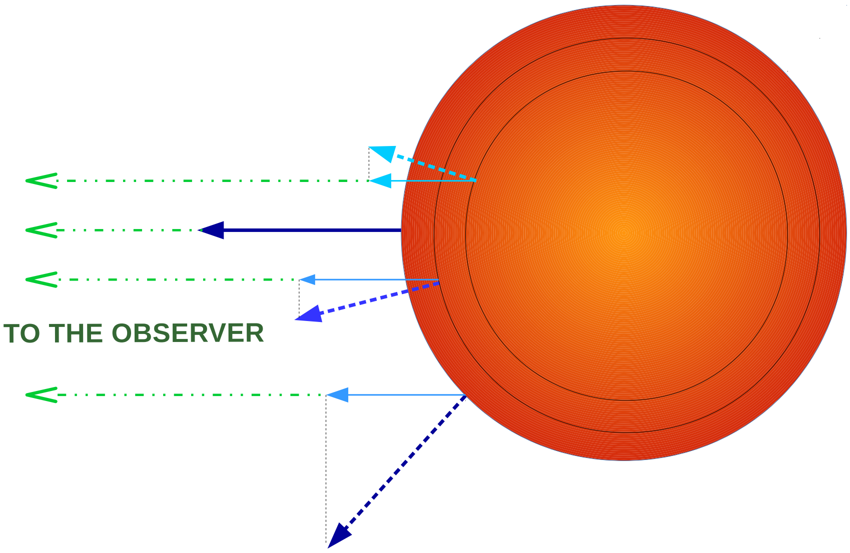

Figure 45: Qualitative depiction of the need to utilize the $p-$ factor. Spectrographs that we use allow for measuring the *effective* (i.e., net, single) radial velocity of the stellar photosphere for a given pulsation phase. However, spectral lines (and their corresponding shifts relative to the reference, laboratory wavelengths) correspond to different layers of the stellar atmosphere that move radially with different velocities at a given phase. Additionally, the radial velocity of a radially-pulsating star corresponds to the velocity of its photosphere only in the geometric center of the observed (but not resolved) stellar disk, and we measure a superposition of radial components of velocity integrated over the whole disk. Limb darkening introduces weights to representations of zones (and the corresponding velocities) at different distances from the center of the stellar disk.

choices fixed for a specific method. That is the reason why consistent methodology must be used for calibration and application of the method.

The B-W method has been most notably used for classical Cepheids. Among the important studies from the last decade there is the paper by Storm et al. (2011), who calibrated the dependence of classical Cepheid $p-$factor on their pulsation period and established the Galactic PL relations for Cepheids using their B-W distances. Gieren et al. (2018) investigated the dependence of Cepheid PL relations on metallicity through the determination of distances to single stars in the Milky Way and the Magellanic Clouds based on the dependence of the $p-$factor on pulsation period by Storm et al.. Researches paid much attention to the calibration of $p-$factors with the aspiration to obtain distances to single stars with precision up to a few percent. However, lately, Trahin et al. (2021) studied the dependence of the $p-$factor on a number of parameters, including the pulsation period for a sample of 63 Galactic Cepheids. They reported a relatively large dispersion of the determined projection factors and have not found any clear correlation with any other quantity. This study suggests that, at least in the case of classical Cepheids, an easy representation of a complex phenomenon using a single parameter could be overly optimistic.

Research on the B-W method for RR Lyrae stars was carried out primarily in the 1980s and early 1990s. Series of studies devoted to the estimation of mean absolute – bolometric and visual – magnitudes of field Galactic RR Lyrae stars and their possible dependence on metallicity were released. They based on the notion of the visual surface brightness S_V (Wesselink 1969, reevaluation by Manduca & Bell 1981), a quantity that binds the effective stellar temperature and the bolometric correction in the $V-$band on the one hand, and the angular diameter and the apparent V magnitude on the other hand.

In one of the series of papers (Carney & Latham 1984; Jones et al. 1987a, 1987b; Jones 1988; Jones et al. 1988a, 1988b, 1992; Carney et al. 1992), the authors assumed values for the $p-$factor from $p = 1.30$ to 1.36. In their second paper (Jones et al., 1987a) introduced an analysis that relied on estimating the stellar apparent bolometric magnitude and effective temperature using the $(V - K)$ color. The authors estimated that this specific method should yield an accuracy for the absolute magnitude of an RR Lyrae star of about 0.1 mag. In the same paper, the authors recognized the influence of shock waves appearing in the atmosphere of RR Lyrae stars (Hill, 1972) that manifested itself as a bump near the minimum brightness in the V light curve and the corresponding anomalous measurements of the radial velocity. This resulted in a poor correspondence between the changes of the radius derived from the radial velocity curve and changes of the angular diameter derived from spectroscopy for pulsation phases affected by a shock. Such phase intervals apparently affected by shocks were rejected in this and in the following studies.

In another series (Cacciari et al. 1989a, 1989b; Clementini et al. 1990), the authors based on $(V - I)$ and $(V - R)$ colors to derive angular diameters of stars. They assumed $p = 1.36$.

Liu & Janes (1990a) performed a similar analysis as Jones et al. (1987a) and, assuming $p = 1.32$, derived absolute magnitudes of 13 field RR Lyrae stars. In a following paper (Liu & Janes, 1990b), they determined absolute magnitudes of 4 stars from the globular cluster M 4.

Yet another series of papers (Fernley et al. 1989, Skillen et al. 1989, Fernley et al. 1990a, Fernley et al. 1990b, Skillen et al. 1993) is based on a different (but qualitatively similar) approach than that deriving from the work of Manduca & Bell (1981). It is the *infrared flux method* of Blackwell & Shallis (1977) that utilizes the well-covered ultraviolet, optical, and NIR photometry to determine the angular diameter at a given pulsation phase. The authors calibrated the mean absolute magnitude and metallicity dependencies for field Galactic RR Lyrae stars in $V-$ and $K-$ bands. They used $p = 1.33$ and noted its 3% uncertainty by comparing their results with those of other researchers.

More recently, Jurcsik et al. (2017a) applied the B-W method to determine distances to 26 RR Lyrae stars from the globular cluster M 3 based on the dependence of the effective temperature and $\log g$ on the optical color $(V - I)_C$ from atmospheric models of Castelli & Kurucz (2003). The authors applied $p = 1.35$, as modeled by Nardetto et al. (2004). In a later work, Jurcsik & Hajdu (2017b) studied the B-W method for Blazhko RR Lyrae stars from M 3. They showed that the distances derived for these stars are not reliable as there is a large discrepancy between the changes of the angular diameter and the radius of a Blazhko star; the distances varied with different modulation phases.

In the era of GAIA parallaxes, a phenomenological determination of $p-$factors for Galactic RR Lyrae stars is possible. Trahin et al. (2018) determined $p = 1.34 \pm 0.07$ for the prototype star *RR Lyr* based on its GAIA DR2 parallax and using *SPIPS* code (Mérand et al., 2015). In my thesis, I am showing the determination of $p-$factors for two RR Lyrae stars, *RX Eri* and *U Lep* based on the *NIR surface brightness method*.

4.3.1 The IRSB method

The surface brightness of an extended celestial object in a given band λ is defined as:

$$S_\lambda := m_\lambda + 2.5 \log A \tag{21}$$

where m_λ is the apparent magnitude integrated over the whole considered area A spanned on the celestial sphere (in fact, A is a solid angle). The surface brightness is a quantity independent of distance (given no extinction) as both the measured flux F_λ and the observed area are inversely proportional to the squared distance of the object. We may easily deduce[31] that in the case of stars S_λ can be written in terms of the stellar angular diameter θ:

[31] Assuming the local flatness of the celestial sphere for small θ.

$$S_\lambda = m_\lambda + 2.5\log\left(\frac{1}{4}\pi\theta^2\right) = m_\lambda + 5\log\theta + 2.5\log\left(\frac{1}{4}\pi\right) \tag{22}$$

Knowing that the amount of energy released from the unit of stellar surface by means of radiation is proportional to T^4 where T is the effective stellar temperature in Kelvin (the Stefan-Boltzmann law), we may write:

$$m_{bol} = -2.5\log T^4 + const. = -10\log T + const. \tag{23}$$

where m_{bol} is the bolometric magnitude, and the constant includes the arbitrary photometric zero point[32].

The bolometric magnitude is related to magnitude in a given band λ through the bolometric correction BC_λ:

$$BC_\lambda = m_{bol} - m_\lambda \tag{24}$$

that depends on the spectral type and luminosity class of a star. It allows us to rewrite the equation (21):

$$S_\lambda = m_{bol} - BC_\lambda + 2.5\log A = -10\log T - BC_\lambda + 2.5\log A + const. \tag{25}$$

Let us consider a quantity that is linearly connected to S_λ (Barnes & Evans, 1976):

$$\log T + 0.1BC_\lambda \tag{26}$$

We will now derive its relation to the stellar angular diameter given in mas (milliarcsec). Keeping in mind the definition of parsec that introduces the astronomical *angle measure of an arc*, we know that mas×kpc=AU, where AU is the astronomical unit. These will be the natural units used in our B-W considerations. The distance to the star is expressed in kpc, its radius R and diameter D are expressed in AU, and its angular diameter θ is expressed in mas. We should re-phrase the distance modulus so that the distance x is expressed in kpc ($x \times 10^3 = r$):

$$(m - M) = 5\log x + 10 \tag{27}$$

Adding that the luminosity $L \propto D^2T^4$ and that the stellar absolute bolometric magnitude is associated with the solar bolometric magnitude through $M_{bol} = M_{bol\odot} - 2.5\log L/L_\odot$, we may continue with (26):

$$\begin{aligned}
\log T + 0.1BC_\lambda &= \log T_\odot + 0.25\log(L/L_\odot) + 0.5\log(D_\odot/D) + 0.1(m_{bol} - m_\lambda) = \\
&= \log T_\odot + 0.25\log(L/L_\odot) + 0.5\log(D_\odot/D) + \\
&+ 0.1[5\log x + 10 + M_{bol\odot} - 2.5\log(L/L_\odot)] - 0.1m_\lambda = \\
&= 0.5\log D_\odot - 0.5\log(D/x) + 0.1M_{bol\odot} + 1 + \log T_\odot - 0.1m_\lambda = \\
&= 0.5\log D_\odot - 0.5\log\theta + 0.1M_{bol\odot} + 1 + \log T_\odot - 0.1m_\lambda
\end{aligned} \tag{28}$$

We may insert $D_\odot = 0.0093\,\mathrm{AU}$, $M_{bol,\odot} = 4.74\,\mathrm{mag}$, and $T_\odot = 5780\,\mathrm{K}$ and thus obtain $\log T + 0.1BC_\lambda = 4.22 - 0.1m_\lambda - 0.5\log\theta$. In their original paper, Barnes & Evans (1976) defined a quantity named the *visual surface brightness*:

$$F_V := 4.2207 - 0.1V_0 - 0.5\log\theta \tag{29}$$

[32] According to the Resolution B2 of the International Astronomical Union from 2015 (`https://www.iau.org/static/resolutions/IAU2015_English.pdf`) it is recommended that in the case of the absolute bolometric magnitude scale the zero point $m_{bol} = 0\,\mathrm{mag}$ corresponds to the an irradiance of $f = 2.518021002... \times 10^{-8} W/m^2$, which corresponds to the solar absolute bolometric magnitude of $M_\odot = 4.739996 \approx 4.74\,\mathrm{mag}$ given the nominal solar luminosity of $L_\odot = 3.828 \times 10^{26}$ W.

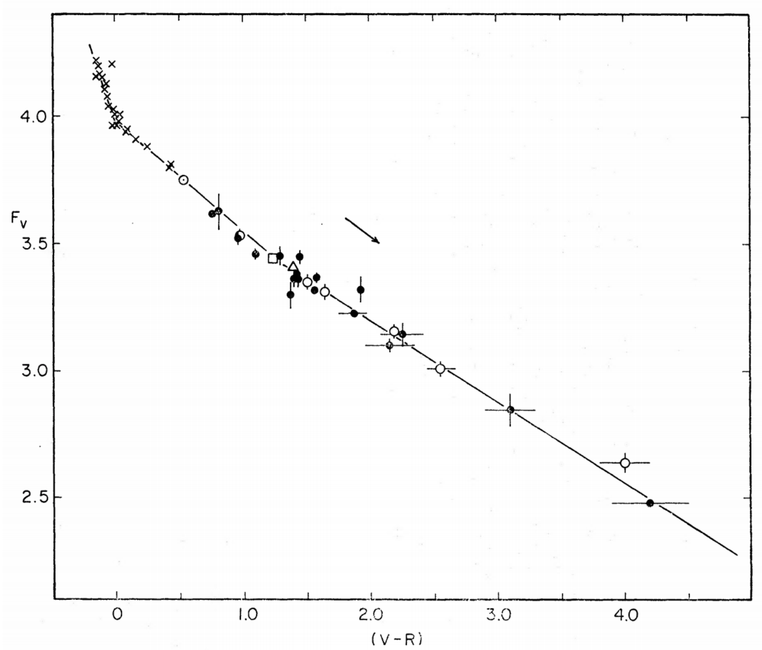

Figure 46: Dependence of the visual surface brightness F_V from the $(V-R)_0$ color as determined by Barnes & Evans (1976). Note that the reddening vector is parallel to the relation in a good approximation. The original figure is taken from `https://articles.adsabs.harvard.edu/pdf/1976MNRAS.174..489B`.

where V_0 is the dereddened $V-$band magnitude. We may expect that F_V depends on stellar color as it is a value derived from the effective temperature and the bolometric correction only. In principle, it could also depend on the metallicity and gravity of objects. Barnes & Evans studied phenomenological correlations between F_V and different optical colors such as $(B-V)_0$, $(V-R)_0$, and $(I-R)_0$. Such relations are known in the literature as the surface brightness-color relations (SBCR). The stellar angular diameters required to calibrate these relations were obtained during lunar occultations and through interferometry. Out of different studied relations, the one depending on $(V-R)_0$ was found to have the smallest scatter. Figure 46 presents that original relation of Barnes & Evans.

Welch (1994) extended the method into the NIR and found that the scatter of the empirical dependence of F_V from $(V-K)_0$ color is significantly lower than that based on merely optical bands for classical Cepheids. Other calibrations followed, and the method became known as the (near-)infrared surface brightness - color technique (IRSB). Fouqué & Gieren (1997) presented a $F_V(V-K)$ calibration for classical Cepheids based on interferometric observations of cool giants and supergiants:

$$F_V = (3.947 \pm 0.003) - (0.131 \pm 0.002)(V-K)_0 \tag{30}$$

Kervella et al. (2004a) calibrated the NIR SBCR for dwarfs and subgiants using interferometry of such stars. The authors found:

$$F_V(Dwarf) = (3.9618 \pm 0.0011) - (0.1376 \pm 0.0005)(V-K)_0 \tag{31}$$

In another paper, Kervella et al. (2004b) calibrated an analog relation for classical Cepheids. They found values of parameters in agreement with the relation of Fouqué & Gieren but more precise:

$$F_V(Ceph.) = (3.9530 \pm 0.0006) - (0.1336 \pm 0.0008)(V-K)_0 \tag{32}$$

The relation for classical Cepheids is also in good correspondence with the relation for dwarfs and subgiants (31). For any given Cepheid color $F_V(Dwarf) - F_V(Ceph.) < 0.005$. Stars of the two luminosity classes have radii between 0.15 and 200 $R_\odot$ and gravities between $\log g = 1.5$ and 5.2. The good agreement between the two relations suggests that the $(V-K)_0$ color is indeed a good tracer of the effective temperature and depends little on the gravity. Di Benedetto (2005) confirmed the convergence between relations for dwarfs and giants, obtaining a difference of about 1%.

Studies also show that SBCR relations including the $(V-K)_0$ color are virtually independent on metallicity (e.g., Thompson et al. 2001, Pietrzyński et al. 2019).

Even though RR Lyrae stars are Population II, metal-poor stars which are hotter than Cepheids, the above arguments suggest that SBCR relations, which were not established based on RR Lyrae stars, may be used to determine their angular diameter with a good precision.

The most recent determinations of SBCR relations include the study of Graczyk et al. (2021), where it is estimated that the relation between the visual surface brightness and $(V-K)_0$ color gives a precision of 1.1% in predictions of angular diameters in the color range $[-0.2; 2.1]$. The relation is nominally derived for dwarfs and subgiants. The work is based on eclipsing binary stars and the relations were calibrated using GAIA EDR3 parallaxes. The visual surface brightness is defined slightly different in that work, as its definition is derived directly from (22); it differs only by the rejection of the constant:

$$S_V := V_0 + 5 \log \theta \tag{33}$$

Thus it is connected to F_V as:

$$F_V = 4.2207 - 0.1 S_V \tag{34}$$

The SBCR relation is given as a fifth-order polynomial of $X := (V-K)_0$:

$$S_V = 2.521 + 1.708 \times X - 0.705 \times X^2 + 0.623 \times X^3 - 0.239 \times X^4 + 0.0313 \times X^5 \tag{35}$$

In summary, the angular diameter (in mas) that might be inserted directly into the B-W equation (19) is given as:

$$\theta = 10^{2(4.2207 - 0.1 V_0 - F_V)} \tag{36}$$

or, alternatively, using S_V as:

$$\theta = 10^{0.2(S_V - V_0)} \tag{37}$$

A big advantage of the *photometric* angular diameter obtained using the IRSB technique based on the$(V-K)_0$ color is that it depends little on the reddening. If we insert the relation of Kervella et al. (2004b) (32) with apparent, reddened photometry into the expression for the angular diameter (36), we get:

$$\begin{aligned} \log \theta &= 2\left[0.2677 - 0.1V + 0.1336(V-K)\right] = \\ &= 2\left[(0.2677 - 0.1V_0 + 0.1336(V-K)_0 - 0.1A_V + 0.1336E(V-K)\right] \end{aligned} \tag{38}$$

Given the extinction ratio of $A_K/A_V = 0.117$ (Table 1), we have $A_V/E(V-K) = 1.1325$ so that the total extinction component above $2 \times [0.1336E(V-K) - 0.1A_V] = 0.041E(V-K) = 0.036A_V$.

I will now describe the methodology leading to determining $p-$factors used in my work. The analysis starts with fits of the well-covered radial velocity curve and light curve in the $V-$ band. However, in the case of the B-W approach, I am not using the fit of the Fourier series but rather a curve interpolating binned data using an *Akima spline* (Akima, 1970) through its implementation in SciPy (Virtanen et al., 2020). Akima spline is a piecewise function made

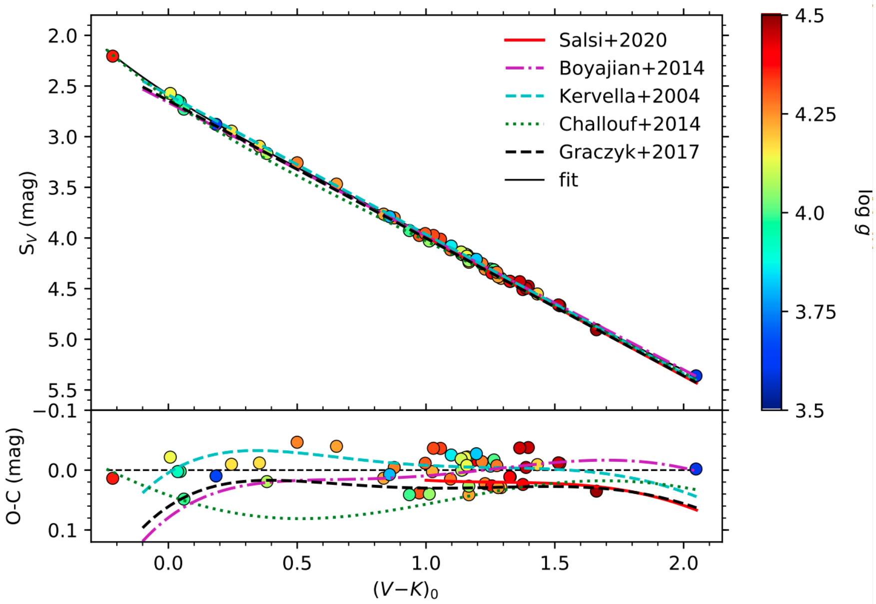

Figure 47: $S_V(V-K)$ surface brightness-color relation of Graczyk et al. (2021). Figure taken from `https://arxiv.org/abs/2103.02077`.

out of cubic polynomials. A valuable property of this mathematical method is that such a spline does not oscillate between data points (through which it passes). Such a behavior allows for a more accurate modeling of periodic physical variations, especially when dealing with a non-uniform coverage of the phase. In my implementation of this method, I fit splines to sets of binned data where every bin is a moving average calculated for adjustable averaging phase range and resolution of bins (i.e., the steps of the moving average are independent from the averaging span). In general, the Akima spline is not a periodic function. In order to force its periodic behavior, I fit a curve to three courses of data over their entire phase: $\phi \in [-1, 2]$.

The integration of the fitted radial velocity curve allows for modeling the radius variations (divided by the $p-$factor). On the other hand, variations of the angular diameter are tracked through SBCR after determining $(V-K)_0$ for a given phase. In my work, I am comparing results obtained using the relations of Kervella et al. (2004a) for dwarfs and subgiants, of Kervella et al. (2004b) for classical Cepheids, and of Graczyk et al. (2021) also for dwarfs and subgiants. While the relation of Graczyk et al. is calibrated in the 2MASS system, the same as my IRIS photometry, Kervella et al. give relation calibrated in the NIR SAAO photometric system. I have transformed K_{2MASS} band into K_{SAAO} using transformation equations given in Koen et al. (2007)[33]. All three relations are calibrated in the Johnson $V-$band – the same as my $V-$band data from VYSOS 16. I have dereddened the photometry using the same approach as in the previous chapter devoted to PL relations[34]. I determine the $(V-K)_0$ color for each $K-$band epoch. The V magnitude for a given phase is interpolated using the corresponding spline fit. The measured K magnitude is subtracted from the modeled V magnitude. Such a choice is purely arbitrary and is dictated by the fact of having usually more K epochs than V epochs. Finally, the angular diameters are determined for phases corresponding to the K magnitude measurements.

The zero phase is also a subject of choice. Like other authors in the case of classical Cepheids

[33]The mean shift resulting from the transformation between the two photometric systems for my stars is (3 ± 9) mmag. It corresponds to the shift of the angular diameter of $(1 \pm 3) \times 10^{-3}$ mas. The determination of such a shift also depends on $(J-H)$ and $(H-K)$ colors.

[34]Dereddened and reddened photometry yield virtually the same, statistically identical results with the corresponding mean angular diameter difference of $\sim 4 \times 10^{-4}$ mas.

(e.g., Storm et al. 2004, 2011; Gieren et al. 2018), I am using the phase of the highest brightness in V as the phase zero point. The integral of radial velocities is calculated relative to this phase. Once again, for each phase of the determined angular diameter, the corresponding value of the integral is taken[35]. Having sets of integrals $x = -2\int [v_r(\phi) - v_{r,0}]\, d\phi$ and angular diameter θ values, we may fit the following relation based on (19):

$$\theta(x) = p\varpi x + \theta_0 \tag{39}$$

The slope of such a relation is the product of the stellar parallax ϖ and its $p-$factor[36]. $\theta_0 = \theta(\phi = 0)$ is the angular diameter corresponding to R_0. As applied by other authors (e.g. Storm et al. 2004, 2011; Gieren et al. 2018) who used the IRSB method, the linear fit is based on the *bisector method* (Isobe et al., 1990) rather than on the ordinary least-squares (OLS) method that prefers one axis over the other. Such fit yields a line that bisects OLS(Y|X) and OLS(X|Y) relations and allows for a more accurate establishment of a relation between the integral of radial velocities and θ rather than a prediction of θ from the value of integral that is non-essential in this case (Storm et al., 2004). I am performing such fits for different phase shifts between the integral of radial velocities and the angular diameter curve[37] $\Delta\phi \in [-0.1, 0.1]$. I am keeping the phase shift that yields the lowest rms around the relation. Phases of θ from the interval $\phi \in [0.8, 1]$ (calculated after the shift) are excluded from the fit due to the possible abnormal mismatch between the course of the angular diameter and the integral curves – similarly to classical Cepheids, the $p-$factor may have an unusual value or the SBCR relation might be even not applicable for this interval of phase due to shocks in the stellar atmosphere (e.g., Sabbey et al. 1995, Bersier et al. 1997). It is also a regular procedure used by Storm et al. (2004), Storm et al. (2011), and Gieren et al. (2018) in the case of classical Cepheids.

Uncertainties of $p-$factors are determined using Monte Carlo simulations through variations of VK magnitudes (the conservative assumption of 0.01 mag of statistical uncertainty for each band), radial velocity values, and parallaxes, given their uncertainties.

Additionally to $p-$factors, I am also determining the mean radii of stars:

$$\langle R\rangle = \frac{\theta_0}{2\varpi} + \langle \Delta R\rangle = \frac{\theta_0}{2\varpi} - p\int\limits_0^1 \int\limits_0^\phi [v_r(\phi') - v_{r,0}]\, d\phi' d\phi \tag{40}$$

where θ_0 is the intersection of the linear obtained using the bisector fit. The mean radius is obtained using both parameters of the fit and assuming a parallax.

4.3.2 Determinations of $p-$factors and mean radii of two Galactic RR Lyraes

I have applied the IRSB technique to two RRab stars - U Lep and RX Eri. Periods of these two stars differ by only about 8 minutes. Figures 48 to 56 depict radial velocity and light curves, integrals of radial velocities, angular diameters obtained from Kervella et al. (2004a), Kervella et al. (2004b), and Graczyk et al. (2021) SBCR, determinations of $p-$factors corresponding to these relations, and finally distributions of $p-$factors resulting from Monte Carlo simulations. Besides $p-$factors, I am also determining distance d to a star given the $p-$factor of the other star – each for the same SBCR. Distances from GAIA calculated as the inverse of parallax, $1/\varpi$, are given for comparison. Finally, I am determining mean radii. Table 20 contains the results. We may see that the distances are recovered with a precision of about 5%. If we assumed that we are using an exact value of p (i.e., with the zero uncertainty), the distance precision would improve to $3-4$%. The mean radii are determined with a precision better than 2%. The obtained $p-$factors are also virtually the same for a given SBCR. Otherwise, they all agree within 1σ (the statistical error).

[35]Numerical integration based on Virtanen et al. (2020), numerical errors are negligible.

[36]After determining the slope, we may obtain p given ϖ or vice versa. Distributions obtained from inversions of GAIA parallaxes are in good approximation symmetric due to their good precision.

[37]One reason for this shift may be related to the finite precision of pulsation period determination. Spectoscopic and photometric data collected at different epochs may be shifted due to the propagation of period error.

star	SBCR	**p**	$\Delta\phi$	d [pc]	$< R >$ $[R_{\odot}]$
U Lep	Kervella et al. (2004a)	$\mathbf{1.46 \pm 0.06}$	0.0435	$1007 \pm 50(35)$	5.47 ± 0.09
	Kervella et al. (2004b)	$\mathbf{1.45 \pm 0.06}$	0.0430	$1001 \pm 48(37)$	5.57 ± 0.09
	Graczyk et al. (2021)	$\mathbf{1.40 \pm 0.06}$	0.0430	$1011 \pm 50(38)$	5.42 ± 0.09
RX Eri	Kervella et al. (2004a)	$\mathbf{1.45 \pm 0.05}$	-0.0190	$584 \pm 30(18)$	5.35 ± 0.07
	Kervella et al. (2004b)	$\mathbf{1.43 \pm 0.05}$	-0.0190	$589 \pm 31(19)$	5.45 ± 0.07
	Graczyk et al. (2021)	$\mathbf{1.41 \pm 0.05}$	-0.0190	$578 \pm 32(19)$	5.30 ± 0.07

Table 20: Results of determinations of $p-$factors through application of the method described in the previous paragraph. Distances d are obtained using p for the other star and the corresponding SBCR. Original GAIA EDR3 parallaxes with Lindegren et al. (2021) corrections yield distances $1/\varpi$(U Lep)$= 1011 \pm 17\,$kpc and $1/\varpi$(RX Eri)$= 573 \pm 8\,$kpc. Statistical uncertainties are calculated as the rms of the distributions. Errors of distances assuming vanishing uncertainty of the $p-$factor are given in parentheses. Mean radii are given in the last column.

Obviously, we are dealing with many arbitrary choices and p depends on a method and its details. Table 21 includes values of p obtained using different approaches with the original one in bold. Other determinations were performed with no phase shift but a limited phase interval and also using epochs from all phases ($\phi \in [0, 1]$) with ($\Delta\phi \neq 0$) and without ($\Delta\phi = 0$) independently determined phase shifts. We can see that the phase cut is necessary in the case of U Lep, as we obtain a much lower, most probably spurious value while taking into account all data (see Figures 50 and 51). It is not the case for the second star. We can see that something unusual is happening near the minima of integrals of both stellar radial velocity curves (Figures 49 and 54). In the case of U Lep the integral is much steeper than the corresponding angular diameter in the same phase range. In the case of RX Eri the integral curve shape also looks very suspicious and does not correspond to the course of the angular diameter. Similar p values obtained for the whole phase interval for this star may be just a coincidence.

While dealing with determinations based on the whole phase interval, we notice that their results do not differ whether we take into account a small phase shift or not. The phase shift is also responsible for taking into account or rejecting different data points from the interval close to $\phi \in [0.8, 1]$. The minimum of the rms of fits for the restricted phase interval is obtained for a specific set of angular diameters. The relatively large discrepancy of p in the case of the limited phase interval with no phase shift, observed for U Lep, is due to a selection effect connected with poor coherence of the radius and the angular diameter phases (Figure 50). A loop appearing in the corresponding plot is apparent. As Storm et al. (2004) report, such shape of the relation results from the unaccounted phase shift. The lower the scatter of the relation, the smaller the influence of selection effects on the slope of the fitted linear.

We may also notice (Figures 49 and 54) that even though the SBCR of Kervella et al. (2004a) yields values of angular diameters that are closer to those obtained using Graczyk et al. (2021) (both relations were determined for dwarfs and subgiants), it is the relation of Kervella et al. (2004b) for Cepheids that gives the value of a $p-$factor closer to that obtained using SBCR of Graczyk et al.. These are the relative courses rather than absolute zero points of angular diameters obtained from the SBCR relations that play a pivotal role in determining the $p-$factor. It is because these are the relative changes of θ and R that influence the slope of the fitted relation (39). Mean radii depend on the absolute values of θ predicted by SBCRs. That is why the relation of Kervella et al. (2004a) gives $\langle R \rangle$ closer to that resulting from Graczyk et al. (2021).

The determined value of $p-$factor depends on a method so it is not directly comparable with values of the parameter obtained using other methods. However, we may notice that my method yields a larger value than derived by Trahin et al. (2018) ($p = 1.34 \pm 0.07$, for the prototype star RR Lyr), but still in agreement within its uncertainty.

star	SBCR	$\phi \in [0, 0.8]$		$\phi \in [0, 1]$	
		$\Delta\phi \neq 0$	$\Delta\phi = 0$	$\Delta\phi \neq 0$	$\Delta\phi = 0$
U Lep	Kervella et al. (2004a)	$\mathbf{1.46 \pm 0.06}$	1.60 ± 0.06	1.23 ± 0.04	1.23 ± 0.04
	Kervella et al. (2004b)	$\mathbf{1.45 \pm 0.06}$	1.47 ± 0.06	1.17 ± 0.04	1.18 ± 0.04
	Graczyk et al. (2021)	$\mathbf{1.40 \pm 0.06}$	1.41 ± 0.05	1.18 ± 0.04	1.18 ± 0.04
RX Eri	Kervella et al. (2004a)	$\mathbf{1.45 \pm 0.05}$	1.50 ± 0.05	1.49 ± 0.03	1.49 ± 0.04
	Kervella et al. (2004b)	$\mathbf{1.43 \pm 0.05}$	1.49 ± 0.05	1.46 ± 0.03	1.46 ± 0.03
	Graczyk et al. (2021)	$\mathbf{1.41 \pm 0.05}$	1.47 ± 0.05	1.46 ± 0.03	1.46 ± 0.03

Table 21: Values of p determined using different approaches.

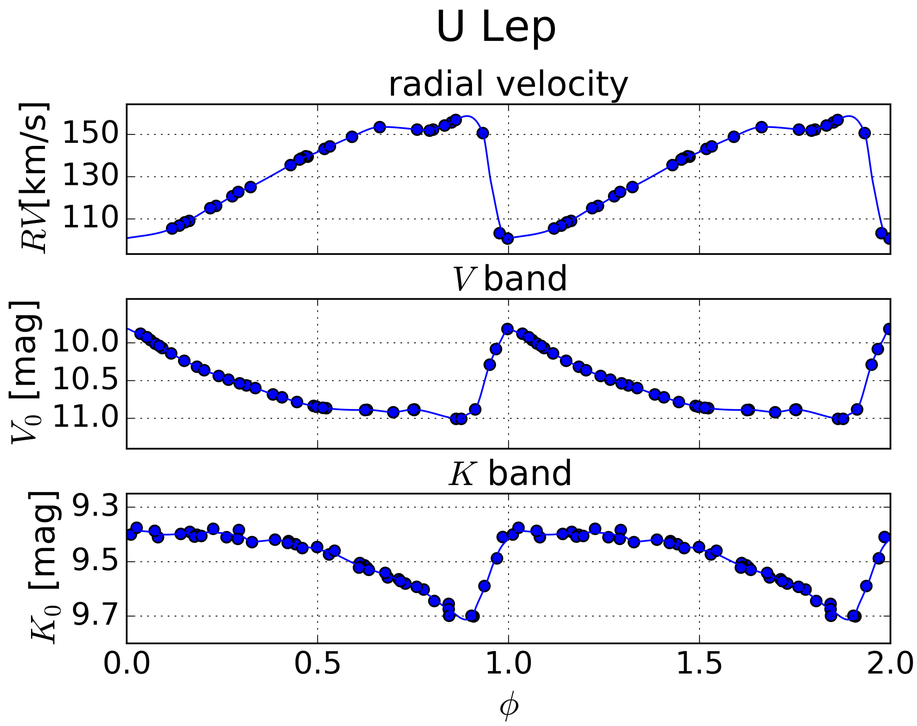

Figure 48: Radial velocity and light curves for U Lep

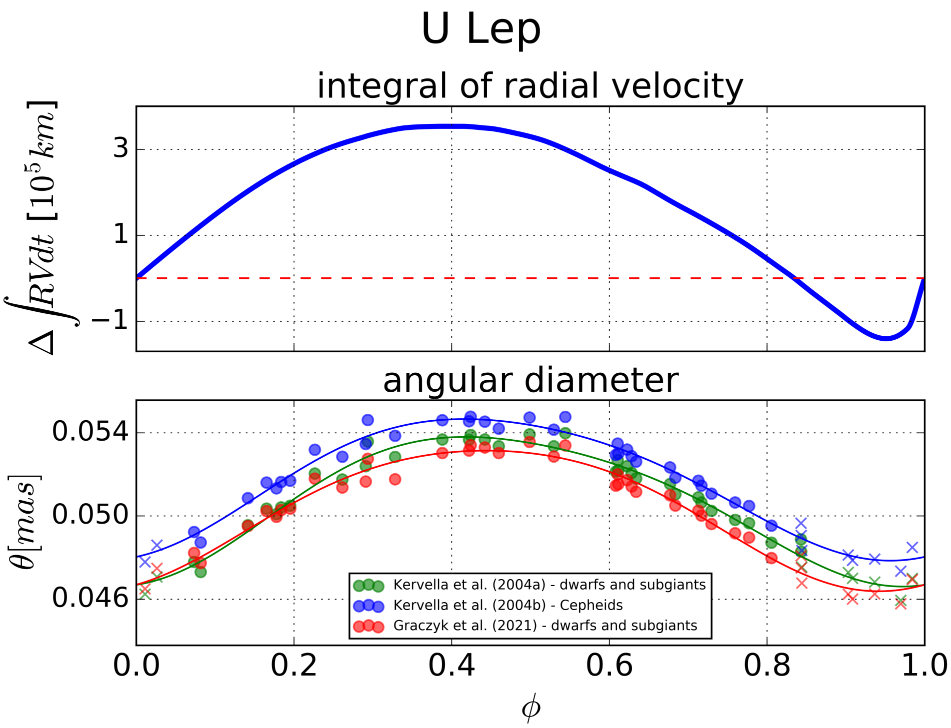

Figure 49: Course of the integral of radial velocity and of the angular diameter of U Lep determined using different SBCRs.

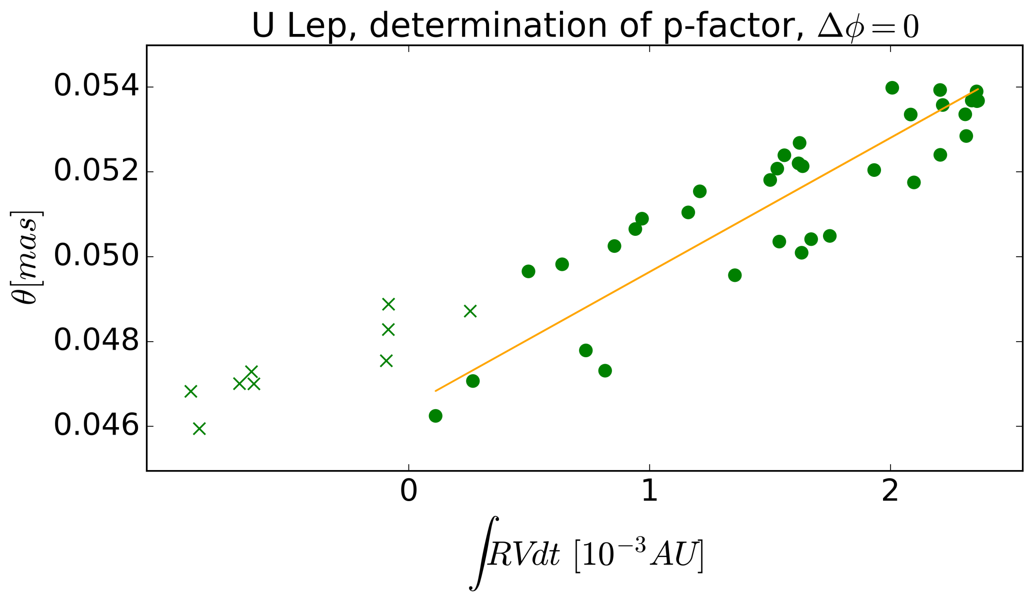

Figure 50: Relation between the integral of radial velocity and angular diameter resulting from the SBCR relation of Kervella et al. (2004a) for U Lep with the limited phase interval and with no phase shift applied. A loop resulting from poor coherence between phases of the two time series, as well as the rejection of points that causes spuriously increased slope of the fitted linear is apparent.

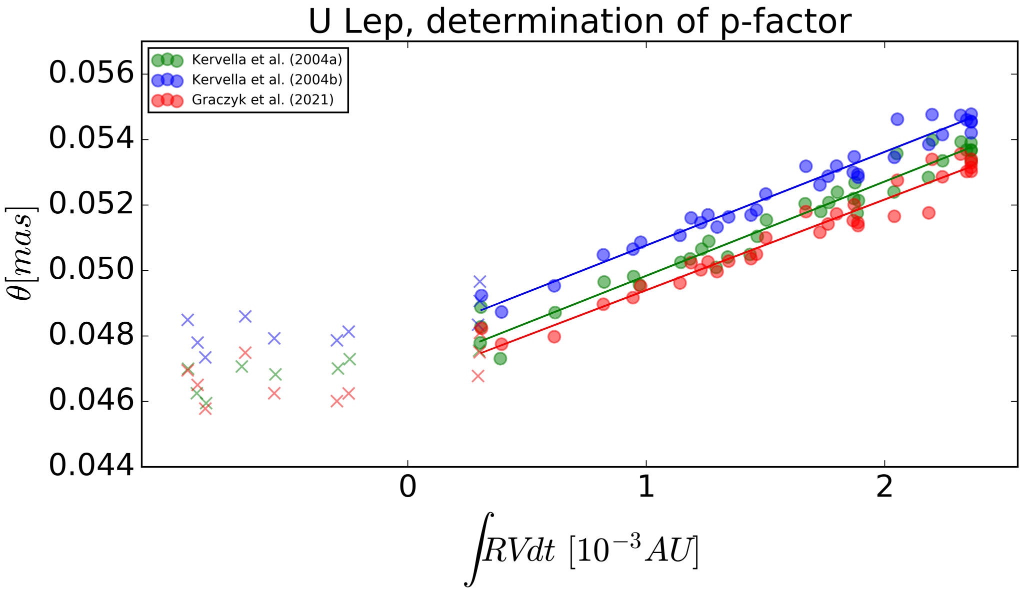

Figure 51: Determination of the $p-$factor and of θ_0 (the intersection) using a bisector fit for U Lep.

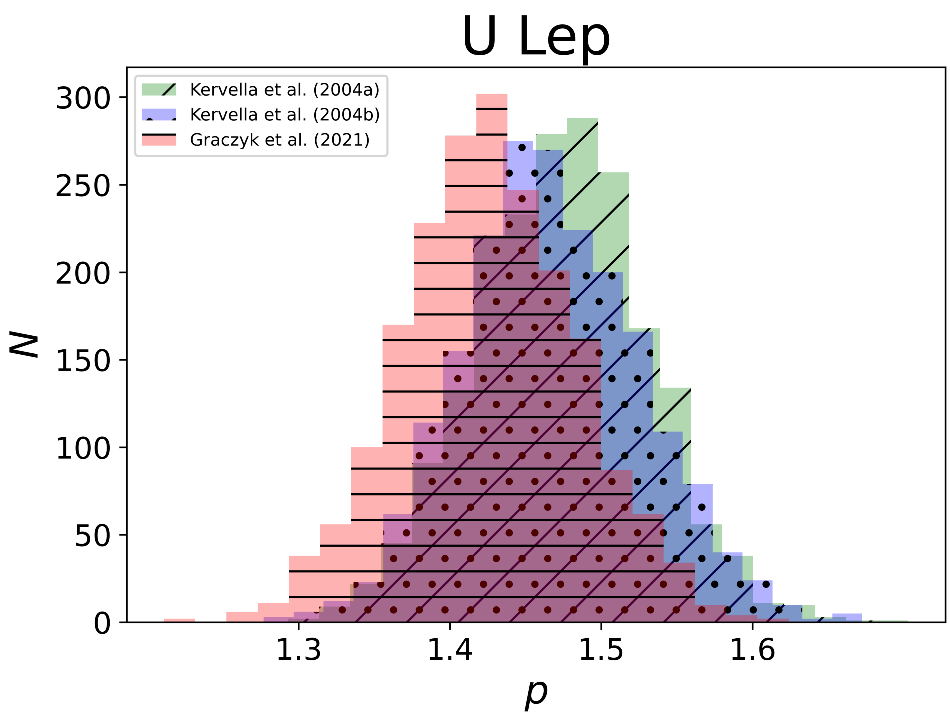

Figure 52: Distributions of p for different SBCRs obtained using Monte Carlo simulations for U Lep.

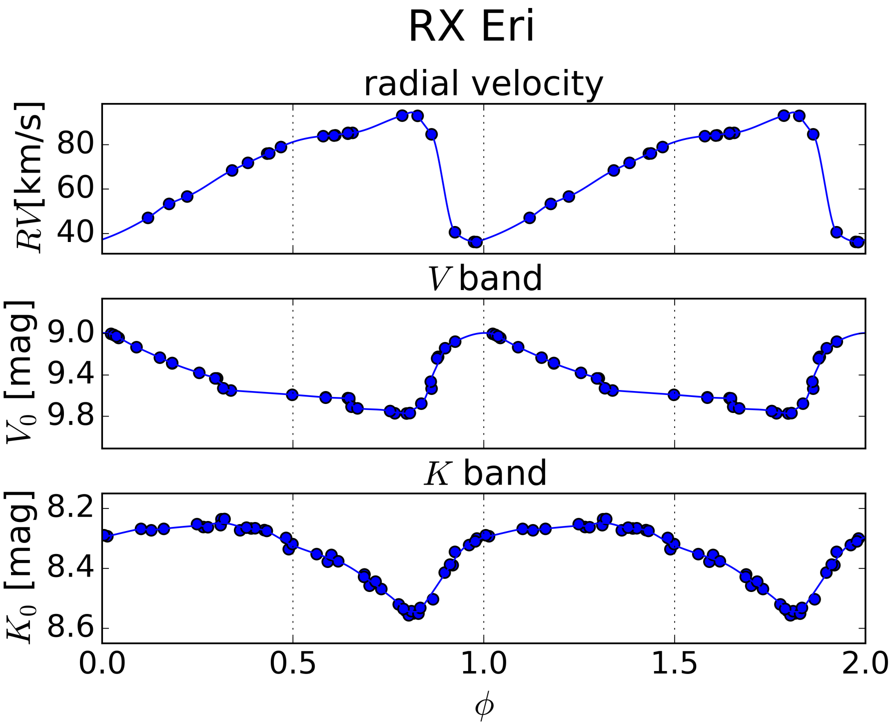

Figure 53: Radial velocity and light curves for RX Eri.

4.3.3 Influence of systematic errors

We immediately notice that the zero point $v_{r,0}$ of the radial velocity curve, recognized as the systemic velocity, neither affects the determination of p, nor θ_0, as it does not influence the values of the integral used in the bisector fit. Consequently, it also does not affect the determination of the mean stellar radius.

Regarding systematic errors of photometry, Figures 57 and 58 depict their influence (for $V-$ and $K-$ bands independently) on determinations of p and $\langle R \rangle$ for U Lep, respectively. Determinations of both p and $\langle R \rangle$ depend more on systematic shifts in K rather than in V.

In the case of the $p-$factor, the influence of systematic errors of photometry on the determination is small, with the approximate change of p of $0.3\,\mathrm{mag}^{-1}$ for the $V-$ band and $1\,\mathrm{mag}^{-1}$ for K. The accuracy of the V photometry, tied up to the Tycho-2 catalog is undoubtedly lower than that of $K-$band photometry but the systematic uncertainty arising from the standardization should not be larger than 0.05 mag (a corresponding shift of p of ~ 0.015). In the case of the $K-$band photometry (tied up to the 2MASS catalog), the estimated systematic error for a single star is $0.025\,\mathrm{mag}$, which corresponds to the shift of p of ~ 0.025. In total, I estimate the systematic uncertainty of p arising from the photometric uncertainties at 0.03, which is around twice smaller than the statistical uncertainty.

In the case of $\langle R \rangle$, the influence of systematic photometric shifts is: $\sim 0.8 R_\odot\,\mathrm{mag}^{-1}$ for V and $\sim 3.3 R_\odot\,\mathrm{mag}^{-1}$ for K. It corresponds to the estimated systematic uncertainty of the mean radii of $0.09 R_\odot$, which is the same as the statistical errors.

Even though I depict here only plotted relations between systematic errors of photometry and the derived parameters p and $\langle R \rangle$ for U Lep, they look virtually the same for RX Eri.

As the determined slope of the fit is a product of p and ϖ, any systematic parallax shift δ_ϖ will have the impact on the shift of $p-$factor that depends on a parallax of a studied object: $\delta_p \propto -\delta_\varpi/\varpi^2$. Given the systematic uncertainty of parallax of $10\,\mu as$, this component of the systematic uncertainty of $p-$ factors is 0.015 and 0.005 in the case of U Lep and RX Eri,

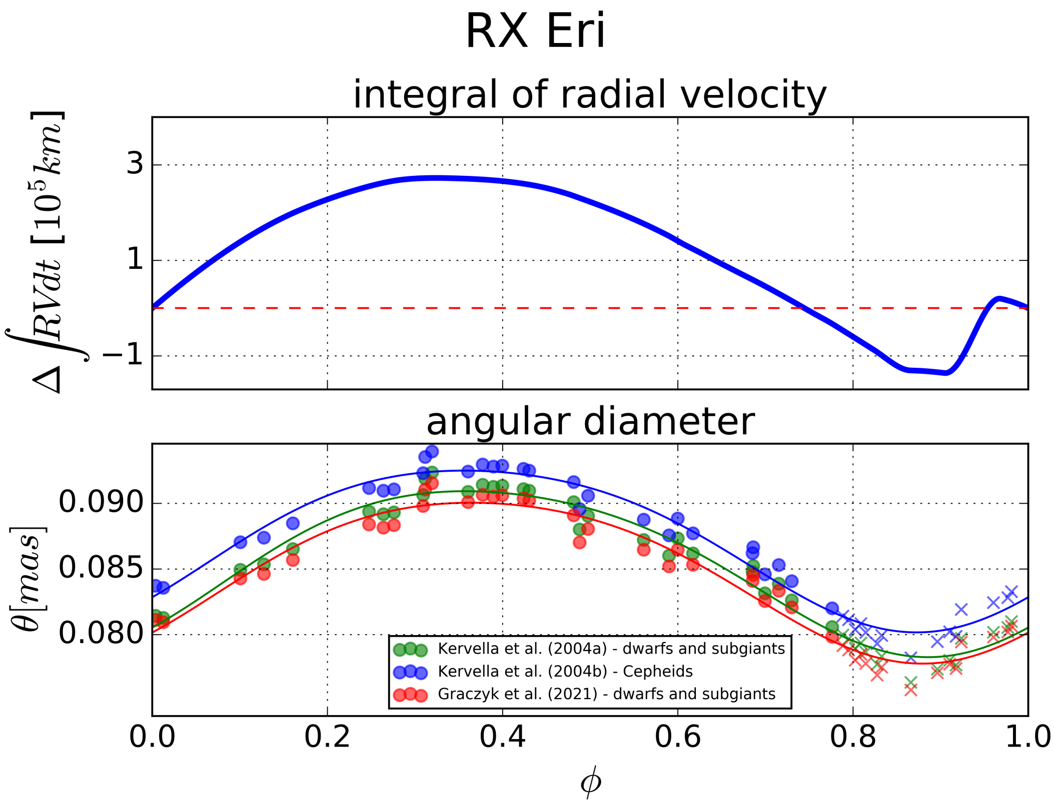

Figure 54: Course of the integral of radial velocity and of the angular diameter of RX Eri determined using different SBCRs.

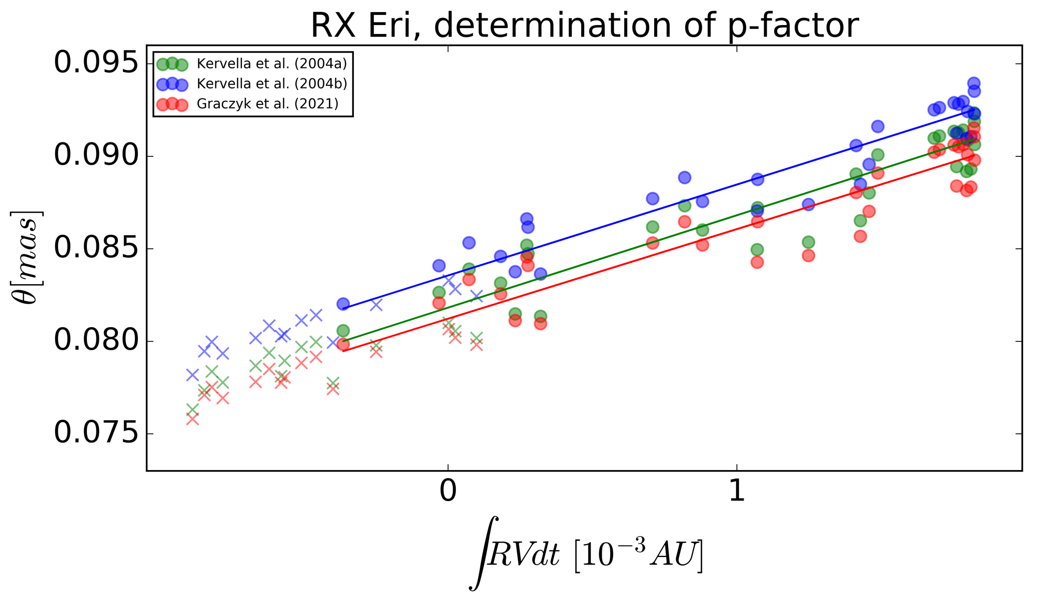

Figure 55: Determination of the $p-$factor and of θ_0 (the intersection) using a bisector fit for RX Eri.

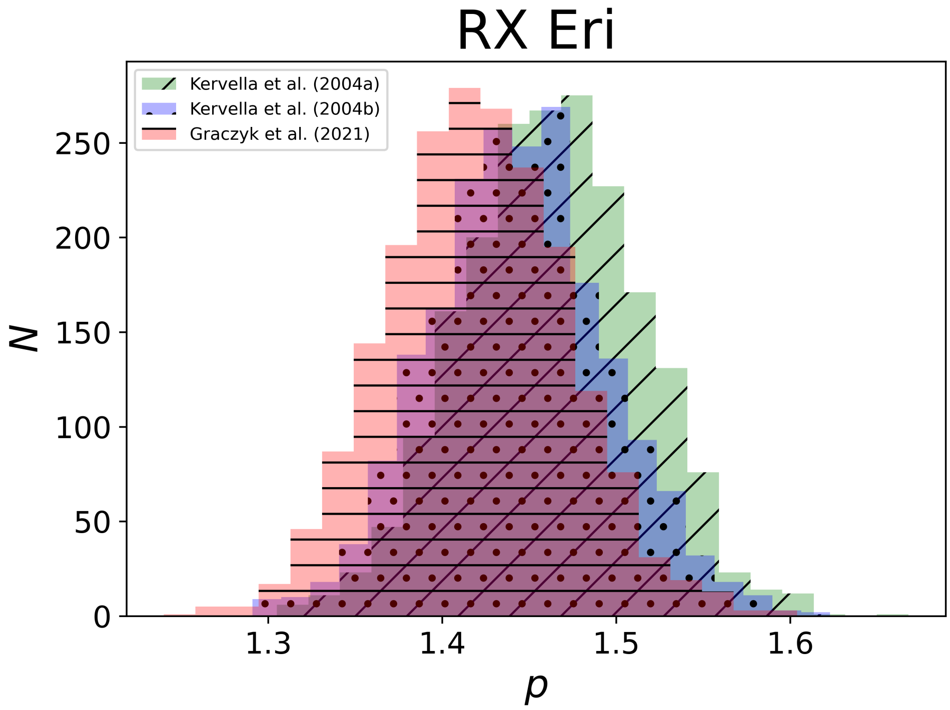

Figure 56: Distributions of p for different SBCRs obtained using Monte Carlo simulations for RX Eri.

respectively. It is significantly smaller than systematic errors arising from photometry.

4.4 Summary

NIR photometry provides excellent opportunities for distance determinations using variable stars, including RR Lyrae stars. It is less affected by extinction than optical photometry, amplitudes of pulsations are smaller, and, in the case of the B-W method, surface brightness-color relations yield angular diameters with better precision.

I have established new PL and PLZ relations for Galactic RR Lyrae stars based on NIR photometry and GAIA EDR3 parallaxes. The zero point of my relations is in very good agreement with the zero point established by RR Lyrae stars from the LMC and the distance to the Cloud obtained from eclipsing binaries of Pietrzyński et al. (2019). Three independent checks have confirmed this fact by fitting relations with period and metallicity slopes of Cusano et al. (2021) and of Muraveva et al. (2015) (both of which are based on the VMC photometry) to my data, and by using my fiducial relations to derive a distance based on Szewczyk et al. (2008) photometry of RR Lyrae stars from the LMC.

Distances obtained using my new relations are smaller by about $0.13 - 0.2$ mag than these based on Bono et al. (2001), Catelan et al. (2004c), Sollima et al. (2008), Dékány et al. (2013) utilized by Szewczyk et al. and Karczmarek et al.. A similar discrepancy is observed when using the zero point established by Benedict et al. (2011) HST parallaxes for 4 Galactic RR Lyrae stars and the VMC photometry (Muraveva et al., 2015). Distances of the Magellanic Clouds reported by Szewczyk et al. correspond to a systematic parallax shift of -0.08 mas relative to GAIA EDR3 parallaxes corrected by the Lindegren et al. (2021) corrections used for the purpose of my calibrations of PL and PLZ relations. It is a shift that is highly unlikely given the uncertainties of parallax corrections of a few μas. Relative distances of Fornax, Carina, and the SMC are discrepant with those resulting from the K photometry of the red clump. The

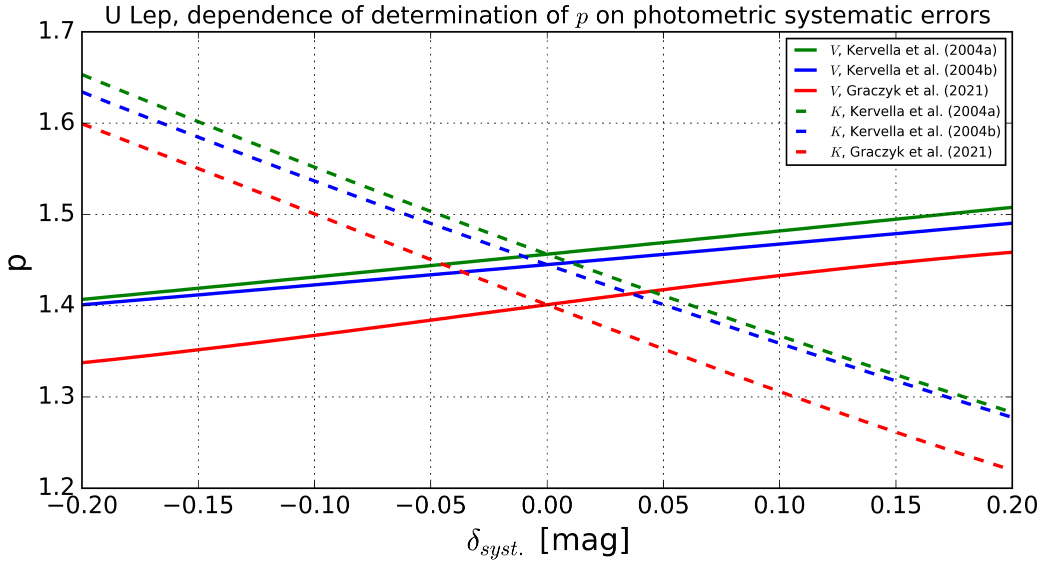

Figure 57: Influence of systematic errors of VK photometry on the determination of the $p-$factor with respect to photometric zero points used in this work.

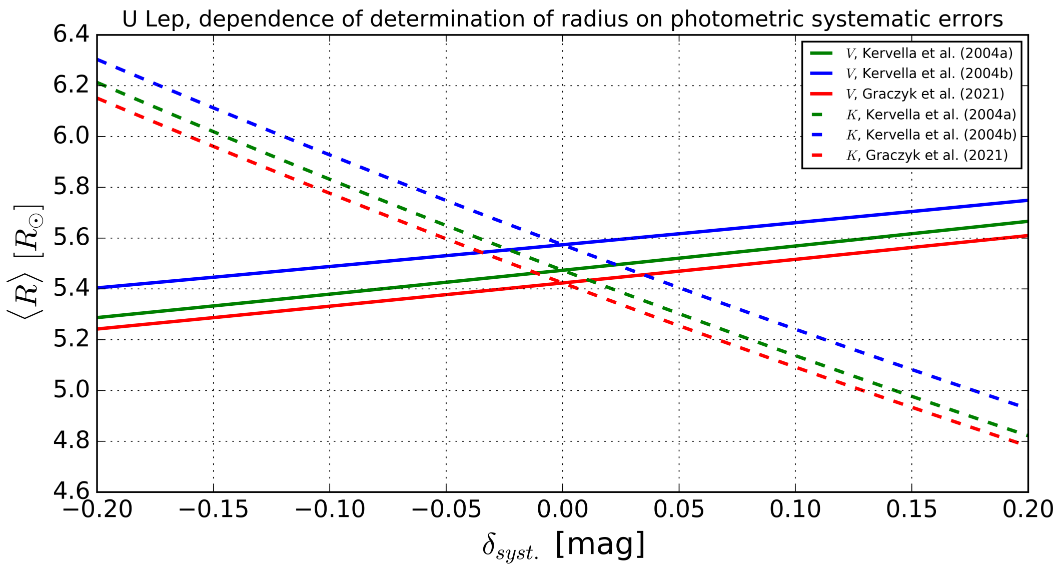

Figure 58: Influence of systematic errors of VK photometry on the determination of the mean radius $\langle R \rangle$ with respect to photometric zero points used in this work.

observed discrepancies may be due to the peculiar positions of the used RR Lyrae stars in their host galaxies, and systematic errors of distances based on the red clump.

In general, distances obtained using PL and PLZ relations for JK bands and the W_{JK} index are in excellent agreement within statistical errors. This is caused by the fact that the adopted mean metallicities of RR Lyrae variables from the analyzed galaxies are similar to metallicities of stars from my calibrating sample. Likewise, it is also because of the small metallicity influence on NIR absolute magnitudes of 0.1 mag/dex, similar to that reported before by, e.g. Sollima et al. (2006), Muraveva et al. (2015), and Cusano et al. (2021). The effect of metallicity introduces distance modulus shifts usually not larger than 0.02 mag, which is comparable to differences resulting from the utilization of the mixed (RRab+RRc) sample rather than just fundamental pulsators (RRab) in distance determinations.

The fundamentalization of periods of RRc stars, especially those being members of other galaxies, is questionable (which is apparent in PL relations for different populations). However, it causes a small distance bias of around 1%. Using just RRab stars yields just slightly larger statistical uncertainties of distances as we are dealing with a smaller span of periods in that case. I estimated the systematic uncertainty of zero point of my PL and PLZ relations of 0.02 mag and systematic uncertainties of my distances of 0.04 mag.

The Baade-Wesselink method of distance determinations is the most complex one discussed in this thesis. As an initial application of the IRSB technique for RR Lyrae stars, I have determined the $p-$factors of two stars, U Lep and RX Eri. I have used three different surface brightness-color relations of Kervella et al. (2004a), Graczyk et al. (2021) (for dwarfs and subgiants), and of Kervella et al. (2004b) (for classical Cepheids); they all yield consistent values of the $p-$factor. The factors of the two stars are also in good agreement. I also had the opportunity to determine the mean radii of the studied stars.

As recognized by other authors before, a phase cut is required near the phase of the minimal radius most probably due to shock waves that cause a discrepancy between the course of the integral of the radial velocity curve and of the angular diameter derived from photometry through SBCR. A slight phase shift between the angular diameter and the integral of radial velocity curve is generally required, similar as for classical Cepheids.

Systematic photometric uncertainties of around a few hundredths of a magnitude do not affect the determination of the $p-$factor (and consequently a distance) much, yielding a bias smaller than the statistical uncertainty. The method requires a robust analysis of a sample of RR Lyrae stars to check the dependence of the $p-$factor on period or metallicity. The analysis of more objects could also allow for improvements of the method and its better adjustment to RR Lyrae stars. The dense coverage of radial velocity and light curves and a good precision of the obtained data are crucial for $p-$factors and distances derived from this method.

Even though the Baade-Wesselink method for RR Lyrae variables is currently not utilized to derive distances to nearby galaxies, when properly calibrated, it may potentially be used to study spatial structures associated with the Population II objects from the nearest neighbors of the Milky Way and within our Galaxy. The new generation of telescopes (JWST, ELT) will allow the Baade-Wesselink method for RR Lyrae stars to reach many galaxies in the volume of the Local Group. The method could also provide corrections to PL and PLZ relations of RR Lyrae stars from nearby galaxies as it already does for classical Cepheids (Gieren et al., 2018).

5 Final conclusions

I have presented three different distance determination methods in my thesis. My calibration of carbon stars as a distance indicator allows for an effective reduction of effects that make luminosity functions of these stars asymmetric and can potentially falsify determinations of distances. The current accuracy of the method is already comparable to that of distances determined from classical Cepheids. A multi-band version of the method could take into account the extinction that affects our measurements. Further improvements will also include the influence of metallicity on mean absolute magnitudes of carbon stars. Accurate parallaxes of carbon stars from GAIA DR4 could allow to study the impact of metallicity on the method. In summary, carbon stars are very promising distance indicators, which will allow to obtain distances to Supernova host galaxies independent of classical Cepheids and the TRGB. Determinations using JAGB stars may contribute to the solution of the Hubble tension and allow for precise determinations of the Hubble constant, especially in the era of the new generation of telescopes.

I have presented new period-luminosity-metallicity relations for RR Lyrae stars. My calibrations show a significant improvement of the accuracy compared to calibrations previously utilized in distance determinations. The zero point of my relations is based on the parallaxes of RR Lyrae variables from GAIA EDR3 determined with a state-of-the-art precision. It is also in agreement with the zero point based on the very accurate distance to the Large Magellanic Cloud determined from detached eclipsing binaries (Pietrzyński et al., 2019). In the case of the Magellanic Clouds and the Fornax and Carina galaxies, my calibration yields distances which are substantially smaller (by about ~ 0.13-$0.2\,$mag, i.e. by $6-10\%$) than those based on previously used calibrations. The obtained discrepancy with the red clump and TRGB distance determinations to Fornax, Carina, and the SMC, based on NIR photometry should be investigated further and can contribute to an improved calibration of these two methods. PLZ relations for RR Lyrae stars can be used to check intermediate methods that calibrate Supernovae. The new generation of telescopes will allow to robustly compare the calibration of PLZ relations for RR Lyrae variables with calibrations of the TRGB, classical Cepheids, and the JAGB method. My fiducial calibrations can already serve for accurate distance determinations from RR Lyrae stars. A future implementation of parallaxes from the next data release of GAIA will only improve them.

The IRSB version of the Baade-Wesselink method applied to two RR Lyrae stars is an introduction to a broader study that will investigate the dependence of $p-$factors of RR Lyrae stars on environmental conditions and various parameters of these stars, such as metallicity and pulsation period. The Baade-Wesselink method for RR Lyrae stars is independent of PL(Z) relations and is in principle geometrical. With well-calibrated $p-$factors, it may provide accurate distance determinations that depend very little on reddening. In my work, I have shown that $p-$factors for RR Lyrae stars can be determined with good accuracy. The next data release of GAIA parallaxes will allow for a true breakthrough in the calibration of the method. Likewise, the next-generation telescopes will allow to implement the method for distance determinations to nearby galaxies, where thousands of RR Lyrae stars are already known.

The date of GAIA Data Release 4, including even more precise parallaxes of nearby stars, has not been announced yet[38]. The release will be based on data gathered during 66 months (5.5 years) of operation. For comparison, the GAIA (E)DR3 is based on 34 months of observations.

Although the most fundamental purpose of calibrations is associated with the accurate calibration of H_0, distance determinations to nearby galaxies are important for many different fields of astrophysics. With uniform and high-quality data, the Cerro Armazones Observatory will provide excellent opportunities to develop the projects described in this dissertation.

[38]GAIA date release scenario is available at: `https://www.cosmos.esa.int/web/gaia/release`.

Acknowledgements

First of all, I would like to thank my supervisor Grzegorz. Thank you for creating wonderful opportunities for young scientists. It has been an honor to work with you. I am also grateful to my 'scientific uncle' - the auxiliary supervisor Marek. You taught me a lot during the last few years and I could always count on you when it comes to advices. I thank Piotrek Wielgórski for the great cooperation we have had during the course of our PhD studies. I would like to thank all members of the Araucaria Project for being part of this well-integrated and ambitious scientific family.

I appreciate the kidness and help of researchers from the Astronomical Institute of the Ruhr University in Bochum, Germany led by prof. Rolf Chini, who also helped me proofread the text of this dissertation. I am grateful to Michael Ramolla for teaching me the operation of OCA, and to Catalina and Sadegh for being wonderful co-observers.

Thank you Marta for your understanding and patience with my imperfections. I thank my family - especially my parents who have shaped me. Monika, Maciek, Bartek i Piotr for being caring and understanding. I am grateful to my older brother for being my mentor in many different fields and skills.

I appreciate the friendship of my buddies from the block. Thank you, Antek, Cysiek, Krzysiek, Mateusz, Michał, Piotr, and Tomek.

The research leading to these results has received funding from the European Research Council (ERC) under the European Union's Horizon 2020 research and innovation program (grant agreements No. 695099 & 951549). The National Science Center financed this research through MAESTRO grant (agreement number UMO-2017/26/A/ST9/00446) and BEETHOVEN grant (agreement number UMO-2018/31/G/ST9/03050). The research was possible also thanks to the grant of the Polish Ministry of Science and Higher Education (decision number DIR/WK/ 2018/09).

This research has made use of the International Variable Star Index (VSX) database, operated at AAVSO, Cambridge, Massachusetts, USA.

Bibliography

Abbott, B. P., Abbott, R., Abbott, T. D. et al. 2017, Nature, 551, 85

Astropy Collaboration, Robitaille, T. P., Tollerud, E. J. et al. 2013, A&A, 558, A33

Akima, H. 1970, Journal of the ACM, 17(4), 589

Arenou, F., Luri, X. 1999, ASPC, 167, 13

Arenou, F., Luri, X., Babusiaux, C. et al. 2018, A&A 616, 17

Baade, W. 1926, Astronomische Nachrichten, 228, 359

Bailer-Jones, C. A. L., Rybizki, J., Fouesneau, M. et al. 2018, AJ, 156, 58

Bailer-Jones, C. A. L., Rybizki, J., Fouesneau, M. et al. 2021, AJ, 161, 147

Bailey, S. I. 1902, Annals of the Astronomical Observatory of Harvard College, 38, 132

Barnes, T. G., Evans, D. S. 1976, MNRAS, 174, 489

Battinelli, P., Demers, S. 2005, A&A, 442, 159

Benedict, G. F., McArthur, B. E., Feast, M. W., et al. 2011, AJ, 142, 187

Bershady, M. A., Lowenthal, J. D., Koo, D. C. 1998, ApJ, 505, 50

Bersier, D., Burki, G., Kurucz, R. L. 1997, A&A, 320, 228

Bersier, D. 2000, ApJ, 543, 23

Bertin, E., Arnouts, S. 1996, A&AS, 117, 393

Bertin, E. 2006, ASPC, 351, 112

Bhardwaj, A. 2020, JApA, 41, 23

Blackwell, D. E. & Shallis, M. J. 1977, MNRAS, 180, 177

Blažko, S. 1907, Astronomische Nachrichten, 175, 325

Bono, G., Caputo, F., Castellani, V. et al. 2001, MNRAS, 326, 1183

Bono, G., Caputo, F., Castellani, V., et al. 2003, MNRAS, 344, 1097

Brahm, R., Jordán, A., Espinoza, N. 2017, PASP, 129, 4002

Bresolin, F., Pietrzyński, G., Gieren, W., Kudritzki, R. P. 2005, ApJ, 634, 1020

Breuval, L., Kervella, P., Wielgórski, P. et al. 2021, ApJ, 913, 38

Cacciari, C., Clementini, G., Prevot, L., Buser, R. 1989a, A&A, 209, 141.

Cacciari, C., Clementini, G., Buser, R. 1989b, A&A, 209, 154

Cacciari, C., Clementini, G., Fernley, J. A. 1992, ApJ, 396, 219

Cardelli, J. A., Clayton, G. C., Mathis, J. S. 1989, ApJ, 345, 245

Carney, B. W. & Latham, D. W. 1984, ApJ, 278, 241

Carney, B. W., Storm, J., Jones, R. V. 1992, ApJ, 386, 663

Carpenter, J. M. 2001, AJ, 121, 2851

Castelli F. Kurucz R. L. 2003, *'New Grids of ATLAS9 Model Atmospheres'*, ed. N. Piskunov, W. W. Weiss and D. F. Gray, IAU Symp., 210, 20

Catelan, M. 2004a, ApJ, 600, 409

Catelan, M. 2004b, ASPC, 310, 113

Catelan, M., Pritzl, B. J., Smith, H. A. 2004c, ApJS, 154, 633

Catelan, M., Smith, H. A. 2015, *'Pulsating Stars'*, Wiley-VCH

Chaboyer B., 1999, in Heck A., Caputo F., eds., *'Post-Hipparcos Cosmic Candles'*. Kluwer, Dordrecht, p. 111

Clementini, G., Cacciari, C., Lindgren, H. 1990, A&AS, 85, 865

Cioni, M. -R. L., Clementini, G., Girardi, L. et al. 2011, A&A, 527, 116

Cohen, M., Wheaton, Wm. A., Megeath, S. T. 2003, AJ, 126, 1090

Crestani, J., Braga, V. F., Fabrizio, M. et al. 2021, ApJ, 914, 10

Cusano, F., Moretti, M. I., Clementini, G. et al. 2021, MNRAS, 504, 1

Cutri, R. M, Skrutskie, M. F., van Dyk, S. et al. 2003, "The IRSA 2MASS All-Sky Point Source Catalog, NASA/IPAC Infrared Science Archive."

Dékány, I., Minniti, D., Catelan, M., et al. 2013, ApJ, 776, L19

Dekker, H., D'Odorico, S., Kaufer, A. et al. 2000, SPIE, 4008, 534

Di Benedetto, G. P. 2005, MNRAS, 357, 174

Drimmel, R., Spergel, D. N. 2001, ApJ, 556, 181

Eddington A. S. 1918, MNRAS, 79, 2

Eddington A. S. 1919, MNRAS, 79, 171

Eddington A. S. 1926, *'The Internal Constitution of the Stars'*, Cambridge University Press

Fabricius, C., Luri, X., Arenou, F. et al. 2021, A&A, 649, 5

Fernley, J. A., Lynas-Gray, A. E., Skillen, I. et al. 1989, MNRAS, 236, 447

Fernley, J. A., Skillen, I., Jameson, R. F., Longmore, A. J. 1990a, MNRAS, 242, 685

Fernley, J. A., Skillen, I., Jameson, R. F., et al. 1990b, MNRAS, 247, 287

Fernley, J. A. 1994, A&A, 284, L16

Fernley, J. A., Barnes, T. G., Skillen, I., et al. 1998, A&A, 330, 515

Fouqué, P., Gieren, W. 1997, A&A, 320, 799

Freedman, W. L., Madore, B. F., Gibson, B. K. et al. 2001, ApJ, 553, 47

Freedman, W. L., Madore, B. F., Scowcroft, V. et al. 2012, ApJ, 758, 24

Freedman, W. L., Madore, B. F., Hatt, D., 2019, ApJ, 882, 34

Freedman, W. L., Madore, B. F. 2020, ApJ, 899, 67

Freedman, W. 2021, ApJ, 919, 16

Gaia Collaboration, Brown, A. G. A., Vallenari, A. et al. 2021, A&A, 649, 1

González-Fernández, C., Hodgkin, S. T., Irwin, M. J. et al. 2018, MNRAS, 474, 5459

Górski, M., Zgirski, B., Pietrzyński, G. et al. 2020, ApJ, 889, 179

Gieren, W., Górski, M., Pietrzyński, G. et al. 2013, ApJ, 773, 69

Gieren, W.; Pietrzyński, G., Nalewajko, K. et al. 2006, ApJ, 647, 1056

Gieren, W., Pietrzyński, G., Soszyński, I. et al. 2005, ApJ, 628, 695

Gieren, W., Pietrzyński, G., Soszyński, I. et al. 2008, ApJ, 672, 266

Gieren, W., Pietrzyński, G., Soszyński, I. et al. 2009, ApJ, 700, 1141

Gieren, W., Pietrzyński, G., Szewczyk, O. et al. 2008, ApJ, 683, 611

Gieren, W., Storm, J., Konorski, P. et al. 2018, A&A, 620, 99

Graczyk, D., Pietrzyński, G., Thompson, I. B. et al. 2014, ApJ, 780, 59

Graczyk, D., Pietrzyński, G., Thompson, I. B. et al. 2018, ApJ, 860, 1

Graczyk, D., Pietrzyński, G., Thompson, I. B. et al. 2020, ApJ, 904, 13

Graczyk, D., Pietrzyński, G., Galan, C. et al. 2021, A&A, 649, 109

Groenewegen, M. A. T. & Marigo, P. 2004, *'Asymptotic Giant Branch Stars'*, H. Springer-Verlag, New York

Herrnstein, J. R., Moran, J. M., Greenhill, L. J., Trotter, A. S. 2005, ApJ, 629, 719

Hill, S. J. 1972, ApJ, 178, 793

Hinshaw, G., Larson, D., Komatsu, E. et al. 2013, ApJS, 208, 19

Hodapp, K. W., Chini, R., Reipurth, B. et al. 2010, SPIE, 7735, 1

Hotokezaka, K., Nakar, E., Gottlieb, O. et al. 2019, Nature Astronomy, 3, 940

Høg, E., Fabricius, C., Makarov, V. V., Urban, S., A&A, 355, 27

Iben, I. 1973, ApJ, 185, 209

Iben, I. 1974, ARA&A, 12, 215

Isobe, T., Feigelson, E.D., Akritas, M.G., Babu, G.J. 1990, ApJ, 364, 104

Jacyszyn-Dobrzeniecka, A. M., Skowron, D. M., Mróz, P. et al. 2016, AcA, 66, 149

Jacyszyn-Dobrzeniecka, A. M., Skowron, D. M., Mróz, P. et al. 2017, AcA, 67, 1

Jones, R. V., Carney, B. W., Latham, D. W., Kurucz, R. L. 1987a, ApJ, 312, 254

Jones, R. V., Carney, B. W., Latham, D. W., Kurucz, R. L. 1987b, ApJ, 314, 605

Jones, R. V. 1988, ApJ, 326, 305

Jones, R. V., Carney, B. W., Latham, D. W. 1988a, ApJ, 326, 312

Jones, R. V., Carney, B. W., Latham, D. W. 1988b, ApJ, 332, 206

Jones, R. V., Carney, B. W., Storm, J., Latham, D. W. 1992, ApJ, 386, 646

Jones, R. V., Carney, B. W., Fulbright, J. P. 1996, PASP, 108, 877

Jurcsik, J., Smitola, P., Hajdu, G. et al. 2017a, MNRAS, 468, 1317

Jurcsik, J., Hajdu, G. 2017b, MNRAS, 470, 617

Karakas, A. I., Lugaro, M., Carlos, M. et al. 2018, MNRAS, 477, 421

Karczmarek, P., Pietrzyński, G., Gieren, W. et al. 2015, AJ, 150, 90

Karczmarek, P., Wiktorowicz, G., Iłkiewicz, K. et al. 2017, MNRAS, 466, 2842

Karczmarek, P., Pietrzyński, G., Górski, M. et al. 2017, AJ, 154, 263

Kaufer, A., Stahl, O., Tubbesing, S. 1999, The Messenger, 95, 8

Kervella, P., Thévenin, F., Di Folco, E., Ségransan, D. 2004a, A&A, 426, 297

Kervella, P., Bersier, D., Mourard, D. et al. 2004b, A&A, 428, 587

Kato, D., Nagashima, C., Nagayama, T. et al. 2007, PASJ, 59, 615

Koen, C., Marang, F., Kilkenny, D., Jacobs, C. 2007, MNRAS, 380, 1433

Kolláth, Z. 2021, ASPC, 529, 117

Kontizas, E., Dapergolas, A., Morgan, D. H., Kontizas, M. 2001, A&A, 369, 932

Kovács, G. 1998, ASPC, 135, 52

Kubiak, M. 1994, *'Gwiazdy i materia międzygwiazdowa'*, Wydawnictwo Naukowe PWN (in Polish)

Kurucz, R. L. 1970, *'Atlas: A Computer Program for Calculating Model Stellar Atmospheres'*, SAO Special Report, 309

Lee, A. J., Freedman, W. L., Madore, B. F. et al. 2020, ApJ, 907, 112

Lee, A. J., Freedman, W. L., Madore, B. F. et al. 2021, ApJ, 923, 157

Lindegren, L., Bastian, U., Biermann, M. et al. 2021, A&A, 649, 4

Liu, T. & Janes, K. A. 1990a, ApJ, 354, 273

Liu, T. & Janes, K. A. 1990b, ApJ, 360, 561

Longmore, A. J., Fernley, J. A., Jameson, R. F. 1986, MNRAS, 220, 279

Luri X., Brown, A. G. A., Sarro, L. M. et al. 2018, A&A, 616, A9

Macaulay, E., Nichol, R. C., Bacon, D. et al. 2019, MNRAS, 486, 2184

Mackey, A. D., Gilmore, G. F. 2003, MNRAS, 345, 747

Macri, L., Ngeow, C.-C., Kanbur, S., Mahzooni, S., Smitka, M. T. 2015, AJ, 149, 117

Madore, B. F. 1982, ApJ, 253, 575

Madore, B. F., Freedman W. L. 2020, ApJ, 899, 66

Madore, B. F., Freedman, W. L., Lee, A. 2021, arXiv:2112.06968

Manduca, A. & Bell, R. A. 1981, ApJ, 250, 306

Marconi, M., Coppola, G., Bono, G. et al. 2015, ApJ, 808, 50

Marigo, P., Girardi, L., Bressan, A. et al. 2008, A&A, 482, 883

Martin C., Plummer H. C. 1915, MNRAS, 75, 566

Mayor, M., Pepe, F., Queloz, D. et al. 2003, The Messenger, 114, 20

McCarthy, M. F. 1994, ASPC, 60, 224

Mérand, A., Kervella, P., Breitfelder, J. et al. 2015, A&A, 584, A80

Miyoshi, M., Moran, J., Herrnstein, James et al. 1995, Nature, 373, 127

Muraveva, T., Palmer, M., Clementini, G. et al. 2015, ApJ, 807, 127

Muraveva, T., Delgado, H. E., Clementini, G. et al. 2018, MNRAS, 481, 1195

Nardetto, N., Fokin, A., Mourard, D. et al. 2004, A&A, 428, 131

Nardetto, N., Poretti, E., Rainer, M., et al. 2017, A&A, 597, A73

Neeley, J. R., Marengo, M., Freedman, W. L. et al. 2019, MNRAS, 490, 4254

Nemec, J.M. 1985, ApJ, 90, 240

Netzel, H., Smolec, R. 2019, MNRAS, 487, 5584

Nikolaev, S., Weinberg, M. D. 2000, ApJ, 542, 804

Oosterhoff, P. Th. 1939, The Observatory, 62, 104

Paczyński, B., Stanek, K. Z. 1998, ApJ, 494, 219

Parada, J., Heyl, J., Richer, H. et al. 2020, MNRAS, 501, 933

Pesce, D. W., Braatz, J. A., Reid, M. J et al. 2020, ApJ, 891, 1

Petersen, J. O. 1973, A&A, 27, 89

Pickering, E. C. 1889, Astronomische Nachrichten, 123, 207

Pickering E. C., Colson H. R., Fleming W. P., Wells L. D. 1901, ApJ, 13, 226

Pietrzyński, G., Gieren, W., Udalski, A. 2003, AJ, 125, 2494

Pietrzyński, G., Górski, M., Gieren, W. et al. 2009, AJ, 138, 459

Pietrzyński, G., Thompson, I. B., Gieren, W. et al. 2010, Nature, 468, 542

Pietrzyński, G., Thompson, I. B., Gieren, W. et al. 2012, Nature, 484, 75

Pietrzyński, G., Graczyk, D., Gieren, W. et al. 2013, Nature, 495, 76

Pietrzyński, G., Graczyk, D., Gallenne, A. et al. 2019, Nature, 567, 200

Pilecki B., Konorski P., Górski M. 2012, IAUS, 282, 301

Pilecki, B., Gieren, W., Smolec, R. et al. 2017, ApJ, 842, 110 *'From Interacting Binaries to Exoplanets: Essential Modeling Tools'*, IAU Symposium, 292, 301

Planck Collaboration: Aghanim, N., Akrami, Y., Ashdown, M. et al. 2020 A&A, 641, 6

Prialnik, D. 2010, *'An Introduction to the Theory of Stellar Structure and Evoluton'*, Cambridge University Press

Pritchet, Christopher J., Richer, Harvey B., Schade, David et al. 1987, ApJ, 323, 79

Raimondo, G., Cioni, M. -R. L., Rejkuba, M., Silva, D. R. 2005, A&A, 438, 521

Richer, H. B. 1981, ApJ, 243, 744

Richer, H. B., Crabtree, D. R., Pritchet, C. J 1984, ApJ, 287, 138

Richer, H. B., Pritchet, C. J., Crabtree, D. R. 1985, ApJ, 298, 240

Riess, A. G., Filippenko, A. V., Challis, P. et al. 1998, AJ, 116, 1009

Riess, A. G., Macri, L., Casertano, S. et al. 2011, ApJ, 730, 119

Riess, A. G., Macri, L. M., Hoffmann, S. L. et al. 2016, ApJ, 826, 56

Riess, A. G., Yuan, W., Macri, L. M. et al. 2021, arXiv:2112.04510

Ripoche, P., Heyl, J., Parada, J., Richer, H. 2020, MNRAS, 495, 2858

Ritter A. 1879, Annalen der Physik, 244, 157

Rucinski, S., M. 2002, AJ, 124, 1746

Sackmann, I. J., Smith, R. L., Despain, K. H. 1974, ApJ, 187, 555

Sandage, A. 1958, Ricerche Astronomiche, 5, 41

Sandage, A. 1981, ApJ, 248, 161

Sandage, A. 1990, ApJ, 350, 631

Schlafly, E. F., Finkbeiner, D. P. 2011, ApJ, 737, 103

Schlegel, D. J., Finkbeiner, D. P., Davis, M. 1998, ApJ, 500, 525

Schwarzschild, M. 1940, Harvard College Observatory Circular, 437, 1

Scowcroft, V., Freedman, W. L., Madore, B. F. et al. 2016, ApJ, 816, 49

Secchi, A. 1868, MNRAS, 28, 196

Shapley, H. 1918, ApJ, 48, 154

Skillen, I., Fernley, J. A., Jameson, R. F. et al. 1989, MNRAS, 241, 281

Skillen, I., Fernley, J. A., Stobie, R. S., Jameson, R. F. 1993, MNRAS, 265, 301

Skrutskie M. F.,Cutri R. M., Stiening R. et al. 2006, AJ, 131, 1163

Smith, B. J., Leisawitz, D., Castelaz, M. W., Luttermoser, D. 2002, AJ, 123, 948

Smolec, R., Soszyński, I., Udalski, A. et al. 2015, MNRAS, 447, 3873

Sollima, A., Cacciari, C., Valenti, E. 2006, MNRAS, 372, 1675

Sollima, A., Cacciari, C., Arkharov, A. A. H. et al. 2008, MNRAS, 384, 1583

Smolec, R. 2021, ASPC, 529, 287

Sabbey, C. N., Sasselov, D. D., Fieldus, M. S. et al. 1995, ApJ, 446, 250

Soszyński, I., Gieren, W., Pietrzyński, G. et al. 2006, ApJ, 648, 375

Soszyński, I., Udalski, A., Szymański, M. K., et al. 2016, AcA, 66, 131

Soszyński, I., Udalski, A., Wrona, M. et al. 2019, AcA, 69, 321

Stetson, P. B. 1987, PASP, 99, 191,

Storm, J., Carney, B. W., Gieren, W. et al. 2004, A&A, 415, 531

Storm, J., Gieren, W., Fouqué, P. et al. 2011, A&A, 534, 94

Suchomska K., Graczyk, D., Smolec, R. et al. 2015, MNRAS, 451, 651

Swan, W. 1857, AnP, 176, 306

Szewczyk, O., Pietrzyński, G., Gieren, W. et al. 2008, AJ, 136, 272

Szewczyk, O., Pietrzyński, G., Gieren, W. et al. 2009, AJ, 138, 1661

Thompson, I. B., Kałużny, J., Pych, W. et al. 2001, AJ, 121, 3089

Tody, D. 1986, SPIE, 627, 733

Trahin, B., Kervella, P., Gallenne, A. et al. 2018, PTA Proceedings, 6, 213

Trahin, B., Breuval, L., Kervella, P. et al. 2021, A&A, 656, 102

Udalski, A., Soszyński, I., Szymański, M. et al. 1999a, AcA, 49, 223

Udalski, A., Soszyński, I., Szymański, M. et al. 1999b, AcA, 49, 437

Udalski, A., Soszyński, I., Szymański, M. K. et al. 2008a, AcA, 58, 89

Udalski, A., Soszyński, I., Szymański, M. K. et al. 2008b, AcA, 58, 329

Watermann, R. 2012, *'Automatisierte Variabilitätsmessungen im Visuellen und Infraroten'*, PhD dissertation (in German), Fakultät für Physik und Astronomie der Ruhr-Universität Bochum, `https://ui.adsabs.harvard.edu/abs/2012PhDT.......276W`

Weinberg, M. D., Nikolaev, S. 2001, ApJ, 548, 712

Welch, D. L. 1994, AJ, 108, 1421

Wesselink, A. J. 1946, Bulletin of the Astronomical Institutes of the Netherlands, 10, 91

Wesselink, A. J. 1969, MNRAS, 144, 297

Whitelock, P. A., Menzies, J. W., Feast, M. W. et al. 2013, MNRAS, 428, 2216

Wielgórski, P., Pietrzyński, G., Pilecki, B. et al. 2021, arXiv:2112.12122

Ventura, P., Dell'Agli, F., Lugaro, M. et al. 2020, A&A, 641, 103

Virtanen, P., Gommers, R., Oliphant, T. E., et al. 2020, NatMe, 17, 261

Yang, T., Birrer, S., Hu, B. 2020, MNRAS, 497, 56

Yoshii, Y., Kobayashi, Y., Minezaki, T. et al. 2014, ApJ, 784, 11

Zgirski, B. 2015, *'Pomiar odległości do galaktyki NGC 7793 na podstawie wielobarwnych zależności okres-jasność dla Cefeid'* - master thesis (in Polish), Wydział Fizyki, Uniwersytet Warszawski

Zgirski, B., Gieren. W., Pietrzyński G., et al. 2017, ApJ, 847, 88

Zgirski, B., Pietrzyński, G., Gieren, W. et al. 2021, ApJ, 916, 19

Appendix: Near-infrared light curves of Galactic RR Lyrae

Mean magnitudes used to establish PL and PLZ relations are denoted with blue horizontal lines.

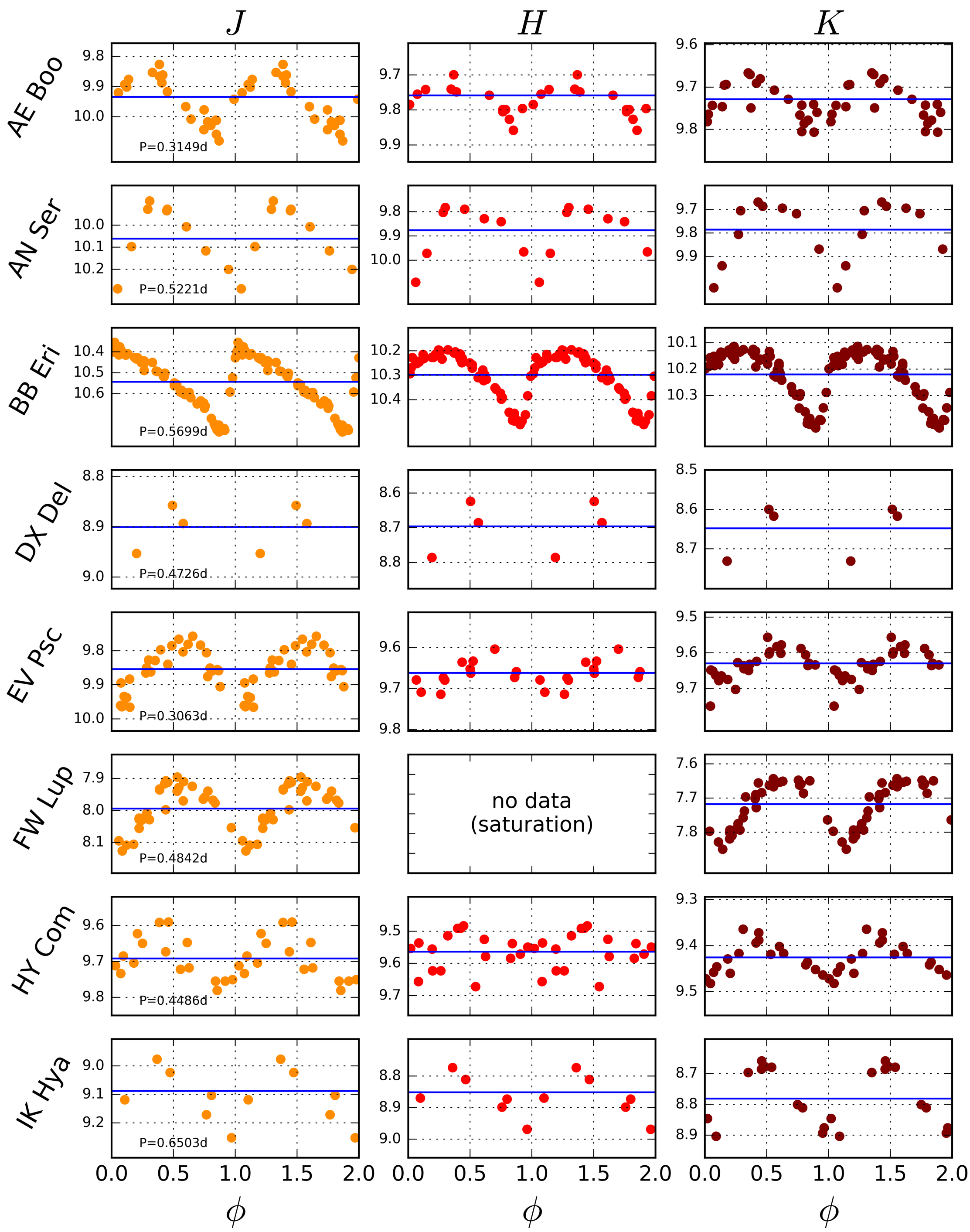

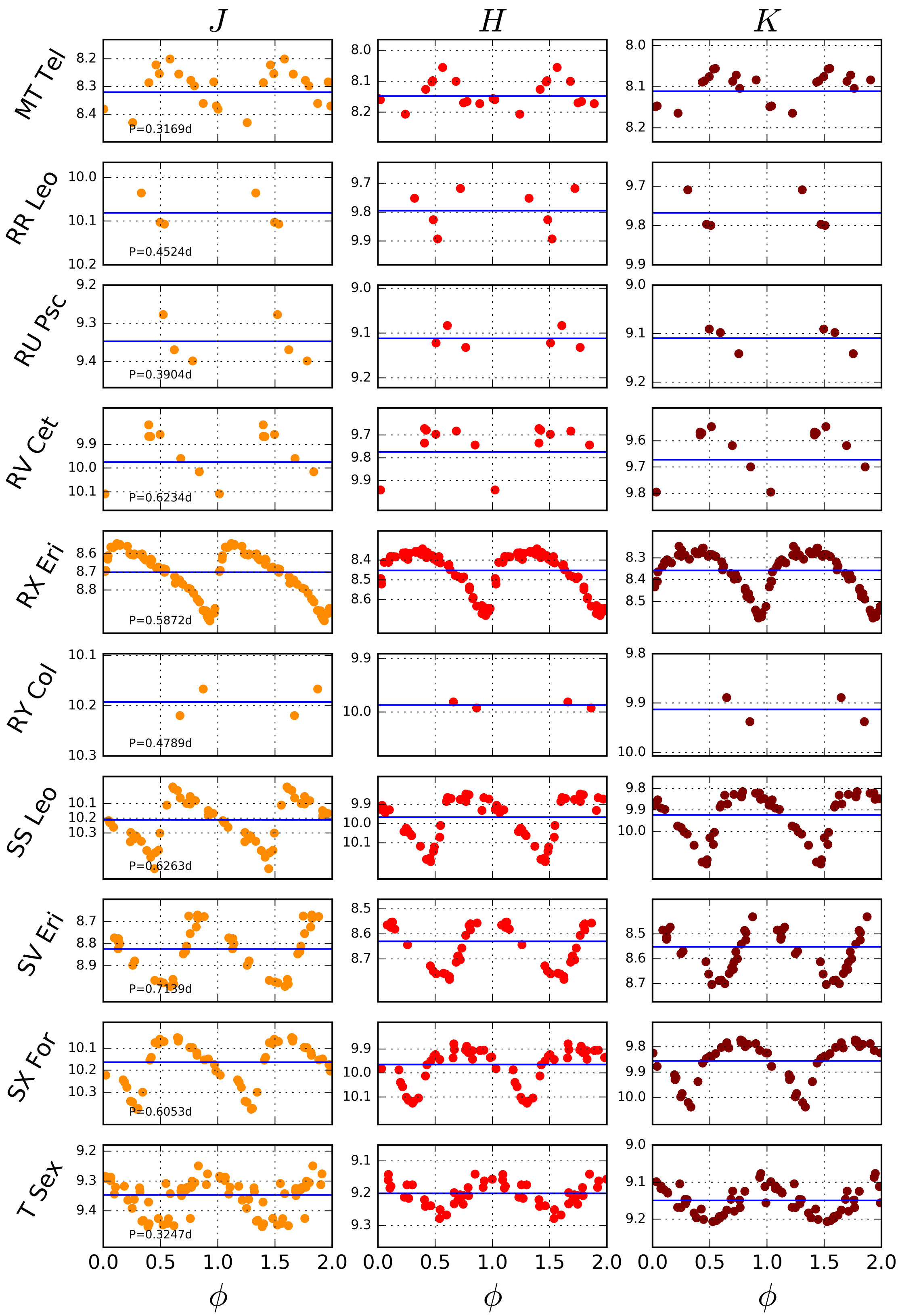
J
H
K
MT Tel
P=0.3169d
RR Leo
P=0.4524d
RU Psc
P=0.3904d
RV Cet
P=0.6234d
RX Eri
P=0.5872d
RY Col
P=0.4789d
SS Leo
P=0.6263d
SV Eri
P=0.7139d
SX For
P=0.6053d
T Sex
P=0.3247d
ϕ

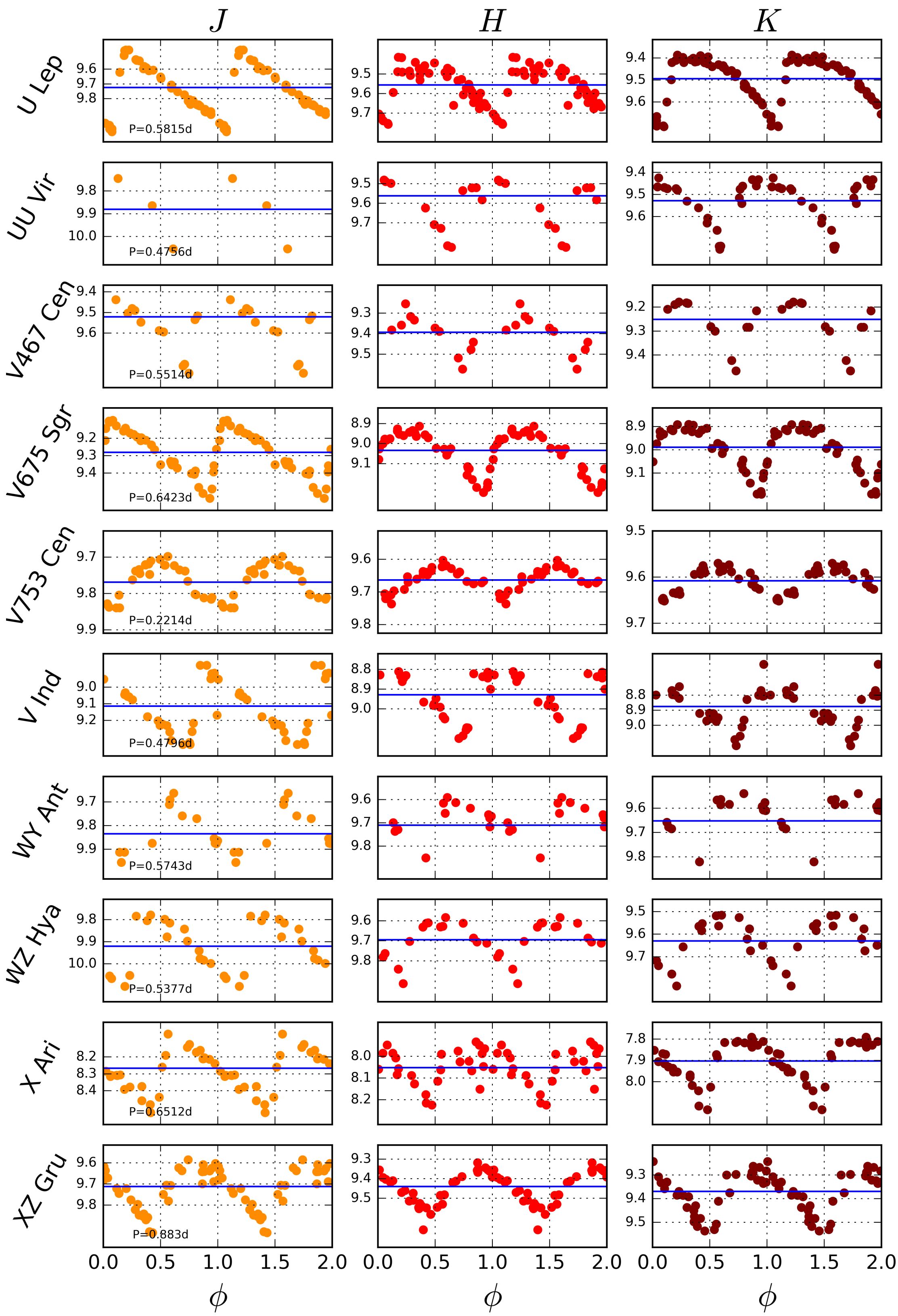

J
H
K
U Lep
P=0.5815d
UU Vir
P=0.4756d
V467 Cen
P=0.5514d
V675 Sgr
P=0.6423d
V753 Cen
P=0.2214d
V Ind
P=0.4796d
WY Ant
P=0.5743d
WZ Hya
P=0.5377d
X Ari
P=0.6512d
XZ Gru
P=0.883d
ϕ